Optimal Control of Mission Design in Multi-Body Models

Majid Salmani
Zentrum für Technomathematik

Dissertation
zur Erlangung des Grades eines Doktors
der Naturwissenschaften
- *Dr. rer. nat.* -
14.12.2012

Gutachter: Prof. Dr. Christof Büskens
Gutachter: Prof. Dr. Alfred Schmidt

I dedicate this dissertation to my family;
to my mother for opening my eyes to the world and showing me the meaning of life and being alive;
to my father for his support, patience and understanding;
and to my siblings and their beautiful families for encouraging me to reach my dreams.

Acknowledgements

I would never have been able to finish my dissertation without the guidance of my supervisor, help from friends, and support from my family.

I would like to express my deepest gratitude to my supervisor Prof. Christof Büskens for his excellent guidance, caring, patience, and providing me with an excellent atmosphere for doing research. I would like also to thank Dr. Matthias Knauer who helped me every time I needed and patiently corrected my mistakes.

I would like to thank friends sitting in the room *Aquarium*, who as good friends, were always willing to help and give their best suggestions.

I would also like to thank my parents, two elder brothers and my sister. They were always supporting me and encouraging me with their best wishes.

Abstract

This dissertation contributes three general steps of space transfer problem. As the first step, this problem is mathematically modelled. Fortunately, it is not an untouched problem, and has been one of the most well-known and challenging problems in mathematics, physics and engineering. Actually, it is known as the *Multi-Body System*, since 18th century till now. During the first step, lots of transfer problem's elements have to be determined. The position, velocity and timing of the start maneuver, the restrictions on position and velocity in the space, especially in the vicinity of the Earth, limits on facilities, etc. are crucial in the mathematical modelling. On the other hand, since the main problem is an interplanetary problem, thus the determination of the final condition is also very important to be exactly understood and obtained.

The second step of the space transfer problem is analysis the mathematical model achieved in the first step. It will be discussed that the system is classified as a chaotic system. After analyzing the behaviour of the system, we would like to control its chaotic behaviour such that some favourite goals are successfully achieved. This step of the study is namely the control of the system. To this end, a new approach is selected which model the transfer problem as an optimal control problem. There are a lot of methods to solve an optimal control problem. Among different classes of solution methods, the direct method is selected which has its own advantages and disadvantages. Its most important advantage is the ability of using the well developed theory of nonlinear programming problem which has been investigated for many decades. The direct method discretizes the transfer optimal control problem and transcribes it into a nonlinear programming problem.

Solving the nonlinear programming problem leads to the optimal solutions, i.e. the optimal trajectory and control. After achieving the optimal solutions, the presented method uses the parametric sensitivity analysis of the discretized nonlinear programming problem and investigates the sensitivity of the optimal solutions with respect to the perturbations. At last, this method contributes a real-time control to correct the violations during the mission.

The numerical results regarding an extensive collection of transfer examples show the applicability of the presented method.

Contents

List of Figures

List of Tables

Chapter 1

Introduction

1.1 Space Transfer

Design capabilities for spacecraft missions to transport the materials have been significantly improved in recent years. These capabilities make the exploration of the space and various observatories possible; the observatories such as the James Webb Telescope [76] and the Terrestrial Planet Finder [59]. A common factor between all these mentioned missions is the destination which is positioned in the vicinity of the libration points in the Sun-Earth system. For being able to stay in such an area, Farquhar first explored trajectory design strategies in the regions of libration points, taking into account periodic solutions of the three-body problem [25]. On the other hand, transportation of spatial telescopes, sensitive optical occupations, large gold coated mirrors and other extremely sensitive and heavy on-board facilities to the periodic destinations considering the huge expenses per kilogram of mass necessitates the development of mission planing that not only keeps the spacecraft in the desired position, but also optimizes the fuel usage and other important factors.

Traditionally, for preliminary design of this kind of missions, the dynamics of two-body problem through the patched conic method has been used. The motion of two bodies is regarded as a well-understood dynamical system with exact analytic solution in the form of conic sections. But in past few decades, the complexity and expectations of mission scenarios have increased such that an expansion of the solution space is required. Specifically, explorations and developments in the vicinity of the libration points are impossible to be modeled accurately in the two-body model. As the number of complicated missions with advanced scientific goals increased, the three-body techniques have been explored to develop mission strategies in the libration point vicinity.

To offer efficient low-energy trajectories that are available throughout more compli-

cated dynamics models of the solar system, such as three-body problem, and satisfy technical, scientific and financial constraints, the existing transfer methods have to be improved. The development of new type of numerical methods coupled with the natural dynamics have had the main role behind the improvements. From these various methods, some of the new observatories take advantage of the *Dynamical System Theory* to offer new insights in multi-body regimes. The methods developed in such an approach are the Target Point Mathod [52] and the Floquet Modes Method [88] which use the idea of invariant manifold tubes from dynamical systems theory.

Another approach incorporates optimization into the mission design process from the commencement, concurrent with the whole engineering goals and requirements. In fact, this approach does take the entire mission design process as an optimal control problem. In this way, the history of control signals and corresponding states (*strategy plan* and *trajectory* in the space application terminology) together construct what is usually called *the mission design* which is supposed to find the optimal maneuvers (amplitude, direction and schedule) to optimize the mission objective and meet the constraints. From control theory point of view, this problem simply means that one is searching for a vector of control variables that when applied to the dynamical system, results in the optimal behavior defined by state variables making objective function to be minimized or maximized [18]. From the system engineering point of view, since the constraints regarding mission, spacecraft and force field, or even location where mission takes place are all simple inputs of a general optimization problem, thus this approach is easier to model the entire problem with the whole details. On the other hand, it is flexible, because of the search space which does not have to be confined to be close to a reference orbit. Indeed, the methods presented in this approach, can search the optimizer in any combination of states (position, velocity and mass), and time with proper thrust. Furthermore, selection of the cost function in the optimization problem is another flexible factor in this approach that can be chosen freely as minimum thrust, minimum fuel use, minimum mission time consumption, minimum amount of maneuvers, a composition of all of them and so on. In addition, if one use a proper method to solve the optimal control problem, the main advantage of this approach comes up which is the possibility to use the theory of parametric sensitivity analysis. Considering the extremely high sensitivity of the periodic orbit transfers with respect to initial conditions, the tools handed by the parametric sensitivity analysis can be used to compute the sensitivities, and then design a method to correct the displacements caused by perturbations.

1.2 Historical Notes

Since the present work incorporates the optimization and mission design in an environment which is defined by multi-body problems, it would be helpful to review briefly the results of previous studies in multi-body problems to see the process and difficulties associated with this field. Furthermore, in order to well understand how this dissertation is relevant to the field of mission design in multi-body models, a historical background of what have been accomplished so far in the fields of interplanetary transfer is provided. Since the knowledge about the three-body problem is basically necessary for working on the other more complicated models, one shall consider studying the three-body problem as the most important branch of this field which one may find it in most textbooks of astrodynamics, see [91] and [97]. There are lots of important contributions since centuries ago developing the three-body problem. The works cited here are tried to be those ones whose contents are either directly used in this dissertation or are fundamentally leading to the topics.

1.2.1 Classical Contributions

The motion of the Sun, the Earth and the Moon has received intense study during centuries all around the world. Since March 15 1079, the announcement date of the most accurate calendar (Persian calendar) by O. Khayyam [7] until works of Johannes Kepler, lots of researches and studies have been investigated regarding asteroid's motions. Although these researches did not develop a workable theory to explain the motion of space bodies, their observations and calculations were useful to similar works afterwards. However Isaac Newton was the person who changed the way by his classic mechanic theory. Whoever talks about mechanics, even celestial mechanics or orbital mechanics, cannot forget his name. He not only solved the general two-body problem, but as the first person, he identified the complexity of the three-body problem in his *Principia* in 1687 too [73]. Unlike the three-body problem which had been left unsolved by him, the motion of two bodies is regarded as a well-known dynamical system with exact conic section-formed analytic solution. Nevertheless, the progress in solving the three-body problem afterwards, has been made under certain simplifications of it. The problem description of the two-body problem is presented in 2.1.1. The famous problem of minimum fuel-consuming transfer of one body to a desired point under a gravitational field of another body is so called *fundamental navigational problem of astronautics* [13]. In 1920's, the first attempts to send rockets to high altitude in an economical manner are made. Indeed, Goddard in 1919 recognized that this problem can be modeled and solved by calculus of variation [13]. But the most famous two-body transfer is the transfer of a satellite from one circu-

lar orbit to another coplanar and cocentric orbit studied first by Hohmann. Hoelker and Solber in 1959 completed the Hohmann's works which was believed to be the minimum fuel trajectory between any two coplanar orbits till that time [47]. To see an extensive list of contributions about the two-body problem, one can refer to [13], [24], [31] and [62]

Besides the two-body problem, Leonhard Euler in the middle of 18th century sought a closed form solution for the three-body problem, but he did not succeed [93]. Joseph-Louis Lagrange used his results to formulate the motion of the Moon under gravitational influence of the Sun and the Earth. He published his famous essay on the three-body problem (*Essai sur le Problème des Trois Corps*) in 1772 [92]. In fact, Lagrange reduced the order of the general three-body problem by the assumption that the third body's mass is infinitesimal and neglectable compared with the other two bodies. This new problem with the extra assumption has been called *Restricted Three-Body Problem*. Not only no closed-form solution to the general three-body problem has ever been found, but also a closed-form solution to the new problem is still unknown. What Lagrange did was the identification of a set of particular solutions for the motion of the third body. He noted that the circular three-body problem yields five equilibrium points. Indeed, Euler had identified the collinear points and Lagrange finished the number five by identifying two equilateral points. For their work, they together were honored by the *Prix de l'Academie de Paris* in 1772 [10]. There were still no closed-form solution to the problem until 1890's when Henri Poincaré proved that no analytical solution for the n-body problem for $n \in \mathbb{N},\ n > 2$ is possible. In 1836, Carl Gustav Jacobi identified an integral and a constant relative to a rotating frame. His determination has combined the conservation low of energy and angular momentum. This two important factors, the constant and the integral, carry his name. After presenting Jacobi integral, lots of efforts had been done searching for more integrals, but Bruns proved that there exists no more integral of motion expressible algebraically as a function of positions and velocities [55]. Some years later in 1890's, Poincaré extended the proof and proved that Jacobi constant is the only integral of motion existing in restricted three-body problem analytically expressible as a function of the system coordinates, masses of the bodies, memonta and the time [95]. Poincarè's insight into the three-body problem and his contributions made most of today's work possible.

1.2.2 Recent Contributions

Poincaré described the periodic orbits as the best tools to explain the dynamical behavior of the three-body problem. After Poincaré's last work in nineteenth century (in 1899), and by the beginning of twentieth century, the three-body problem was a well-defined

problem. But, there were lots of unanswered questions in the study of this problem, specifically about the periodic solutions. The first person who found the periodic orbits in the three-body problem was George Darwin [23]. In the early 1900s, Hill, Moulton and Plummer were seeking periodic orbits in the vicinity of libration point, see [46], [71], [80] and [81]. Moulton indeed developed several analytical approximation to the linearized equations derived from equations of motion. However in 1912, Sundman derived an infinite series solution to the general three-body problem, but it converges quite slow. Indeed, it needs to calculate 1.0E8,000,000 terms to produce a useful solution for a practical purpose, see [90] and [84]. Despite efforts regarding three-body problem and its periodic orbits, till 1960‘s no big progress in their calculation happened. In the 1960‘s, by using modern computers and numerical techniques, a huge number of contributions entered upon identification and compution of the periodic orbits. The authors presented lots of families of planar as well as three-dimensional periodic orbits [16]. One of these authors was Michel Hènon who has a significant role in this study, see [40],[41],[42],[43] and [44]. In 1968, Farquhar used the word *Halo* to describe three-dimensional periodic orbits in the vicinity of libration points, which has been accepted in the terminology [25]. Researchers continued identifying the periodic and quasi-periodic orbits in 1970's, see [27], [38], [98], [63] and [67]. One of the most important contributions belongs to David Richardson who used the Lindestedt-Poincarè method to produce analytically the periodic orbits up to a certain order [83]. Howell presented a numerical method to compute families of periodic orbits near all three collinear points [49]. Jeff Parker in 2007 presented a good study about the orbits in three-body problem. One can refer to his PhD dissertation as a complete reference devoted to show lots of possible orbits [77].

Since the subject of this dissertation is to study the space transfer, therefore a review of the works which have been done in this field is also useful. As mentioned before, the Hohmann transfer is developed as the most important transfer using two-body problem as its underlying system dynamics by Walter Hohmann [48]. But the problem of transferring in three-body model is not as simple as two-body problem, since the trajectories are not conic orbits and there are a few analytical tools available for this problem. Therefore, the challenge of mission design on the three-body problem have been gained many studies during last decades. Because of dependence of transfer investigation in three-body problem on numerical approaches, these transfers have not been investigated extensively until 1960's. McGehee and D'Amario were the first persons who took advantage of new computers combining the analytical and numerical techniques to study trajectories in the three-body problem. Subsequently, in August 12, 1978, a spacecraft designated as the *International Sun-Earth Explorer-3* (ISEE-3) was launched and then after 102 days was injected into a periodic orbit around first libration point in the Sun-Earth system. Since

that event, several texts have described libration point transfers. In 1991, invariant manifold became utilized in determining transfers, see [32] and [33]. The authors followed the dynamical system approach to transfer problem. The particular Earth-halo transfers have been studied in [51] incorporating aspects of [32]. The same problem with extra constraints in launch conditions has been studied in [51] and [9].

Since the problem of three bodies is one of the famous chaotic systems, it attracted also some researchers working on chaotic dynamical systems. There are two main approaches to control a chaotic system. First approach exploit a series of small and wisely chosen perturbations to the system to maintain the desired periodic orbit. In another approach, an appropriate continuous controlling signal is injected into the system, see [36], [8] and [70]. Despite all this distributions, a few works took advantage directly of optimal control theory, methods and post-optimality analysis. Lawden in 1963 only developed some theoretical results and investigated the necessary conditions that must be satisfied by an optimal impulsive trajectory [61]. His works founded the core of transfer optimization using *primer vector*. In [64] and [54], the authors extended his works regarding optimization with primer vector. They investigated some ways to develop their methods to be able to solve the problem with some extra constraints (especially inequalities on control variables), free time, various boundary conditions, and so on. One can find a good discussion about optimal transfers between libration points using primer vector in [45]. Recently, Infeld considered the whole mission design problem in three-body model as an optimal control problem [53]. She used the pseudospectral method to solve the optimal control problem with some simple constraints. The most important work that used optimal control theory is [87]. The authors have not explained about the solving method. They tried to design a mission correcting method which can be handled offline before commencement of the mission. The latter work is very important in the recent contributions, since it did not use the traditional correcting method, the so called *Targeting Method*. This targeting method first had been applied in GENESIS mission, see [65] and [50]. Gómez et al. studied a two-maneuvers correction in [35]. They also showed that their results agree qualitatively and quantitatively with those obtained with optimal control software in [87]. Design the real-time correction strategies which is studied in this dissertation have never been worked before.

1.3 Real Missions Planned on Three-Body Model

A brief overview of the missions planned on three-body trajectories shows the challenging research field *Libration Point Mission Design* as it had to be well-investigated in these missions. Several missions have been planned and operated on the three-body trajectories

since August 12, 1978, when ISEE-3 spacecraft was launched, see [11] and [77]. Also, there are expensive and important missions going to take place in future to investigate the scientific and technological goals. In this section, some of previous missions as well as future planned missions are briefly described.

ISEE-3/ACE was the first libration point mission which was launched on August 12, 1978. One of the *International Sun-Earth Explorer 3*'s purposes was to examine in detail the structure of the solar wind near the Earth and the shock wave that forms the interface between the solar wind and Earth's magnetosphere [75]. Since this mission is one of the most interesting missions which last until now, its story has been explained a little more in detail [75]. After launch, it was placed in a halo orbit

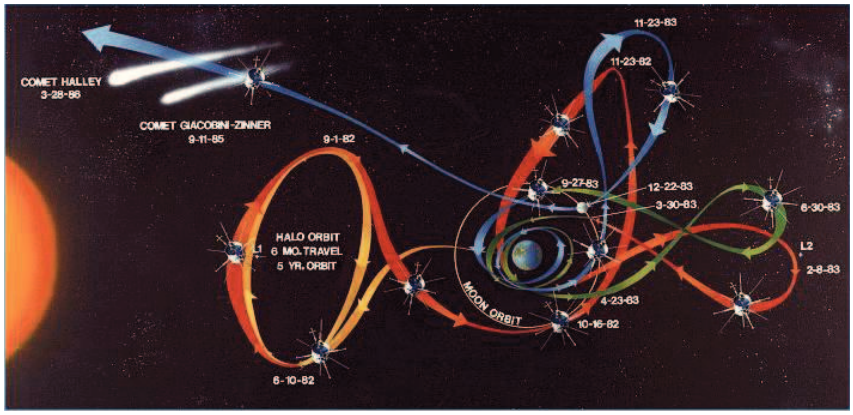

Figure 1.1: The trajectory and time schedule of ISEE-3/ICE [1]

about the first libration point in the Sun-Earth system where it continuously monitored changes in the near-Earth interplanetary medium. In 1982, ISEE-3 began the magnetotail and comet encounter phases of its mission. A maneuver was conducted on June 10, 1982, to transfer the spacecraft from its position to the second libration point. After several passes through the Earth's magnetotail, with gravity assists from lunar flybys in March, April, September and October of 1983, a final close lunar flyby (119.4 km above the Moon's surface) on December 22, 1983, caused the spacecraft renamed to the *International Cometary Explorer* (ICE) and ejected it out of the Earth-Moon system and injected it into the tail of Comet Giacobini-Zinner. This happened on June 5, 1985. The Figure 1.1 shows the long path of ISEE-3/ICE. Farquhar has presented a complete analysis of this flight in [26]. The operation has been terminated in 1997, and the spacecraft will arrive the vicinity of the Earth in August 2014.

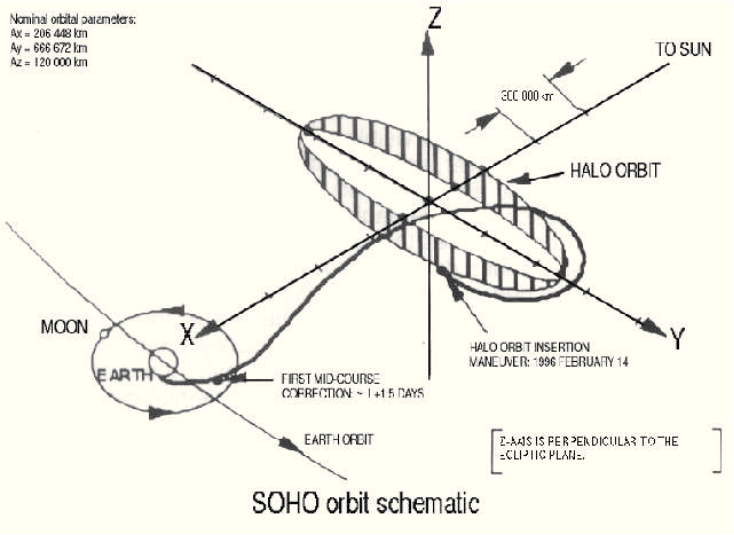

Figure 1.2: The trajectory of SOHO [3]

SOHO or the *Solar and Heliospheric Observatory*, launched on 2nd December 1995, with 1850 kilograms of mass, costed about one thousand million Euro, is a project of international collaboration between ESA[1] and NASA[2] to study the Sun from its deep core to the outer corona and the solar wind [2]. SOHO was designed for a nominal mission lifetime of two years, but because of its spectacular successes, the mission was extended five times (in 1997, 2002, 2006, 2008, and 2010). This allowed SOHO to cover an entire eleven years solar cycle and the rise of the new cycle. SOHO is currently approved through the end of 2012. The interesting fact about this mission is that the control of the spacecraft was lost in June 1998, and only restored three months later through efforts of the SOHO recovery team almost with no ill effects. The Figure 1.2 shows a plot of the way passed by SOHO.

WMAP or the *Wilkinson Microwave Anisotropy Probe* mission, stared on June 30, 2001, with 840 kilograms payload, reveals conditions as they existed in the early universe by measuring the properties of the cosmic microwave background radiation over the full sky [4]. To minimize environmental disturbances (especially sunlight) and maximize observing efficiency, WMAP observes from a Lissajous orbit about the second libration point of the Sun-Earth system. The trajectory to reach the observing station consisted of three lunar phasing loops, see Figure 1.3. The Lissajous orbit (the maximum planar and out of planar amplitudes) has been selected such that the WMAP-Earth vector remains between 1 and 10 degrees off the Sun-Earth vector to satisfy communications requirements. Station-keeping maneuvers are required

[1] European Space Agency, Europe
[2] National Aeronautics and Space Administration, USA

about four times per year to maintain the orbit.

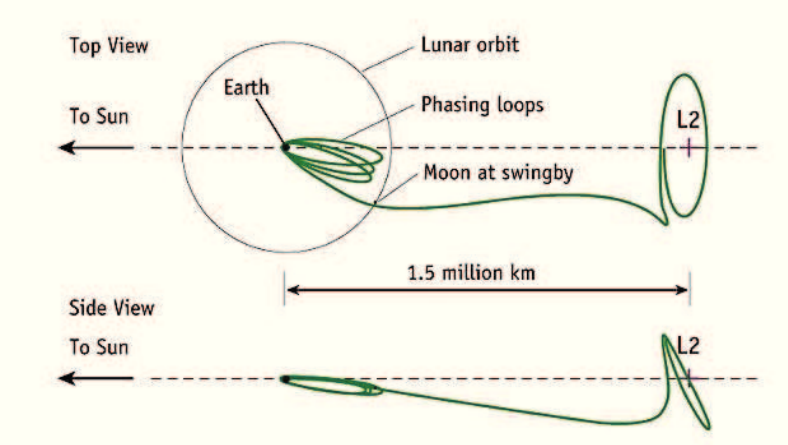

Figure 1.3: The trajectory of WMAP [4]

ACE or the *Advanced Composition Explored* was launched on August 25, 1997 as an explorer program mission. It is carrying six high-resolution sensors and three monitoring instruments, samples low-energy particles of solar origin and high-energy galactic particles with a collecting power 10 to 1000 times greater than past experiments [5]. ACE performed a direct insertion into a Lissajous orbit with 150,000 kilometers y-amplitude around the first libration point of the Sun-Earth system, see Figure 1.4. ACE was the first mission to follow the quasi-periodic Lissajous pattern [11]. The spacecraft has enough propellant on board to maintain the orbit until 2024. Three types of maneuvers (attitude, orbit and spin) have been used since July 2001 to control ACE. Orbit maneuvers use $3^{lbm}/_{year}$ of fuel per year and keep the spacecraft bound to the libration point. Attitude maneuvers use $6^{lbm}/_{year}$ and are required to maintain the antenna constraint. With this strategy, fuel use is $9^{lbm}/_{year}$ total, see [5] and [89].

Genesis was launched on August 8, 2001, The purpose of this mission was to observe the solar wind, entrap its particles and return them to Earth. To this end, it was injected into a halo orbit around the first libration point in the Sun-Earth system. Its direct and quick flight to the halo orbit took almost three months. At arrival, the spacecraft's large thrusters fired to put it into the halo orbit. Genesis completed five periods which took 850 day, nearly 80 percent of the mission's total time to collecting solar winds samples. Because of the position of the landing site and the unique geometry of Genesis' flight path, the spacecraft could not make a direct

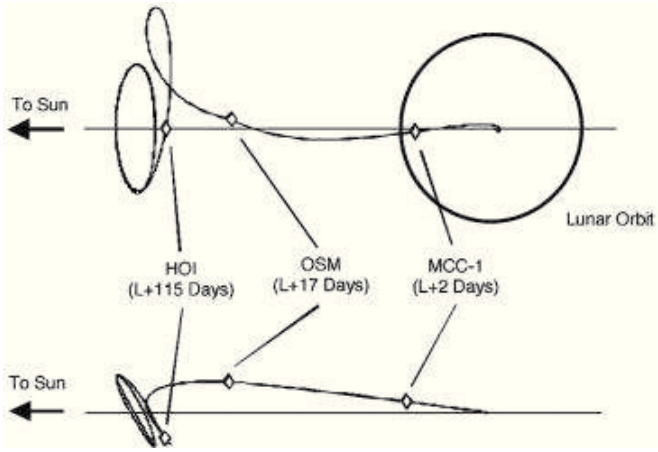

Figure 1.4: The trajectory of ACE [89]

approach and still make a daytime landing. In order to allow the Genesis helicopter crews an opportunity to capture the return capsule in daylight, Genesis mission navigators designed an orbital detour toward the second libration point. Figure 1.5 shows the 3 millions kilomeres-long trajectory of Genesis.

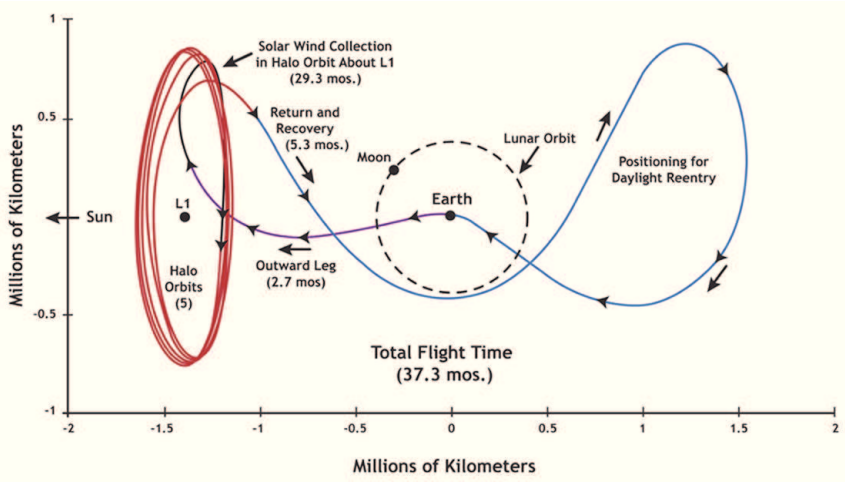

Figure 1.5: The trajectory of GENESIS [6]

Other Past Libration Point Missions are also operated in last years. *Herschel Space Observatory* is operated by ESA on 14 May 2009. It has the largest single mirror ever built for a space telescope. The mission designed as a formation mission joint with ESA's Planck spacecraft. The next day, 15 May 2009, a trajectory control maneuver

was performed as planned to fine-tune Herschel's trajectory. The destination of Herschel is Lissajous orbit about the second libration point of the Sun-Earth system [79]. Another mission is so called Eddington which despite the schedule (2008), ESA records its status as cancelled.

James Webb Space Telescope is an international collaboration between NASA, ESA, CSA[1], scheduled for launch in 2014. Webb will observe primarily the infrared light from faint and very distant objects [76]. To avoid swamping the very faint astronomical signals with radiation from the telescope, the telescope and its instruments must be very cold. To this end, Webb has a large shield that blocks the light from the Sun, the Earth, and the Moon. The normal of the Webb's sun-shield should stay orthogonal to the Sun-Earth surface. Therefore, the best place that the Sun, Earth and Moon are in about the same direction, is the second libration point of the Sun-Earth system.

Other Future Missions such as *Global Astrometric Interferometer for Astrophysics* (GAIA), Terrestrial Planet Finder [12], *International X-ray Observatory* (IXO) and Darwin are plans which will use the libration point of the Sun-Earth system to locate their instruments. The GAIA is a project in ESA that will be launched in 2012 and then will be placed in a Lissajous orbit about the second libration point in the Sun-Earth system. IXO is a joint effort of NASA, ESA, and JAXA[2] combines a large X-ray mirror with powerful new instrumentation that will explore the high energy Universe. The study of project named Darwin ended in 2007 with no further activities planned.

1.4 Present Work

The focus of the current effort is to investigate and develop the methods and techniques to mission design in the three-body problem as well as the four-body problem. As reviewed before, the traditional approach of mission design selects an appropriate initial reference on an appropriate orbit with a reasonable in-plane and out-of-plane amplitudes. This is the first step in the methodology to develop an initial approximation that meets the mission design criteria. Finding such an initial approximation is one of the most difficult tasks during the mission design process, because of the chaotic dynamics in this region. Therefore, it is preferred to choose the initial approximation from the existing trajectories. Of course, selecting an initial approximation in such a way causes some problems

[1] Canadian Space Agency
[2] Japan Aerospace Exploration Agency

such as satisfying the requirements of the current design criteria. However, the errors associated with the initial approximations do not permit the integrated trajectory to be accurate enough and directly acceptable as a solution. After determination of the initial approximation, it should be improved such that an acceptable solution to the three-body problem is obtained. Some methods are proposed to improve the initial guess, e.g. [68], but in spite of their feasibility, they need a solid knowledge of the problem and a lot of user interactions. It should be mentioned that augmenting the effects of additional forces besides gravity fields, such as solar radiation pressure, which has not been considered in initial approximation, imposes extra necessities.

After improving the initial approximation, this approach integrates the states of the system through the vector field to get close to the Earth (mission's initial position). This is a searching procedure that consumes much efforts to reach initial position, velocity and the corresponding time windows. The most important problem which arises in this step is the necessity of having a process to make the trajectory to be continuous in position, velocity and time. Moreover, transfers designed in such a way need also to be the lowest fuel-consuming choice. That induces extra effort to use some sophisticated techniques for optimization. Techniques such as differential correction process which requires to derive a relationship between a given patch point and the states of the system. Furthermore, since the region between the Earth and the libration points has highly unstable dynamics, it causes high sensitivity to the orbits regarding even a tiny change. Therefore, if the underlying model requires to be a little different, even simpler, the whole search has to be done again. The problem will be the same, if one wants to add a constraint on the system dynamics. On the other hand, these difficulties continue also to the design of correction maneuvers. Since there is not enough knowledge about the behavior of the system regarding the errors, the whole correction strategy, i.e. the magnitude and timing, is non-optimal. This means that the method for effective recovery is not a natural resultant of the mission design procedure.

The whole discussion holds for obtaining an approximation in four-body problem, with additional difficulty which is the augmenting solar perturbations that are often too large for the linear differential correction process. To get over these difficulties, this work continues the optimization approach to the mission design problem. Indeed, choosing the reference orbit concurrently with satisfying the constraints, makes another promising approach that is the aim of this work. It will be shown that changing the constraint, constructing more complicated force model, modifying objective of the mission and even the mission region are easy. Since there is no reference approximation, these methods search a less restricted space to reach the minimum-fuel trajectory. This will illustrate how this approach opens new windows to the mission design field and gives the ease of

adjusting the components of the mission. Methods for solving the problem modeled in this way are also very important. In fact, there are two methods to solve an optimal control problem, the direct method and the indirect method. They shall be reviewed in next sections. The method used in this dissertation is a direct method which transcribes the continuous optimal control problem into a discrete nonlinear programming problem with a partially discretization scheme. This transcription results in the most important resultant of this dissertation which is the real-time control of the mission. Upon commencement of this work, the correction maneuvers were limited to the use of pre-designed off-line strategies. One of the goals of this investigation is the determination of a more efficient, systematic and mathematical method that identify accurately the maneuvers to correct the errors. Indeed, the handed means to systematically characterize the correction maneuvers develops a real-time control to be used as a tool to quickly evaluate the correction strategies in order to meet the given mission design requirements. This is the main focus of this dissertation. To this end, this dissertation also tries to contribute the tools to the optimization theory as well as the interplanetary mission design.

1.4.1 Dissertation Organization

To present the approaches and results, this dissertation is organized in the following manner.

Chapter 2 In this chapter, the underlying vector fields and their properties which are going to be studied are explained with particular emphasis on the circular restricted three-body problem. This problem is formulated including the explanation of the simplifying assumptions, nondimensionalization, derivation of the equations of motion, libration points and so on. After that, the four-body problem will be explained based on various types of original three-body problems..

Chapter 3 The solutions of the three-body problem is studied. Furthermore, the quasi-periodic and periodic solutions are also explained with a strong emphasis on the periodic orbits, their computation methods and stability analysis. Additionally, an introdustion to the invariant manifolds is also prepared in this chapter.

Chapter 4 A brief intoriduction to the theory of optimization is presented. Two main categories of optimization, the static or discrete optimization and optimal control theory, are explained. A method to discretize an optimal control problem and transcribe it into a nonlinear programming problem is investigated such that one can use extra useful tools such as parametric sensitivity analysis.

Chapter 5 In this chapter, the transfer optimal control problem in different regimes such as three- and four-body problems is introduces. The basic elements of the control problem plus different extra requirements are determined. This problem is then tried to be solved by the method used in fourth chapter to achieve the optimal solutions to be used in next chapter.

Chapter 6 The optimal solution reached in the previous chapter is considered as an unperturbed solution. We try to design the new strategy for mission correction to conquer the errors taking place during the mission.

Chapter 7 The whole dissertation will be reviewed in a short glance. It makes the difficulties of the approaches and methods more clear and gives a view to the possible future works.

Chapter 2

Dynamics of Multi-Body Systems

The foundation of this dissertation lies on an understanding of the multi-body problem. Investigation of the issues involved in solving transfer problems requires knowledge of the celestial mechanics and initial discussion detailing relevant background information. Space transfer missions are designed traditionally as patched conic sections. This means that the space was divided into some subspaces which only two bodies at a time were considered. Then the trajectory was designed separately as a conic section in every subspace. This method and its factors result in a very good approximation which can be used in more complex models such as *Patched Three-Body Problem*. To reach the point that the whole components of various available models are understandable, we shall study the general multi-body problem first. Then, the special cases such as two-, three- and four-body problems shall be explained.

2.1 Multi-Body Problem

The n-body problem is the problem of predicting the motion of a group of particles that interact with each other. The only interaction between these bodies is the gravitational attraction. This problem can be identified as following; given sets of mass, position and velocity of n bodies (three-dimensional position and three-dimensional velocity) at a specified time, determine the position and velocity of each particle afterwards. Using the Newton's law of universal gravitation, the force on i-th particle generated by j-th particle is

$$\vec{F_i} = G\frac{m_i m_j}{|r_{ij}|^3}\vec{r}_{ij}, \tag{2.1}$$

where m_i and m_j are the masses of i-th and j-th bodies, r_{ij} is the distance between them, F_i is the gravitational force between these two masses exploited on i-th body, and G is

the universal gravitational constant which is equal to 6.673E−11 $^{Nm^2}/_{kg^2}$. By reducing 2.1 to two independent one-body equations, one can determine the equation of the motion of the center of mass (*barycenter*). Considering the attraction due to the rest $n-2$ particles, the inertial acceleration of particle i with respect to the their barycenter is

$$\ddot{\vec{r}}_i = \frac{\sum_{j\neq i}^{n} G\frac{(m_i m_j)}{|r_{ij}|^3}\vec{r}_{ij}}{m_i} \tag{2.2}$$

where r_i is the distance of the desired body to the barycenter. The system of differential equations governing motion of the whole n bodies possess ten integrals of motion. The conservation of linear momentum generates six integrals, the conservation law of angular momentum possesses three, and the conservation of energy in the system also possesses another one. Since the system 2.2 is of the second order of three-component position vectors r of each body, therefore one needs $6n$ integrals of motion to solve the system 2.2. Besides two-body problem that will be discussed in Section 2.1.1, the n-body problems for $n > 2$ possesses no closed-form solution.

2.1.1 Two-Body Problem

In classical mechanics, the problem of two bodies describes the motion of two particles that interact only with each other. The only influence between these two bodies is the gravitational attraction. Common examples for such a problem include a satellite orbiting a planet, a celestial body orbiting another one, or classical electron orbiting an atomic nucleus. This is a general physical law derived from empirical observations by what Newton called induction. It states that every point mass in the universe attracts every other point mass with a force that is directly proportional to the product of their masses and inversely proportional to the square of the distance between them. From 2.2 for $n = 2$, the equation describing the motion of one of these bodies can be obtained. Let us suppose that the first body is a celestial body and the second one is a spacecraft. The Equation 2.2 can be used also to calculate the position of a spacecraft with respect to a celestial body. Note that the mass of the spacecraft is very small with respect to a planet and can be neglected. The ordinary differential equation 2.2 for $n = 2$ is solved analytically [91], and the position vector of the spacecraft with respect to the barycenter (which is almost on the surface of the planet) can be described by

$$\vec{r} = \frac{a(1-e^2)}{1+e\cdot\cos(\theta)}, \tag{2.3}$$

where a is the *semi-major axis* of the spacecraft's orbit, the argument θ is called *true anomaly*, and e is the eccentricity of the orbit. This equation is in polar coordinates for a conic section, and it indicates that all two-body problem solutions are conic sections. For $e = 0$, it will be a circle with radius $p = a(1 - e^2)$. For $0 < e < 1$ it is an ellipse with radii a and $b = a\sqrt{1 - e^2}$. For $e = 1$ it is a parabola and for $e > 1$ it will be a hyperbola. It is worthy of note to mention to another approach reaching the solution of the two-body problem, since it underlies much of the general works in three-body problem. As mentioned in Section 2.1, the equations system of motion in two-body problem has $6 \times 2 = 12$ degrees of freedom. To have a concrete analytical expression, one has to have exactly twelve integrals of motion, i.e. as many as degrees of freedom. The way to get ten integral of motions has been mentioned in Section 2.1, which uses the law of conservation of energy, the conservation of angular momentum, the conservation of linear momentum. The rest two integrals can be provided by Kepler's first two laws. These twelve integrals determine a concretely characterized solution as 2.3, see [94].

2.1.2 Three-Body Problem

The three-body problem is one of the most challenging historical problems during the last centuries, see Section 1.2. It describes the motion of three particles under pure mutual gravitational forces, thus it is an n-body problem with $n = 3$. From 2.2, the gravitational force on one body with mass m_1 is

$$m_1\ddot{\vec{r}}_1 = -G\frac{m_1 m_2}{|\vec{r}_{12}|^3}\vec{r}_{12} - G\frac{m_1 m_3}{|\vec{r}_{13}|^3}\vec{r}_{13}, \tag{2.4}$$

where $\vec{r}_1$ is the position vector of the first body with respect to the origin, and $\vec{r}_{12}$ and $\vec{r}_{13}$ are the position vector of the second body and the third body with respect to the first one, respectively. As a special case of the n-body problem, similar expressions can be derived for the motion of other two bodies. Furthermore, as a subset of general n-body problem, this problem retains ten integrals of motion described in Section 2.1. However, the Kepler's laws do not apply to the problems with more than two bodies. Additionally, the three-body problem needs $6 \times 3 = 18$ integrals of motion to be completely solvable. Therefore, the general three-body problem has eight degrees of freedom, and a complete analytical solution is impossible. To proceed to study this problem, several simplifications can be used which are presented as additional assumptions in the sequence.

RTBP is the abbreviation of the three-body problem with extra assumption which restricts the mass of one body to be infinitesimal and negligible relative to the mass of other two bodies. The other two bigger bodies are so called primaries and they

are supposed to move in a two-body manner around their barycenter. Due to the motion of two primaries, this problem possesses two extra integrals of motion caused by Kepler's laws. Note that such an assumption is common in studying astrodynamics. The three-body problem augmented by the new assumption is called *Restricted Three-Body Problem* (RTBP).

CRTBP or *Circular Restricted Three-Body Problem* is the same RTBP with an assumption which restricts the motion of two primaries to circular orbits around their barycenter. This problem also possesses one extra integral of motion which is so called Jacobi integral, see Section 2.1.2.4. Additionally, the circular motion of primaries makes it possible to model the motion of the third body (infinitesimal mass) in the rotating frame. This is a huge advantage of this assumption that contributes lots of useful properties of the three-body problem.

PCRTBP or *Planar Circular Restricted Three-Body Problem* assumes the motion of all three bodies to be in one plane. This problem has eventually three degrees of freedom.

Since most of the dynamics in the vicinity of the Earth and the Moon have been traditionally modelled as the circular restricted three-body problem, this dissertation also applies this model wherever refers to the three-body problem afterwards unless it is clearly mentioned as the general three-body problem. Since the main underlying dynamical model in this study is the three-body problem, we shall describe it in more detail.

2.1.2.1 Reference Frame

To proceed to formulate the mathematical model after assuming more restrictions on the general three-body problem, the coordinate system in which the motion can be described shall be established. To this end, first assume that $m_1 > m_2$. Suppose that X-Y-Z denotes the requisite inertial coordinates with the origin located at the barycenter B, where the X-axis is directed toward the periapses of the orbit of the smaller primary m_1. The X-Y plane spanned by the X-axis and the Y-axis coincides with the plane of primaries motion. The right handed triad rule generates the Z-axis. The origin of the rotating coordinate frame $\hat{X}$-$\hat{Y}$-$\hat{Z}$ also positioned at the barycenter when the $\hat{X}$-axis is directed toward the smaller primary m_1, $\hat{Z}$-axis is the same as Z-axis and $\hat{Y}$-axis completes the right handed triad. Let θ denotes the angle which represents the orientation of the new coordination system with respect to the X-Y-Z coordination frame. Then one can describe one of these frames in terms of the other one and vice-versa. The transformation between inertial (sideral) and rotating (synodic) frames is explained in more details in

Appendix. Note that $\theta = \omega_{m_2} s$, where ω_{m_2} is a quantity which is so called *mean motion* in celestial mechanics, and s denotes the time, so the symbol t is preserved to denote the time later in the three-body problem in synodic frame.

2.1.2.2 Equations of Motion in Inertial Frame

Let ξ and η denote the abscissa and ordinate of the third body m_3, (ξ_1, η_1) and (ξ_2, η_2) show the same quantities for m_1 and m_2 in the sideral frame, respectively. We have

$$\begin{aligned} \frac{d^2\xi}{ds^2} &= \frac{\partial F}{\partial \xi}, \\ \frac{d^2\eta}{ds^2} &= \frac{\partial F}{\partial \eta}, \end{aligned} \tag{2.5}$$

where F is calculated by 2.2 for $n = 3$. Since

$$\begin{aligned} \xi_1 &= a\cos(\theta), \text{ and } \xi_2 = -b\cos(\theta), \\ \eta_1 &= a\sin(\theta), \text{ and } \eta_2 = -b\sin(\theta), \end{aligned} \tag{2.6}$$

where a and b are the distance of m_1 and m_2 to the barycenter respectively, the Equation 2.5 becomes

$$\begin{aligned} \frac{d^2\xi}{ds^2} &= -G\frac{m_1(\xi - \xi_1)}{\rho_{13}^3} - \frac{m_2(\xi - \xi_2)}{\rho_{23}^3}, \\ \frac{d^2\eta}{ds^2} &= -G\frac{m_1(\eta - \eta_1)}{\rho_{13}^3} - \frac{m_2(\eta - \eta_2)}{\rho_{23}^3}, \end{aligned} \tag{2.7}$$

where ρ_{13} and ρ_{23} are the distance of the third body with respect to the second and the third bodies, respectively. Since the force F contains the time explicitly because of the motion of the primaries, presenting these equations in synodic frame to neglect dependence on the time is reasonable. After straightforward calculation, the equations of motion in synodic frame are [91]

$$\begin{aligned} \frac{d^2\bar{\xi}}{ds^2} - 2\omega_{m_2}\frac{d\bar{\eta}}{ds} - \omega_{m_2}^2\bar{\xi} &= -G\frac{m_1(\bar{\xi} - b)}{\bar{r}_{13}^3} - \frac{m_2(\bar{\xi} + a)}{\bar{r}_{23}^3}, \\ \frac{d^2\bar{\eta}}{ds^2} + 2\omega_{m_2}\frac{d\bar{\xi}}{ds} - \omega_{m_2}^2\bar{\eta} &= -G\frac{m_1\bar{\eta}}{\bar{r}_{13}^3} + \frac{m_2\bar{\eta}}{\bar{r}_{23}^3}, \end{aligned} \tag{2.8}$$

which $\bar{r}_{13}$ and $\bar{r}_{23}$ are the distances of the third body to the first and the second primaries respectively, indicating that in the synodic frame, the new distances have no explicit dependence on the time. Despite the complicated appearance of the new system, especially the first derivative terms, the only useful integral of motion can be obtained directly from

this system.

2.1.2.3 Nondimensionalization

To make the three-body problem more general in the derivations, it is useful to define the coordinates in a nondimensionalized manner. With this attempt, the equations of motion will be independent of quantities like G, a, b, m_1, m_2 and ω_{m_2}. To this end, suppose $l = a + b$ is the distance between two primaries, $M = m_1 + m_2$ and $t = \omega_{m_2} s$. The only parameter which will appear in the system is μ that is

$$\mu = \frac{m_2}{M}. \tag{2.9}$$

By straightforward calculation [91], the equations of motion in the sideral frame is

$$\begin{aligned} \frac{d^2\bar{\xi}}{dt^2} &= -(1-\mu)\frac{(\bar{\xi} - \mu\cos(t))}{\bar{r}_{13}^3} - \frac{\mu(\bar{\xi} + (1-\mu)\cos(t))}{\bar{r}_{23}^3}, \\ \frac{d^2\bar{\eta}}{dt^2} &= -(1-\mu)\frac{(\bar{\eta} - \mu\sin(t))}{\bar{r}_{13}^3} - \frac{\mu(\bar{\eta} + (1-\mu)\sin(t))}{\bar{r}_{23}^3}. \end{aligned} \tag{2.10}$$

Now, the equations of the motion will be derived using dimensionless variables. It is clear that the dimensionless equations of motion of third body in synodic frame is the simplest form of three-body problem. With augmenting the equation regarding out-of-plane variable z to the system, one can derive the three-body problem as following

$$\begin{aligned} \ddot{x} - 2\dot{y} - x &= -(1-\mu)\frac{x+\mu}{r_{13}^3} - \mu\frac{x-1+\mu}{r_{23}^3}, \\ \ddot{y} + 2\dot{x} - y &= -(1-\mu)\frac{y}{r_{13}^3} - \mu\frac{y}{r_{23}^3}, \\ \ddot{z} &= -(1-\mu)\frac{z}{r_{13}^3} - \mu\frac{z}{r_{23}^3}, \end{aligned} \tag{2.11}$$

where r_{13} and r_{23} are the distances of the third body with infinitesimal mass from the bigger and smaller primary, respectively, i.e.

$$r_{13}^2 = (x+\mu)^2 + y^2 + z^2, \tag{2.12}$$

$$r_{23}^2 = (x-1+\mu)^2 + y^2 + z^2. \tag{2.13}$$

Note 2.1.1. In 2.11, it is clear that this system only depends on one parameter $0 \leqslant \mu \leqslant 1$ which is the ratio of the smaller primary's mass to the total mass in the system. The value $\mu = 0$ or $\mu = 1$ corresponds to a unit mass at the origin. The value $\mu = \frac{1}{2}$ also corresponds to two bodies with equal masses positioned with equal distance from the

origin with mass $\frac{1}{2}$. However, $1-\mu$ is also the parameter denoting the mass of the bigger primary in the dimensionless synodic frame. Therefore the total mass is unity as well as the distance, since all distances occurring in the equations were made dimensionless by dividing by l. The dimensionless time t can be interpreted as the longitude of the smaller primary. It is actually a measure of the angle by which the synodic frame has rotated for actual time s. An interesting resultant of the nondimensionalization in the Sun-Earth three-body problem is that the unit of the rotation rate of the system is the same angular velocity of the Earth rotating the Sun.

The parameter μ for the Sun-Earth three-body system equals to $\mu = 3.0404025\text{E}-6$, and for the Earth-Moon system is equal to $\mu = 1.2150604\text{E}-2$. The quantities and information about the Sun-Earth and the Earth-Moon as well as the Sun-Jupiter three-body systems have been gathered and summarized in Table 2.1. The information presented in this table are based on the Reference [94].

2.1.2.4 Jacobi Integral

Suppose that

$$U = \frac{1}{2}(x^2+y^2) + \frac{1-\mu}{r_{13}} + \frac{\mu}{r_{23}}, \tag{2.14}$$

as a pseudo-potential. The equations of motion 2.11 can be rewritten in terms of partial derivatives of U as following

$$\begin{aligned} \ddot{x} &= \frac{\partial U}{\partial x} + 2\dot{y}, \\ \ddot{y} &= \frac{\partial U}{\partial y} - 2\dot{x}, \\ \ddot{z} &= \frac{\partial U}{\partial z}. \end{aligned} \tag{2.15}$$

This system of equations present the third body's equations of motion in dimensionless synodic frame. Multiply the equations 2.15 by $2\dot{x}$, $2\dot{y}$ and $2\dot{z}$ respectively, sum the result together and then integrate, we will have

$$\dot{x}^2+\dot{y}^2+\dot{z}^2 = (x^2+y^2) + 2\frac{1-\mu}{r_{13}} + 2\frac{\mu}{r_{23}} - C, \tag{2.16}$$

which is indeed

$$C = 2U - \|\vec{v}\|_2^2, \tag{2.17}$$

where $\vec{v} = (\dot{x}, \dot{y}, \dot{z})^T$ is the vector of velocities. The Equation 2.17 is the *Jacobi's integral of motion* and the constant C is so called *Jacobi's Constant*. This constant is one of the most important aspects in studying the three-body problem. The Jacobi constant of a

Quantity	the Sun-Earth System		the Earth-Moon System		the Sun-Jupiter System	
μ	3.04040250E-6		1.2150604E-2		9.5454943E-4	
	SU[a]	Dimensionless	SU	Dimensionless	SU	Dimensionless
l[b]	149597870 km	1	384403 km	1	7.784E8 km	1
m_1[c]	1.9891E30 kg	$1-\mu$	6.0477E24 kg	μ	1.9891E30 kg	$1-\mu$
m_2[d]	5.9742E24 kg	$1-\mu$	7.3483E22 kg	μ	1.8970E27 kg	μ
a[e]	454.8377 km	μ	4670.692 km	μ	742360.08 km	μ
b[f]	149597415 km	$1-\mu$	379729.31 km	$1-\mu$	777657639.9 km	$1-\mu$
t	365.24 days	2π	27.28 days	2π	4320.60 days	2π

Table 2.1: The quantities of the Sun-Earth, the Earth-Moon, and the Sun-Jupiter three-body systems.

[a] Standard Units
[b] Distance between two primaries
[c] Mass of the bigger primary
[d] Mass of the smaller primary
[e] Distance of the bigger primary from the barycenter
[f] Distance of the smaller primary from the barycenter

spacecraft cannot change unless some extra forces besides gravitational forces perturb it. If no maneuver is applied to the spacecraft at a particular position, its Jacobi constant cannot increase more than the upper bound $2U$. On the other hand, if it performs a maneuver to increase the velocity, the Jacobi constant will be decreased. In the case of no extra force and maneuver, the spacecraft cannot move freely in whole space. Regions that spacecraft cannot reach are so called *forbidden region*.

2.1.2.5 Zero-Velocity Curves

The Jacobi's constant of the motion in the rotating frame leads to an equation relating the velocity of the massless particle to its position. If one maps out the Jacobi constant in the neighborhood of the primaries, it can be seen that the potential of the three-body system in the synodic frame is a function of the distance. For given values of Jacobi's constant, it is possible to construct curves in the plane on which the velocity vanishes. Indeed, the countours of Jacobi's constant's map are these zero-velocity curves. The zero-velocity curves for the Sun-Earth three-body problem are shown in the Figure 2.1. Since the parameter μ in this system is very small, the curves are not distinctively clear in this figure. To see these curves clearly, the zero-velocity curves for the Earth-Moon three-body system are shown in Figure 2.2, and one can see the zoomed out vicinity of the Moon in the Figure 2.3. The point denoted by L_i, for $i = 1, \ldots, 5$ are the libration points which will be discussed in Section 2.1.2.6. If a zero-velocity curve is closed, the particle

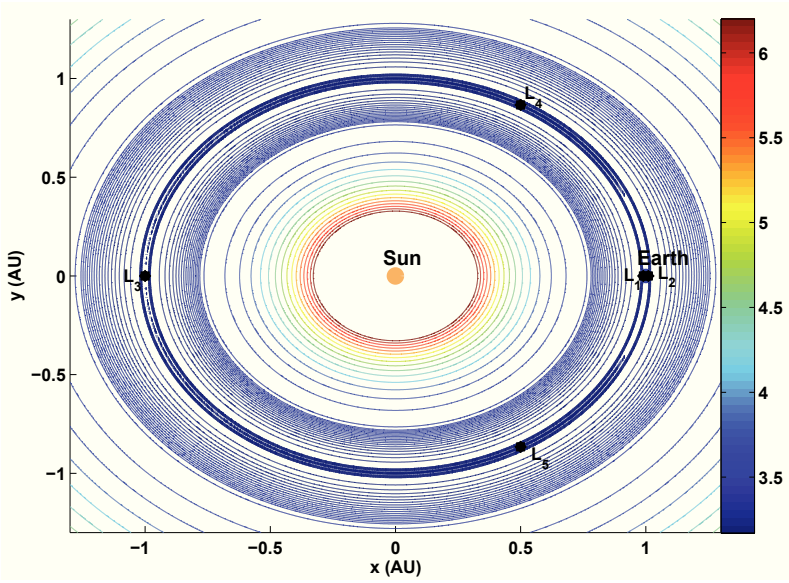

Figure 2.1: The zero-velocity curves for the Sun-Earth three-body problem

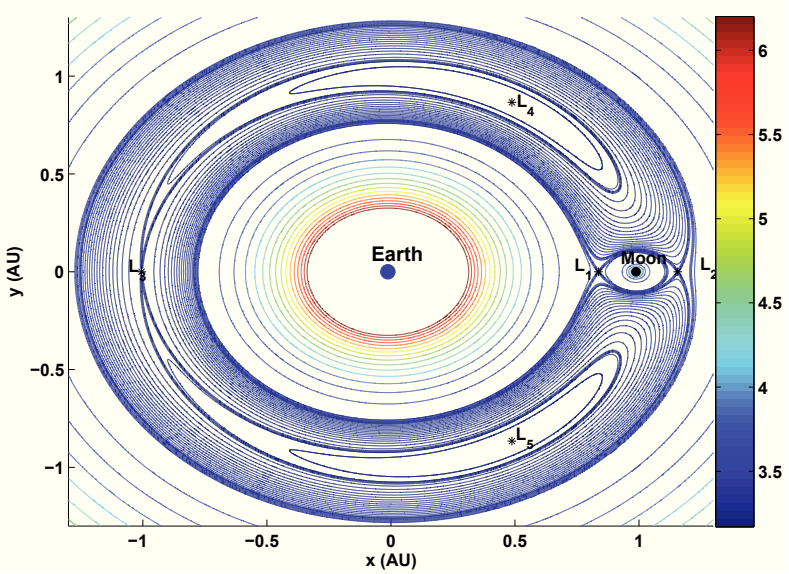

Figure 2.2: The zero-velocity curves for the Earth-Moon three-body problem

cannot escape from the interior of the closed zero-velocity curve unless it placed there with a different constant of the motion than the value used to construct the curve. The third body with infinitesimal mass without any maneuver (such as thrust in the case of spacecraft) cannot change its Jacobi constant. Therefore, it only can reach the regions in the space which is feasible for this constant. The Figures 2.4 and 2.5 show the forbidden regions in the Sun-Earth and the Earth-Moon three body systems, respectively. The trajectories shown in these figures are propagated in the space. The trajectory in Figure 2.4 is propagated with Jacobi constant $C = 3.00659$ and lasts for almost 160 years, and one can see that it cannot cross over the forbidden region and go beyond the Earth's orbit. Additionally, the trajectory of Figure 2.5 is shown for $C = 3.02869$ and lasts for almost three-months. One can see that the third body can cross over the lunar orbit around the Earth on the feasible region. Generally, in the Earth-Moon three-body system, the third body can reach any position if it has a Jacobi constant lower than $C = 2.98800$. A good example to see the restriction of forbidden region is the Oterma comet's trajectory which is shown in Figure 2.6.

2.1.2.6 Equilibrium Points

The zero-velocity curves discussed in the Section 2.1.2.5 can be used to show the existence of three unstable stationary points in the three-body problem, see Figures 2.1 and 2.2. They are actually saddle points in the sense that, if the particle is placed at one of these

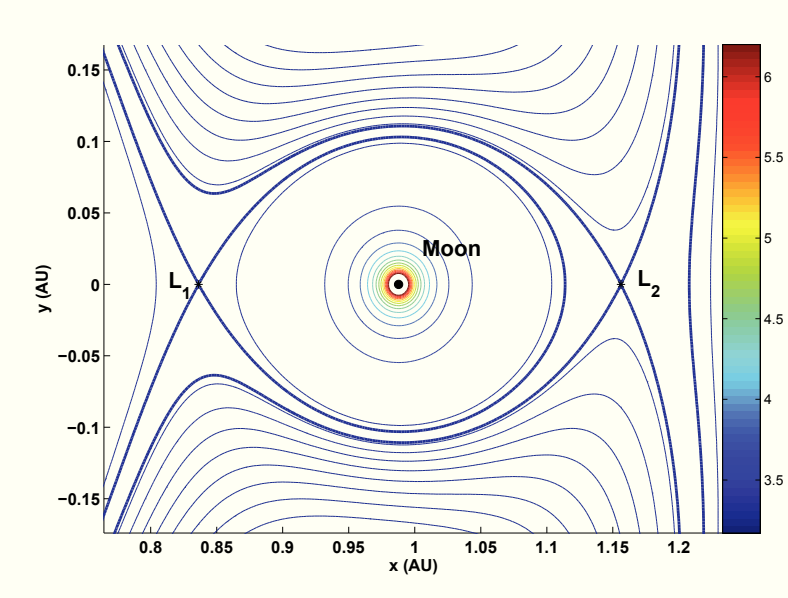

Figure 2.3: The zero-velocity curves for the Earth-Moon three-body problem in the vicinity of the Moon

points, the slightest perturbation will cause it to move far away. One can see the zoomed out Figure 2.3 which shows clearly two saddle points named L_1 and L_2. On the other hand, there are also two other points equilaterally located in Figures 2.1 and 2.2 seen as two peaks. These five points are indeed located at which the instantaneous summation of all forces including centrifugal and gravitational forces is zero. Therefore, if a particle is placed exactly at these points without velocity and there also is no perturbation applied on the particle, then the particle will remain at the same point forever. These five points are so called the *Libration Points*. Due to the Lagrange's identification of these points [92], they are also called the *Lagrange Points*[1]. The expressions leading to computation of the libration points are available from the equilibrium conditions which are

$$\begin{aligned} \frac{\partial U}{\partial x} &= 0, \\ \frac{\partial U}{\partial y} &= 0, \\ \frac{\partial U}{\partial z} &= 0, \end{aligned} \tag{2.18}$$

where U is defined as 2.14. Figure 2.7 shows the locations of the five libration points in the synodic frame. The μ-parameter is selected in the manner that one can distinct

[1]Due to the Dynamical System terminology, these point are also called the equilibrium points or stationary points regarding that they vanish the system of equations of motion.

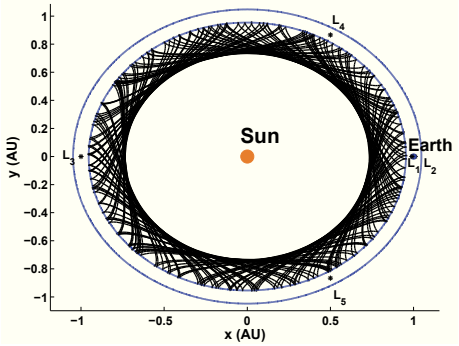

Figure 2.4: The forbidden region for $C = 3.00659$ in the Sun-Earth three-body problem

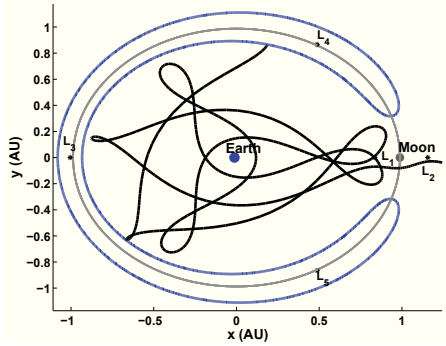

Figure 2.5: The forbidden region for $C = 3.02869$ in the Earth-Moon three-body problem

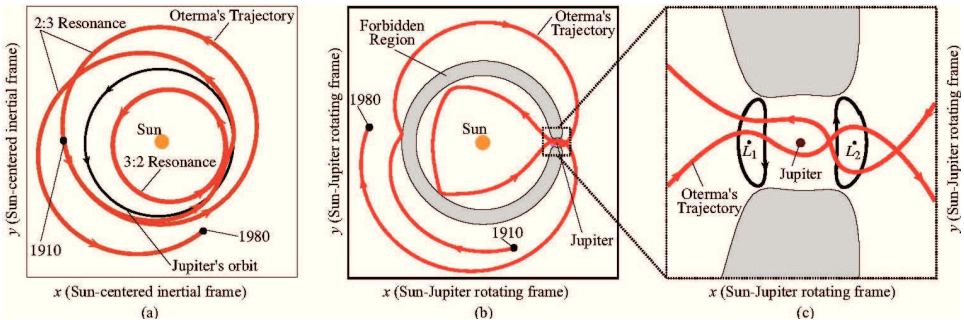

Figure 2.6: The trajectory of the comet Oterma and the forbidden region in the Sun-Jupiter three-body problem

the barycenter and the bigger primary. The μ-parameter of the three-body problem corresponding to this figure is $\mu = 0.121506$. As in the Figure 2.1, three of the Lagrange points lie along the x-axis. These points, L_1, L_2 and L_3, are called the collinear points. The interior one located between the primaries is the first Lagrange point and labeled L_1. The point on the far side of the smaller primary m_2 is denoted by L_2. The point on the far side of the bigger primary m_1 is shown by L_3. Additionally, the remaining two points are the vertices of a equilateral triangle positioned above and below the x-axis. They are denoted by L_4 and L_5, respectively, and called equilateral libration points. In the circular restricted three-body problem, each libration point is located at a constant distance from the barycenter. In the more general elliptic three-body problem, the libration points still exist, but they oscillate continuously. The location of the libration points vary as a function of the parameter μ. This is shown in the Figures 2.8 and 2.9. Since the location of equilateral points always make equilateral triangle, their y-coordinates are constant and

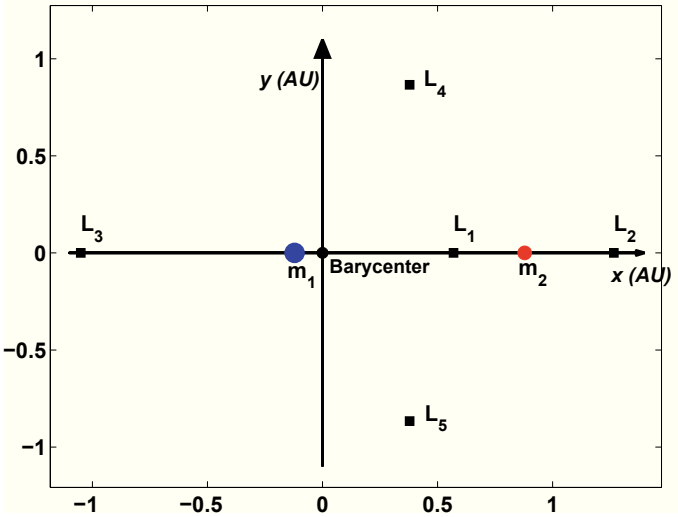

Figure 2.7: Locations of the libration points corresponding to $\mu = 0.121506$

have not been shown. The parameter μ is considered to vary between zero and 0.5, since for $0.5 < \mu \leqslant 1$ the bigger and smaller primaries will switch. Furthermore, when μ goes to zero, the points L_1 and L_2 approach the smaller primary and L_3 approaches -1. Note that in the case $\mu = 0.5$, the distances L_1-L_2 and L_1-L_3 are equal. Since the locations of the Lagrange points are functions of μ, then the corresponding Jacobi constant of each Lagrange point where $\|v\|_2$ equals to zero, is also a function of μ. Figures 2.10 and 2.11 show the Jacobi constant C of each Lagrange point varying as a function of μ

2.1.3 Four-Body Problem

The problem of four bodies is a well-known problem that studies the motion of the fourth body under the pure gravitational effects of the other three bodies. In the study of solar system, there are interesting four-body systems such as the Sun-Earth-Moon-spacecraft, the Sun-Jupiter-Saturn-spacecraft and etc. Specifically, in the study of the environment in the vicinity of the Earth, the motion of a spacecraft under the gravitational forces of the Sun, Earth and Moon may be affected directly by all three bodies. This can be a more realistic system to model the motion of the spacecraft. We shall study the four-body problem in some specific forms which are the patched three-body and the bicircular models.

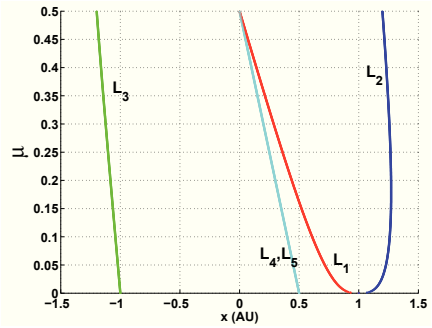

Figure 2.8: The position of the libration points L_i, $i = 1, \ldots, 3$ as functions of μ. The μ-axis is scaled linearly

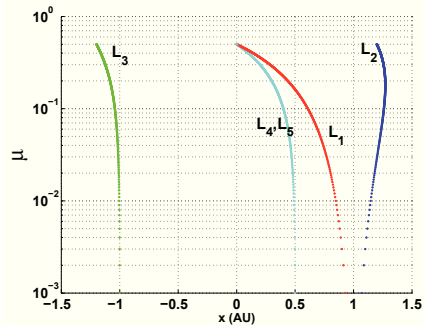

Figure 2.9: The position of the libration points L_i, $i = 1, \ldots, 3$ as functions of μ. with logarithmically scaled μ-axis

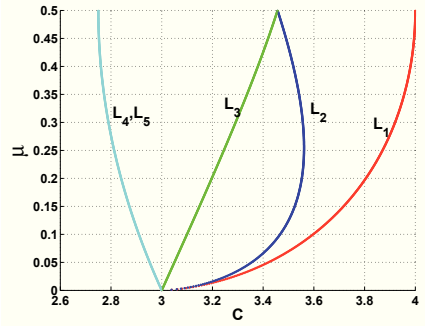

Figure 2.10: The Jacobi's constant C of the libration points L_i, $i = 1, \ldots, 5$ as functions of μ with the linear scaled μ-axis

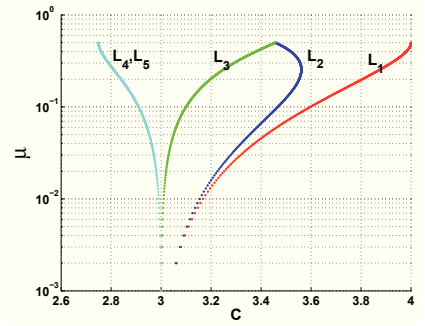

Figure 2.11: The Jacobi's constant C of the libration points L_i, $i = 1, \ldots, 5$ as functions of μ with logarithmically scaled μ-axis

2.1.3.1 Patched Three-Body Problem

As mentioned before, trajectories for interplanetary missions have been designed by using the conic sections. The trajectory of the spacecraft was divided into pieces in which the influence of only one body is considered. This is so called the *Patched Conic* or *Patched Two-Body* approximation of the multi-body problem. The trajectory of the Voyager probes have been designed by this method and worked very well. The dividing step is the most important step of this method which uses a criterion. This criterion is known as the *sphere of influence*, in which the second body's influence is taken into account. As one expects, this method cannot model accurately the motion on a low-energy trajectory. In such a trajectory, the influences of both primaries have the same order of magnitude. In this case, a new patched model must be used which is called *Patched Three-Body Model*. This model uses separated three-body problems to approximate the four-body system.

Let consider the Sun-Earth-Moon-spacecraft four-body problem. When the spacecraft reaches the vicinity of the Moon (in a sphere of the Moon with a certain radius), the equations of motion is described by the equations of motion in the Earth-Moon three-body problem. This holds unless the spacecraft exits the mentioned sphere. Then the motion is modeled by the Sun-Earth three-body problem. The sphere of influence and its boundary are computed in the same way as patched two-body problem. Design of the trajectories in the patched three-body model by the traditional methods shows some difficulties, especially in the configuration of the initial guess. On the other hand, to use the patched model, these methods ignore other perturbations. We will study the mission design in this model, so one can see the ease of the problem in the optimal control approach, even with additional perturbation such as solar radiation pressure. Note that once the spacecraft reaches the boundary of the spheres of influence and crosses the boundary, its states should be transferred to the other coordinate system. To compute the radius of a primary's sphere of influence centered at the primary, one can use the gravitational forces exploited on the infinitesimal body. Then the sphere of the influence can be identified as the surface where the massless body's motion is equally affected by both primaries. Briefly, the radius of the sphere of influence of the smaller body is roughly equal to

$$r_{si} = \mu^{2/5}, \tag{2.19}$$

where the parameter μ is the ratio of the smaller body's mass to the bigger one's mass. The Equation 2.19 is a special case corresponding to the primaries with circular orbits. In general form, the radius of a body's sphere of influence in an elliptical orbit about the bigger body is

$$r_{si} = a\mu^{2/5}, \tag{2.20}$$

where a is the semi-major axis of the elliptical orbit. Once the bicircular models based on the Sun-Earth three-body problem and the Earth-Moon three-body model are explained in the Section 2.1.3.2, one serious question will arise which will be discussed in the Section 2.2.

2.1.3.2 Bicircular Model

In this section, the motion of the fourth body with infinitesimal mass in field of the other three massive bodies m_1, m_2 and m_3 will be discussed. In this model the bodies m_2 and the m_3 are in circular motion about their barycenter. And it is assumed that the system m_2-m_3 together as one body rotates in a circular orbit around the other body m_1. This model is so called the *bicircular model*, and the most important instance of

this model is the Sun-Earth-Moon model. This bicircular model can be presented in two ways. First model is derived from the Earth-Moon three-body system with augmenting the gravitational influence of the Sun. And the second bicircular model is derived from the Sun-Earth three-body system with extra term of the Moon's gravitational force.

A. Bicircular Model Derived from the Earth-Moon CRTBP

This model is the same bicircular model mentioned earlier with an additional assumption

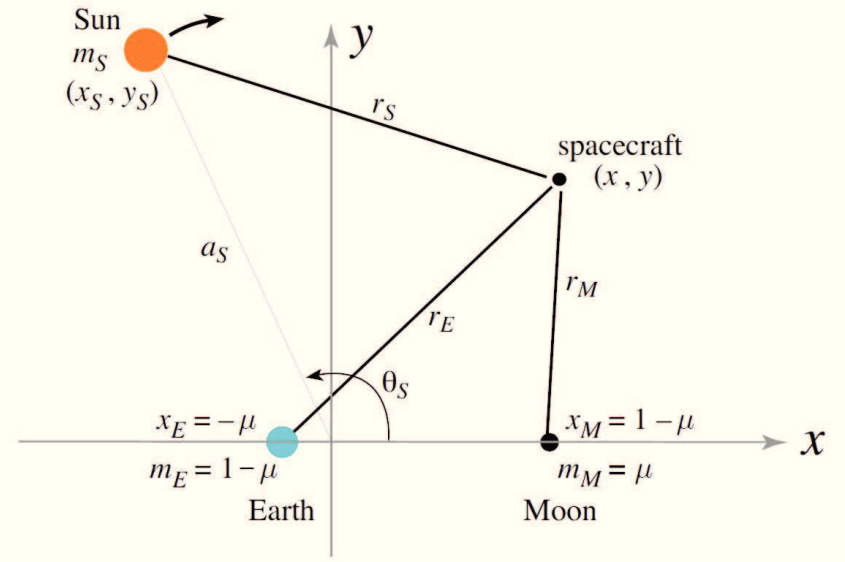

Figure 2.12: The Sun-Earth-Moon-spacecraft bicircular four-body model derived from the Earth-Moon three-body problem in the synodic frame [58]

$m_1 \gg m_2 \gg m_3$. Let us consider the Sun-Earth-Moon-spacecraft four-body system. And suppose the spacecraft does not affect the motion of the primeries [34]. The Earth and the Moon are assumed to revolve around their barycenter as the circular restricted three-body system with the parameter μ, Equation 2.11. After that, this model put the Sun and the Earth/Moon[1] in a circular restricted three-body system. Note that the orbits of all three primaries are in the same plane. Since the basic system from which the bicircular model has been derived was the Earth-Moon three-body system, thus the units of mass, length, time and therefore the angular velocity are the same as the Earth-Moon three-body problem, i.e. μ and $1-\mu$ are the masses of the Moon and the Earth, respectively, and the distance between them equals to one. Let m_S and a_S denote the Sun's mass

[1]The Earth and the Moon are considered as one body revolving around the Sun, and it is shown by Earth/Moon. Although Earth-Moon might be a better way to show this concept, the Earth/Moon is common in the terminology.

and semi-major axis in the mass and length units of the Earth-Moon three-body system, respectively. The x- and y-axes are directed as Figure 2.12. This figure shows the Earth-Moon circular restricted three-body problem in the synodic frame. Therefore, the Earth and the Moon are fixed points and the Sun moves with the mean motion ω_S around their barycenter. The x- and y-coordinates of the Sun are denoted by x_S and y_S, and given by

$$x_S = a_S \cos(\theta_S), \tag{2.21}$$
$$y_S = -a_S \sin(\theta_S), \tag{2.22}$$

where $\theta_S = (1-\omega_S)t + \theta_{S_0}$ is the phase of the Sun with the initial value θ_{S_0}. Then equations of motion of the infinitesimal body (spacecraft) in the dimensionless synodic Sun-Earth-Moon reference frame are

$$\begin{aligned}
\ddot{x} &= 2\dot{y} + x - (1-\mu)\frac{x+\mu}{r_{PE}^3} - \mu\frac{x-1+\mu}{r_{PM}^3} - m_S\frac{(x-x_S)}{r_{PE}^3} - m_S\frac{x_S}{a_S^3},\\
\ddot{y} &= -2\dot{x} + y - (1-\mu)\frac{y}{r_{PE}^3} - \mu\frac{y}{r_{PM}^3} - m_S\frac{(y-y_S)}{r_{PS}^3} - m_S\frac{y_S}{a_S^3},\\
\ddot{z} &= -(1-\mu)\frac{z}{r_{PE}^3} - \mu\frac{z}{r_{PM}^3} - m_S\frac{z}{r_{PS}^3},
\end{aligned} \tag{2.23}$$

where r_{PE} and r_{PM} and r_{PS} are the distances of the spacecraft to the Earth, and the Moon and the Sun, respectively. Indeed,

$$r_{PE}^2 = (x+\mu)^2 + y^2 + z^2, \tag{2.24}$$
$$r_{PM}^2 = (x-1+\mu)^2 + y^2 + z^2, \tag{2.25}$$
$$r_{PS}^2 = (x-x_S)^2 + (y-y_S)^2 + z^2. \tag{2.26}$$

The parameters of the mentioned bicircular system are

$$\begin{aligned}
\mu &= 1.215060\text{E}-2,\\
m_S &= 328900.54,\\
a_S &= 388.81114,\\
\omega_S &= 0.925195985520.
\end{aligned}$$

The time and distance scales are the same as the Earth-Moon three-body problem mentioned in the Table 2.1.

B. Bicircular Model Derived from the Sun-Earth CRTBP

In this model, the Sun and the Earth are revolving in circular orbit around their barycenter

and the Moon is moving in a circular orbit around the center of the Earth. To get the spacecraft's equations of motion, we begin with the Sun-Earth three-body problem. Let the distance between the Sun and the Earth be taken as unity. The coordinates with respect to the Sun-Earth system is used, such that the positions of the Sun and the Earth are fixed at $(-\mu, 0)$ and $(1-\mu, 0)$, respectively. Let m_M be the parameter of the Moon in the same non-dimensional mass units as the Sun-Earth three-body system. In this frame, the Sun and the Earth hold and Moon moves about the barycenter of the Sun-Earth system on a circle with radius R_M, in the non-dimensional distance units. The angular velocity of the Moon in these synodic coordinates and the phase of the Moon are denoted by ω_M and θ_M, respectively, which θ_M at $t = 0$ is θ_{M_0}. The x- and y-coordinates of the Moon may then be described respectively by

$$\begin{aligned} x_M &= R_M \cos(\theta_M), \\ y_M &= R_M \sin(\theta_M), \end{aligned} \tag{2.27}$$

where $\theta_M = \omega_M t + \theta_{M_0}$. The equations of the motion of the spacecraft in the bicircular system in the Sun-Earth synodic reference frame are then equal to the equations of motion of the same spacecraft in the Sun-Earth three-body system with the new contributions due to the Moon,

$$\begin{aligned} \ddot{x} &= 2\dot{y} + x - (1-\mu)\frac{x+\mu}{r_{PS}^3} - \mu\frac{x-1+\mu}{r_{PE}^3} - m_M\frac{(x-x_M)}{r_{PM}^3}, \\ \ddot{y} &= -2\dot{x} + y - (1-\mu)\frac{y}{r_{PS}^3} - \mu\frac{y}{r_{PE}^3} - m_M\frac{(y-y_M)}{r_{PM}^3}, \\ \ddot{z} &= -(1-\mu)\frac{z}{r_{PS}^3} - \mu\frac{z}{r_{PE}^3} - m_M\frac{z}{r_{PM}^3}, \end{aligned} \tag{2.28}$$

with

$$\begin{aligned} r_{PS}^2 &= (x+\mu)^2 + y^2 + z^2, \\ r_{PE}^2 &= (x-1+\mu)^2 + y^2 + z^2, r_{PM}^2 = (x-x_M)^2 + (y-y_M)^2 + z^2, \end{aligned}$$

where μ and $1-\mu$ are the parameters describing the ratio of masses of the Earth and the Sun, respectively, to the sum of both masses. Furthermore, r_{PS}, r_{PE}, and r_{PM} are the distances of the third body to the Sun, the Earth, and the Moon, respectively. The values of the parameters for the Sun-Earth-Moon-spacecraft bicircular four-body problem

derived from the Earth-Moon three-body problem are briefly as following

$$\mu = 3.034040\text{E} - 6$$
$$m_M = 3.694262\text{E} - 8$$
$$R_M = 2.635651\text{E} - 3$$
$$\omega_M = 12.368869.$$

In the Sun-Earth-Moon-spacecraft bicircular four-body system **??**, time is scaled by the period of the Sun and Earth around their barycenter of mass (one year). Hence, the time unit equals to $T/2\pi$ where T = one year = 31557600 s. Position is also scaled by the average Sun-Earth distance (L = 149597870 km) and therefore velocities are scaled by $2\pi L/T = 29.786$km/s which is the Earth's average velocity around the Sun.

2.2 Discussion

In the Section 2.1.3.1, the concept of sphere of influence for the patched two-body system has been extended to the patched three-body system. And the patched three-body model has been explained for the Sun-Earth-Moon-spacecraft four-body problem. Now, one can consider the same discussion for two bicircular four-body systems, i.e. the bicircular models derived from the Earth-Moon CRTBP and the Sun-Earth CRTBP. As explained in the first bicircular model, the new contributions due to the Sun is added to the Earth-Moon CRTBP. This bicircular model is a good approximation for the Earth-Moon CRTBP, and works very well for the near-Moon environment. Also, the contribution due to the Moon is augmented to the Sun-Earth CRTBP to make the second bicircular model. This model is also generally a better approximation of the dynamics than the Sun-Earth CRTBP. Nevertheless, in the first bicircular model, since the Sun's gravity does not perturb the motion of the Earth or the Moon, therefore the system does not satisfy the Newton's equations. Furthermore, the motion of the three primaries in the second bicircular model is not coherent, hence, the motions in this model also do not satisfy the newton's equations. The question which arises now is; How can one define a sphere of influence centered at the Moon with system dynamics as bicircular of form A inside, and bicircular of form B outside? and the other question is; Considering the fact that neither the bicircular model of form A nor B, satisfy the Newton's equations, how the energy changes when the spacecraft crosses the boundary of sphere of influence?

Chapter 3

The Three-Body Problem

This chapter is devoted to explain the three-body problem in more details. Since one of the goals of this dissertation is the optimal control of mission design in the three-body system, therefore the modeling, analyzing and constructing the full model and its solutions shall be discussed. On the other hand, various four-body models which are going to be used in this study, use the particular solutions of the three-body problem. Studying the three-body problem is much more difficult than the two-body problem, considering exsitance of no analytical solution. This lack of analytical solution makes the researchers to use approximated analytical expressions and numerical methods to reach a certain set of solutions. In the sequential sections, we shall study the existance of various types of solutions in three-body problem, and the methods to calculate and compute them.

3.1 Solutions of CRTBP

As mentioned in Section 2.1.2.6, there exist five points in every three-body problem which are its most basic solutions. Among these points, the first two collinear ones have attracted more interests than the other ones, since they are located in the vicinity of the smaller body. Unfortunately, these two points are unstable in the sense that if a small perturbation is exploited to a particle placed at one of these two points, the particle will depart from the point. This instability does not finish the story of libration points, because there are numerous families of orbits which provide good positions to place the particle.

3.1.1 Periodic and Quasi-Periodic Orbits

The three-body problem possesses several types of solutions other than libration points. Periodic and quasi-periodic orbits of two- and three-dimensions are families of important solutions which attracted much efforts. Most of the authors have referred to the

quasi-periodic orbits as *Lissajous Orbits*. The most important property of the periodic and Lissajous solutions is their boundedness. They are bounded, especially in the z- and y-directions which make the control and communication possible. Usually, there is no problem regarding the eclipses, especially when the Moon blocks the Earth which causes a communication outage. Another property of these orbits is the low fuel-consuming station keeping strategies. To achieve these solutions, there are several methods which are categorized in three main categories listed below.

Analytical Expansion which is mainly based on the works of Richardson [83]. Using higher order expansions of this method results very accurate approximations. This high order expansion is useful for high energy trajectories, since once the energy increases, the nonlinear terms in the expansion become important. The WMAP's Lissajous orbit and JWST's halo orbit are two important instances of orbits which are calculated accurately using this method. Nevertheless, because of symbolic computation required to implement this methods, most of researchers and designers usually prefer to use the numerical methods.

Numerical Method which is indeed based on the shooting techniques. These techniques are usually difficult, but in case of three-body problem with exploiting some constraints such as the symmetry of the system, one can numerically construct various types of halo orbits. The main body of this method is based on the work of Howell presented in 1984 [49]. We frequently use this method to construct the halo orbits in the three-body problem. It is explained in more detail in the sequential sections.

Poincaré Section is a convenient way to achieve the periodic and quasi-periodic orbit, especially the stable orbits. Because Poincaré map preserves many properties of periodic and quasiperiodic orbits of the original system and has a lower dimensional state space, it is often used for analyzing the original system. After recording the piercing points on the Poincaré surface, one can identify a periodic orbit as a fixed-point in the plane and a quasi-periodic orbit as a closed loop.

3.1.1.1 Analytical construction of orbits

To analytically calculate periodic and quasi-periodic orbits, one can use the Richardson's analytical approximation [83]. This expression results in a very good characterization of the periodic solutions.

First, the origin of the synodic frame is required to be translated to one of the collinear Lagrange points. Then we transform the variables in the three-body problem to the new

frame. The new position coordinates are defined as

$$\begin{aligned} x_L &= x - (1 - \mu \pm \gamma_L), \\ y_L &= y, \\ z_L &= z, \end{aligned} \tag{3.1}$$

where γ_L is the nondimensional distance of the Lagrange points to the smaller primary. The sign preceding γ_L depends on the Lagrange point under consideration. It is plus for the L_2 point and minus for the L_1 and L_3 points. Since the position is only translated by some constant value in synodic frame, the velocities and the accelerations in the new translated coordinate system are

$$\begin{aligned} \dot{x}_L &= \dot{x},\ \ddot{x}_L = \ddot{x}, \\ \dot{y}_L &= \dot{y},\ \ddot{y}_L = \ddot{y}, \\ \dot{z}_L &= \dot{z},\ \ddot{z}_L = \ddot{z}. \end{aligned} \tag{3.2}$$

After translating the coordinates, the next step is to expand the equations of motion about the Lagrange point under consideration [83]. This expansion is

$$\begin{aligned} \ddot{x}_L - 2\dot{y}_L - (1 + 2c_2)x_L &= \sum_{n=2}^{\infty}(n+1)c_{n+1}\rho^n P_n(\frac{x}{\rho}), \\ \ddot{y}_L + 2\dot{x}_L - (1 - c_2)y_L &= \sum_{n=3}^{\infty} c_n y \rho^{n-2} \tilde{P}_n(\frac{x}{\rho}), \\ \ddot{z}_L + cz_L &= \sum_{n=3}^{\infty} c_n z \rho^{n-2} \tilde{P}_n(\frac{x}{\rho}), \end{aligned} \tag{3.3}$$

where P_n is the n-th Legendre polynomial of the first kind, ρ is the distance from the considered libration point, and

$$\begin{aligned} \tilde{P}_n(\frac{x}{\rho}) &= \sum_{k=0}^{[(n-2)/2]} (3 + 4k - 2n) P_{n-2k-2}(\frac{x}{\rho}), \\ c_n &= \frac{(-1)^n}{(\pm\gamma_L)^3}(\mu + \frac{(1-\mu)\gamma_L^{n+1}}{(1 \pm \gamma_L)^{n+1}}). \end{aligned} \tag{3.4}$$

A special case of the analytical approximations is the linear approximation which permits existance of specific type of solution in the vicinity of the collinear Lagrange points. Indeed, this approximation of the three-body problem allows the existence of periodic

and quasi-periodic orbits. If the linear term of the Taylor expansion (3.3) is taken, then we have the linearized equations of motion as

$$\begin{aligned} \ddot{x}_L - 2\dot{y}_L - (1+2c_2)x_L &= 0, \\ \ddot{y}_L + 2\dot{x}_L - (1-c_2)y_L &= 0, \\ \ddot{z}_L + c_2 z_L &= 0, \end{aligned} \tag{3.5}$$

where c_2 is

$$c_2 = \frac{1-\mu}{(1\pm\gamma_L)^3} + \frac{\mu}{(\pm\gamma_L)^3}. \tag{3.6}$$

The equation regarding z_L in (3.5) is independent from x_L and y_L, and describes a simple harmonic motion. The remaining four-dimensional linear first order system has a characteristic equation as

$$\sigma^4 + (2-c_2)\sigma^2 + (1+2c_2)(1-c_2) = 0, \tag{3.7}$$

which has two real and two complex roots. Therefore, the general solution can be written as

$$\begin{aligned} x_L &= A_1 e^{\epsilon t} + A_2 e^{-\epsilon t} + A_3\cos(\tilde{\sigma}t) + A_4\sin(\tilde{\sigma}t), \\ y_L &= -k_1 A_1 e^{\epsilon t} + k_1 A_2 e^{-\epsilon t} - k_2 A_3\cos(\tilde{\sigma}t) + k_2 A_4\sin(\tilde{\sigma}t), \\ z_L &= B_1\cos(\tilde{\nu}t) + B_2\sin(\tilde{\nu}t). \end{aligned} \tag{3.8}$$

Due to the exponential terms in (3.8), the particle can move with no bound. However, the motion can be adjusted to be bounded by carefully selecting the appropriate initial conditions. The resulting equations then can be presented as

$$\begin{aligned} x_L &= -kA_x\cos(\lambda t+\phi), \\ y_L &= A_x\sin(\lambda t+\phi), \\ z_L &= A_z\sin(\nu t+\psi). \end{aligned} \tag{3.9}$$

Equation (3.9) describes that the periodic and quasi-periodic orbits can be identified by six variables. They are the in-plane and out-of-plane amplitudes, A_x and A_z, the in-plane and out-of-plane frequencies, λ and ν, and phase angles ϕ and ψ for in-plane and out-of-plane motion, respectively. The Figure 3.1 show one lissajous orbit which after projection on a two-dimensional plane has been shown in Figure 3.2. Although the orbit shown in these figures last for twenty years, its motion is bounded. Several types of Lissajous orbit obtained by different in-plane and out-of-plane frequencies are shown in Figure 3.3. Note

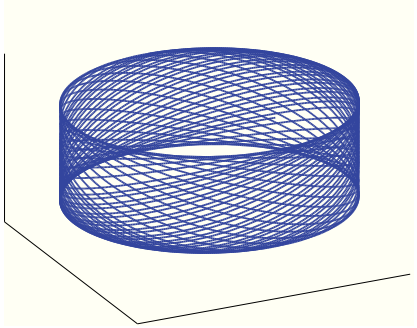

Figure 3.1: A Lissajous orbit in three-dimensional view

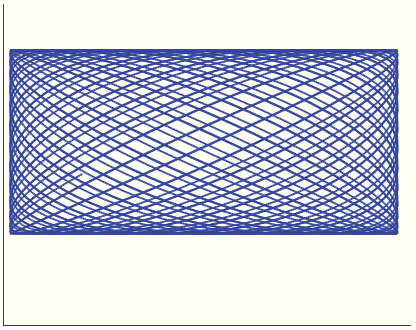

Figure 3.2: A Lissajous orbit in two-dimensional view

that if two frequencies λ and ν equal to each other or commensurate, the resulting orbit will be a periodic orbit. In other cases it will be a quasi-periodic or Lissajous orbit. In the special case when these two frequencies are equal, the resulting periodic orbit is known as *Halo Orbit*. If the out-of-plane amlpliude equals to zero, then the orbits handed by (3.9) will be a planar orbit which is known as *Lyapunov Orbit*. As one expects, there are infinite number of periodic orbits in the three-body problem. To classify these orbits, one can use the symmetry of the three-body problem, i.e., if the problem allows an orbit to exist, then it also permits a symmetric orbit to exist which is indeed the reflection of the original one across the x-y plane. This allows the classification of the periodic orbits into two genral classes of *Northern*[1] and *Southern*[2] families. Indeed, if the maximum out-of-plane component is above the x-y plane ($z > 0$), then the orbit is classified as a northern family, and otherwise it is classified as the southern family. Figure 3.4 shows two halo orbits (blue lines) around Lagrange points L_1 and L_2 concurrent with two their corresponding symmetrical orbits (red lines). The linear approximation which has been used to analytically construct the orbits, gives a qualitatively good approximation of the dynamics found in the three-body problem. This property of the linear approximation leads to the numerical method for constructing periodic orbits which will be discussed in Section 3.1.1.2. However, one should be cautious about the very high A_z-amplitude periodic orbits which cannot be approximated accurately by the linear approximation. In this case, higher order approximations should be used [83].

[1] known also as the Class I family
[2] known also as the Class II family

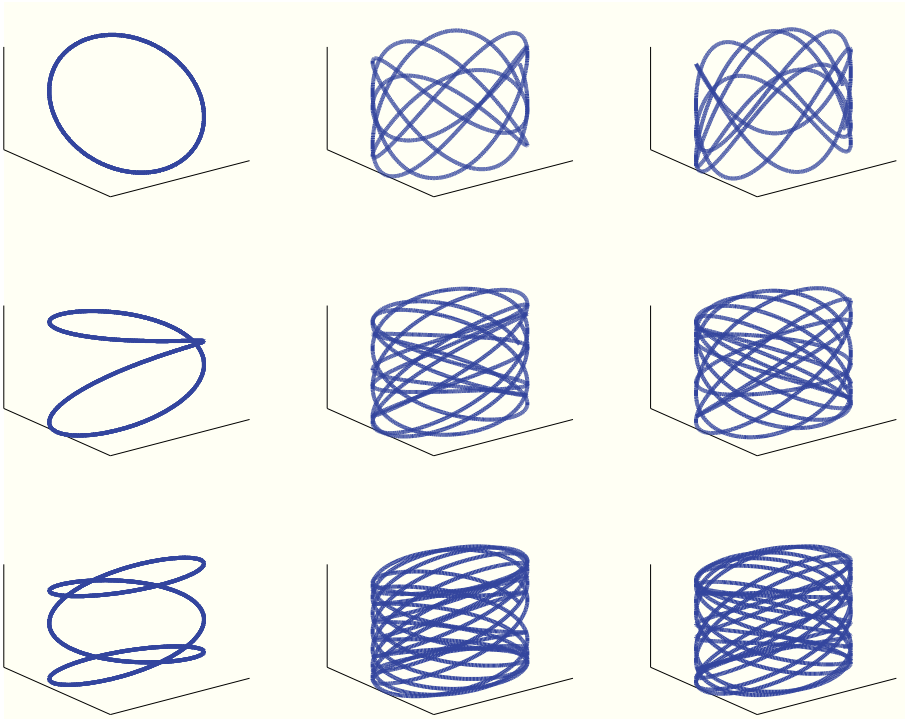

Figure 3.3: Various types of Lissajous orbits with different in-plane and out-of-plane amplitudes and frequencies, viewed in 3-dimensional frame. The curves on the left are periodic. The rest of curves are Lissajous orbits which have been propagated for for almost two years.

3.1.1.2 Numerical construction of halo orbits

This section is mainly based on the numerical method presented in [49] in 1984. The shooting technique is used to numerically construct a periodic orbit by targeting a single state. To construct by this method, first the state transition matrix should be introduced which is associated with the equations of motion. This matrix approximates the propagation of even a slight deviation. One can use this matrix to adapt the initial conditions regarding satisfying some other conditions. The state trasition matrix is usually denoted by $\Phi(t, t_0)$ and is governed by 36 first order ordinary differential equations as follows

$$\dot{\Phi}(t, t_0) = A(t)\Phi(t, t_0), \tag{3.10}$$

with the initial conditions $\Phi(t_0, t_0) = I_6$, which I_6 is the 6×6 identity matrix. And

$$A(t) = \frac{\partial \dot{\mathbf{x}}(t)}{\partial \mathbf{x}(t)}, \tag{3.11}$$

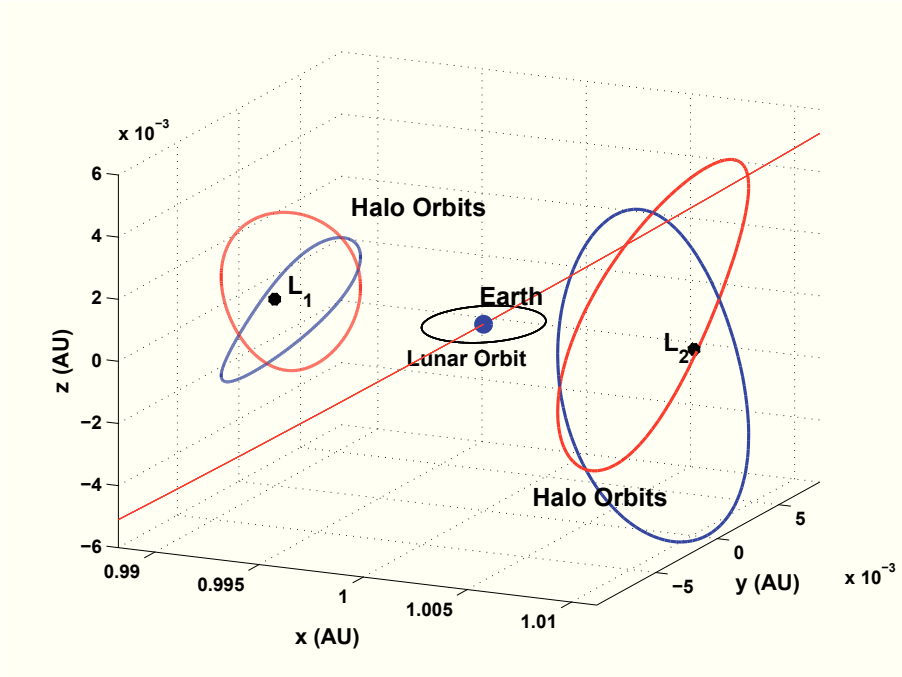

Figure 3.4: Two halo orbits around Lagrange points L_1 and L_2 (blue lines). The other two halo orbits (red lines) are obtained only using symmetrical property of the three-body problem.

when state vector $\mathbf{x} = (x, y, z, \dot{x}, \dot{y}, \dot{z})^T$ is the vector of position and velocity variables. For the three-body problem $A(t)$ has the following form

$$A(t) = \left(\begin{array}{c|c} \mathbf{0}_3 & I_3 \\ \hline U_{xx} & 2\Omega \end{array}\right) \tag{3.12}$$

where $\mathbf{0}_3$ represents the 3×3 matrix of zeros, I_3 is the 3×3 identity matrix and

$$U_{xx} = \frac{\partial^2 U}{\partial \mathbf{x}^2} = \begin{pmatrix} \frac{\partial \ddot{x}}{\partial x} & \frac{\partial \ddot{x}}{\partial y} & \frac{\partial \ddot{x}}{\partial z} \\ \frac{\partial \ddot{y}}{\partial x} & \frac{\partial \ddot{y}}{\partial y} & \frac{\partial \ddot{y}}{\partial z} \\ \frac{\partial \ddot{z}}{\partial x} & \frac{\partial \ddot{z}}{\partial y} & \frac{\partial \ddot{z}}{\partial z} \end{pmatrix}, \text{ and } \Omega = \begin{pmatrix} 0 & 1 & 0 \\ -1 & 0 & 0 \\ 0 & 0 & 0 \end{pmatrix}, \tag{3.13}$$

with the same U defined as (2.14). Given a set of initial states as $\mathbf{x}_0$, numerical integration of the equations of motion is sufficient to construct the corresponding trajectory. However, to construct trajectories with specific charcteristics such as halo orbits, the simultaneous integration of both the equations of motion and the differential equations governing the

state transition matrix is required. Therefore, the construction of a halo orbit with this method needs simultaneous integration of a system consists of 42 ordinary differential equations. The obtained elements of the state transition by integration of the Equation (3.10) represent the relationship between the linearized states at two time instants t and t_0 which is defined as

$$\Phi(t,t_0)=\frac{\partial \mathbf{x}(t)}{\partial \mathbf{x}(t_0)}=\begin{pmatrix} \frac{\partial x(t)}{\partial x(t_0)} & \frac{\partial x(t)}{\partial y(t_0)} & \cdots & \frac{\partial x(t)}{\partial \dot{z}(t_0)} \\ \frac{\partial y(t)}{\partial x(t_0)} & \frac{\partial y(t)}{\partial y(t_0)} & \cdots & \frac{\partial y(t)}{\partial \dot{z}(t_0)} \\ \vdots & \vdots & \ddots & \vdots \\ \frac{\partial \dot{z}(t)}{\partial x(t_0)} & \frac{\partial \dot{z}(t)}{\partial y(t_0)} & \cdots & \frac{\partial \dot{z}(t)}{\partial \dot{z}(t_0)} \end{pmatrix}. \tag{3.14}$$

The state transition matrix contains the full informations of every point along the trajectory propagated by equations of motion and this matrix.

To construct a halo orbit, we use their symmerty property which means that they are symmetric with respect to the x-z plane, piercing this plane twice a period. Suppose that $\mathbf{x}_0$ is a point on the periodic orbit on the plane $y=0$, and $\mathbf{x}_{T/2}$ is the state of the next crossing point of the plane. For these orbits to be symmetric and periodic, $\mathbf{x}_0$ and $\mathbf{x}_{T/2}$ have to be set to

$$\mathbf{x}_0=(x_0\ 0\ z_0\ 0\ \dot{y}_0\ 0)^T, \tag{3.15}$$

$$\mathbf{x}_{T/2}=(x_{T/2}\ 0\ z_{T/2}\ 0\ \dot{y}_{T/2}\ 0)^T. \tag{3.16}$$

Assume that we start from an initial guess which is close enough to the state of the periodic orbit. The transition matrix at $\frac{T}{2}$ can be used to adjust the initial values of the nearby periodic orbit to make the states at $\frac{T}{2}$ to be $\dot{x}_{T/2}=\dot{z}_{T/2}=0$. This adjustment can be calculated from

$$\delta\mathbf{x}_{T/2}\approx\Phi(T/2,0)\delta\mathbf{x}_0+\frac{\partial \mathbf{x}}{\partial t}(T/2)\delta(T/2). \tag{3.17}$$

One should note that the term $\frac{\partial \mathbf{x}}{\partial t}$ in (3.17) has to be calculated at $T/2$. In some literatures it is written as $\frac{\partial \mathbf{x}}{\partial t}(0)$ which is wrong. The Equation (3.17) may be used as a differential corrector to get the desired changes in the final state, i.e. at $\frac{T}{2}$. The desired changes in the final state is the change in the $\dot{x}$ and $\dot{z}$. After forward integration until the next x-z plane cross, we obtain

$$\tilde{\mathbf{x}}_{\tilde{T}/2}=(x_{\tilde{T}/2}\ 0\ z_{\tilde{T}/2}\ \dot{x}_{\tilde{T}/2}\ \dot{y}_{\tilde{T}/2}\ \dot{z}_{\tilde{T}/2})^T. \tag{3.18}$$

The deviation of y is zero, since the integration has been applied until the x-z plane cross.

Therefore

$$\delta \mathbf{x}_{T/2} = (x_{T/2}\ 0\ z_{T/2}\ -\dot{x}_{T/2}\ \dot{y}_{T/2}\ -\dot{z}_{T/2})^T. \tag{3.19}$$

Now by using (3.17) with allowed initial corrections as $\delta \mathbf{x}_0 = (\delta x_0\ 0\ \delta z_0\ 0\ \delta \dot{y}_0\ )^T$, we have

$$\begin{pmatrix} \delta x_{T/2} \\ 0 \\ \delta z_{T/2} \\ -\dot{x}_{T/2} \\ \delta \dot{y}_{T/2} \\ -\dot{z}_{T/2} \end{pmatrix} \approx \Phi(T/2, 0) \begin{pmatrix} \delta x_0 \\ 0 \\ \delta z_0 \\ 0 \\ \delta \dot{y}_0 \\ 0 \end{pmatrix} + \begin{pmatrix} \dot{x} \\ \dot{y} \\ \dot{z} \\ \ddot{x} \\ \ddot{x} \\ \ddot{x} \end{pmatrix} \delta \frac{T}{2}, \tag{3.20}$$

where

$$\delta \frac{T}{2} = \frac{-\phi_{21}\delta x_0 - \phi_{23}\delta z_0 - \phi_{25}\delta \dot{y}_0}{\dot{y}}, \tag{3.21}$$

which the ϕ_{ij} is the ij-th entry of the state matrix Φ. If it desired to change only z_0 and

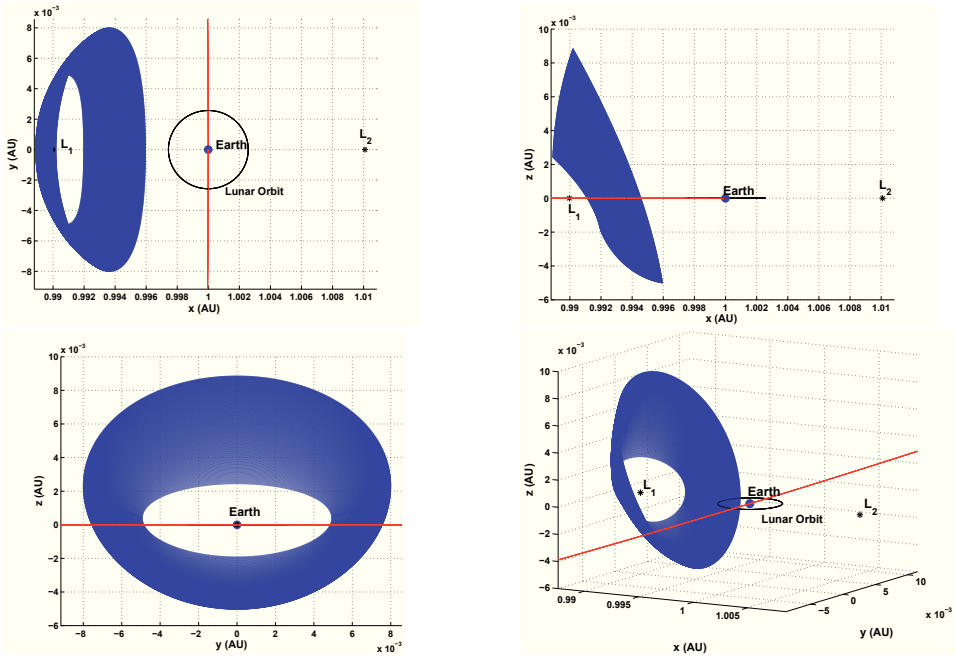

Figure 3.5: The two- and three-dimensional view of a family of almost 200 halo orbits around the Lagrange point L_1 in the Sun-Earth three-body system.

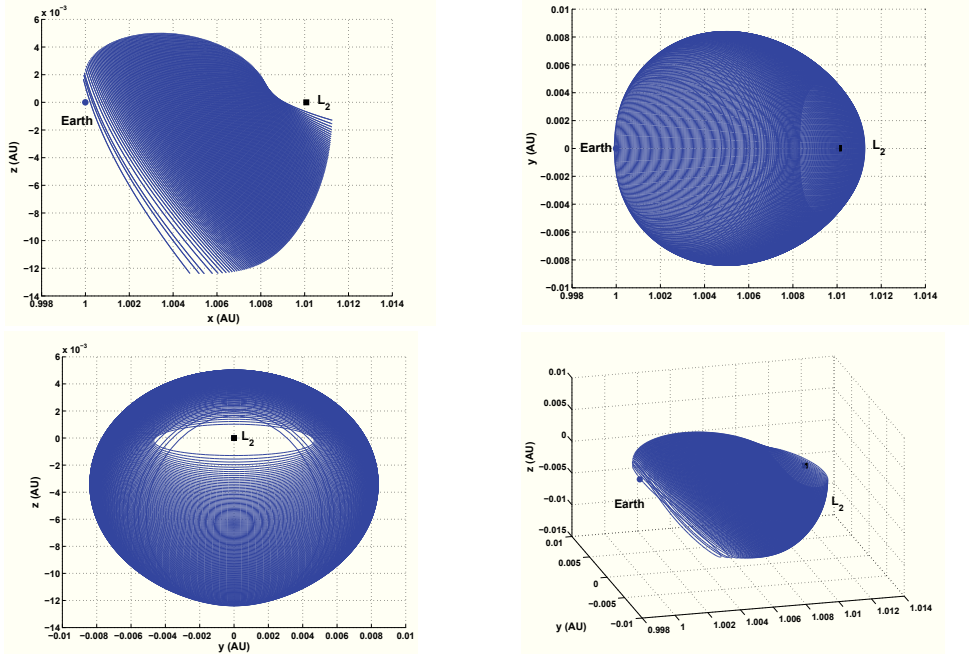

Figure 3.6: The two- and three-dimensional view of a family of almost 200 halo orbits around the Lagrange point L_2 in the Sun-Earth three-body system.

$\dot{y}_0$ and leave x_0 fixed, the correction of the initial guess will be as

$$\begin{pmatrix} \delta z_0 \\ \delta \dot{y}_0 \end{pmatrix} \approx \left(\begin{pmatrix} \phi_{43} & \phi_{45} \\ \phi_{63} & \phi_{65} \end{pmatrix} - \frac{1}{\dot{y}} \begin{pmatrix} \ddot{x} \\ \ddot{z} \end{pmatrix} (\phi_{23} \ \phi_{25}) \right)^{-1} \begin{pmatrix} -\dot{x}_{T/2} \\ -\dot{z}_{T/2} \end{pmatrix}. \tag{3.22}$$

And if it is desired to keep z_0 fixed and correct x_0 and $\dot{y}_0$, we have

$$\begin{pmatrix} \delta x_0 \\ \delta \dot{y}_0 \end{pmatrix} \approx \left(\begin{pmatrix} \phi_{41} & \phi_{45} \\ \phi_{61} & \phi_{65} \end{pmatrix} - \frac{1}{\dot{y}} \begin{pmatrix} \ddot{x} \\ \ddot{z} \end{pmatrix} (\phi_{21} \ \phi_{25}) \right)^{-1} \begin{pmatrix} -\dot{x}_{T/2} \\ -\dot{z}_{T/2} \end{pmatrix}. \tag{3.23}$$

Because of the linearization of the system in order to produce this algorithm, this methodology converges to a periodic halo orbit usually with three or four iterations [49]. On the other hand, it is not necessary to compute the second half of the orbit, because of the symmetry about x-z plane. Figure 3.5 shows a family of halo orbits around the Lagrange point L_1. As it can be seen in the projection on the x-z plane, most of the orbits' bodies are above the x-y plane. Hence this family is classified as a northern family of halo orbits. Figure 3.6 shows also a family of halo orbits around the Lagrange point L_2 in different two- and three-dimensional views. This family consists of almost 200 halo orbits with a wide range of in-plane and out-of-plane altitudes. The period of these orbis varies be-

tween 110 and 200 days. The shortest and longest period belong to the halo orbits which are the closest ones to the L_2 and the Earth, respectively. The family of orbits shown in Figure 3.6 are classified as southern orbits, since the maximum out-of-plane components of all orbits are under the x-y plane. These orbits concurrent with their corresponding symmetrical northern orbits are shown in Figure 3.7. The northern orbits are computed using only the symmetric property of the three-body problem.

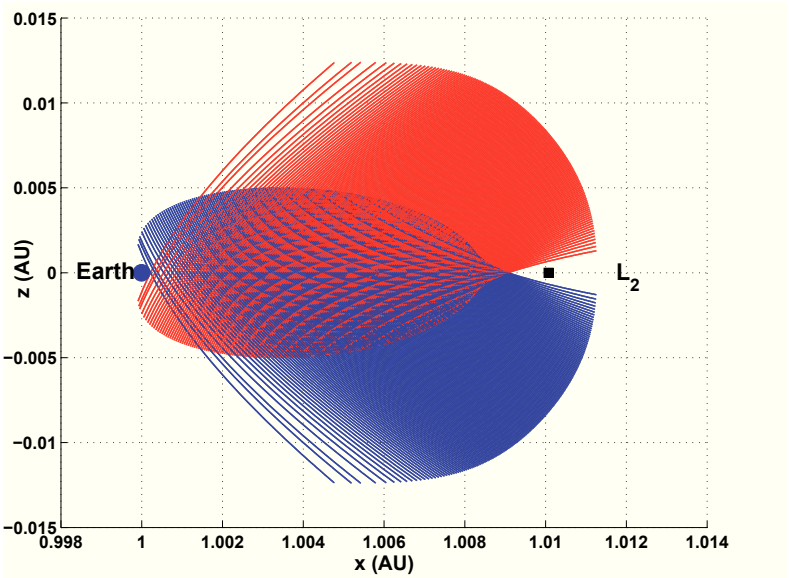

Figure 3.7: A family of halo orbits around L_2 point in the Sun-Earth system. The period of this family varies between 100.05 days till 182.17 days.

3.2 Stability Analysis

To reach useful information about the behaviour of the three-body problem, one can use the theory of dynamical system. However, despite lack of analytical solution, much qualitative information is typically available about local behaviour. For the three-body system, the local behaviour near a particular reference solution can be frequently determined from the linear approximation of the system. The reference solution can be any type of solution, namely an equilibrium point, a quasi-periodic or a periodic orbits. Note that using linear approximation restricts the analysis of the phase space to be only in the vicinity of the reference solution. To review briefly the local behaviour of the flow in the vicinity of a reference solution, suppose a general continuous nonlinear vector field such

as the three-body system as

$$\dot{x} = f(x). \tag{3.24}$$

The vector of states x is real and defined in a n-dimensional space, $x \in \mathbb{R}^n$. The reference solution $\bar{x}$ is supposed to be known. If $x = \bar{x} + y$ which y is the variations of the states, and ingnor the higher order terms, the linear differential equation governing y is

$$\dot{y} = A(t)y, \tag{3.25}$$

where $A(t)$ is an $n \times n$ matrix which generally can be time varying. However, for the special case when $\bar{x}$ is an equilibrium point, it is constant. The solution of (3.25) for the constant matrix A can be written as

$$y(t) = Pe^{\Lambda t}P^{-1}y(0), \tag{3.26}$$

where the matrix P transforms A to its Jordan normal form, and the matrix Λ is a block diagonal matrix which has the same eigenvalues as A. Without loss of generality, suppose that the eigenvalues of A are distinct real scalars λ_i for $i = 1, \ldots, n$. Thus,

$$y(t) = \sum_{i=1}^{n} c_i e^{\lambda_i t} v_i, \tag{3.27}$$

where v_i is the i-th eigenvector of A corresponding to the engenvector λ_i, and the scalars c_i are the integration constants which can be determined from the initial conditions. The solution of (3.25) in the form (3.27) makes it easy to address the concept of stability. To this end, suppose that $\lambda_1, \ldots, \lambda_s$ are s eigenvalues which their real parts are negative, $\lambda_{s+1}, \ldots, \lambda_{s+u}$ are u eigenvalues with positive real parts, and $\lambda_{s+u+1}, \ldots, \lambda_{s+u+c}$ are the pure imaginary eigenvalues. Then the stable, unstable and center subspaces of $\mathbb{R}^n$ are [78] defined as

$$\begin{aligned} E^s &= span\{v_1, \ldots, v_s\}, \\ E^u &= span\{v_{s+1}, \ldots, v_{s+u+1}\}, \\ E^c &= span\{v_{s+u+1}, \ldots, v_{s+u+c}\}. \end{aligned} \tag{3.28}$$

If the initial point lies on each of these stable, unstabl or center subspaces, then the solution will stay in the same subspace for all time. This demonstrates the concept of invariance. Indeed, the subspace $E \subseteq \mathbb{R}^n$ is invariant, if for any set of initial conditions in E the solution belongs to E for all time. The mentioned subspaces are related to the

invariant manifolds which is explained in the following theorem [37].

Theorem 3.2.1. *Suppose that $\bar{x}$ is a hyperbolic equilibrium point of the system (3.24). Then there exists local stable and unstabole manifolds $W^s_{loc}(\bar{x})$ and $W^u_{loc}(\bar{x})$ of the same dimensions as stable and unstable subspaces at $\bar{x}$. Furthermore, The stable and unstable manifolds are tangent to the stable and unstable subspaces, respectively.*

The manifolds are also invariant. The manifolds referred in this dissertation are global manifolds which can be obtain by numerical integration through the vector field over a larger time interval. Figure 3.8 shows the first equilibrium point of the three-body system and its stable and unstable subspaces and manifolds. Indeed, the manifols shown in this figure as W^s and W^u are global manifolds. Note that the manifolds are tangent to the subspaces and beyond the vicinity of equilibrium point, they branch out into subspaces and manifolds. The instability of the collinear libration points of the three-body problem

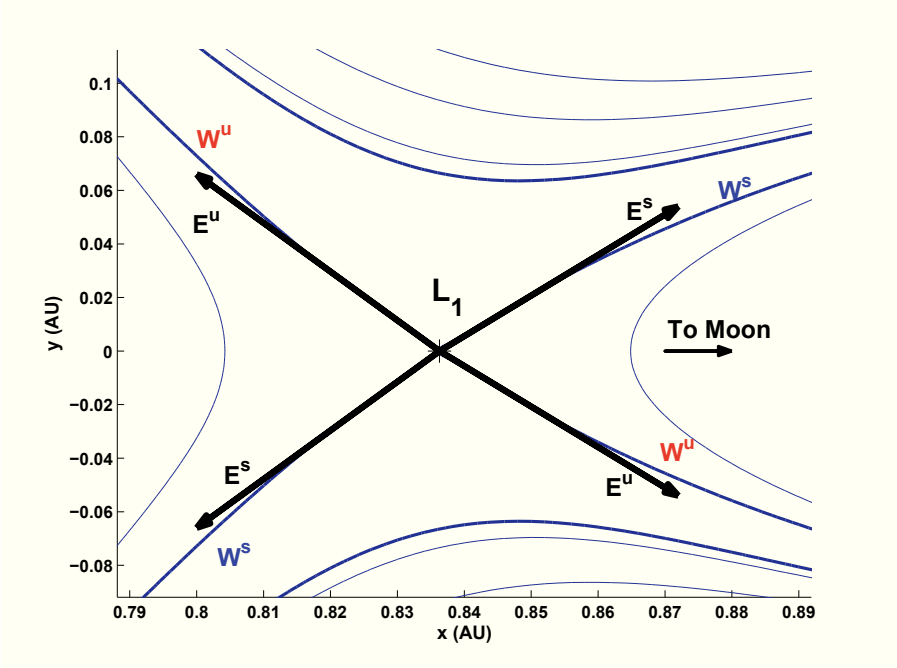

Figure 3.8: The stable and unstable subspaces and manifolds corresponding to the equilibrium point L_1 in the Earth-Moon three-body system

is a strong motivation to look for another types of solutions which are stable. Among the solutions of the three-body problem, periodic orbits are frequently used as a reference solution for investigating the nonlinear system. Consideration of a periodic orbit as a reference solution for the linearization makes the matrix A in (3.25) to be time-varying.

To use the priodicity of a periodic orbit in stability analysis, most of the works use the monodromy matrix. The monodromy matrix is the same state transition matrix associated with the periodic orbit after one period of the motion.The eigenvalues of the monodromy matrix can be used to estimate the local geometry in the vicinity of the periodic orbit. Due to the Floquet theory [95], the state transition matrix $\Phi(t, t_0)$ can be rewritten as

$$\Phi(t, t_0) = F(t)e^{Jt}F^{-1}(t_0), \tag{3.29}$$

where J is a block diagonal matrix which its diagonal elements are the Floquet multipliers. Since $F(t)$ is a periodic matrix, i.e. $F(T) = F(t_0)$, therefore

$$\Phi(T, t_0) = F(t_0)e^{JT}F^{-1}(t_0), \tag{3.30}$$

thus

$$e^{JT} = F^{-1}(t_0)\Phi(T, t_0)F(t_0), \tag{3.31}$$

where T is the period of the orbit. The eigenvectors of the monodromy matrix are equal for all the fixed points on the periodic orbit, but the associated eigenvectors vary in direction at each fixed point [95]. From (3.31), we have

$$\lambda_i = e^{\varpi_i T}, \tag{3.32}$$

$$\varpi_i = \frac{1}{T}\ln(\lambda_i), \tag{3.33}$$

where ϖ_i are the Poincaré exponents. Due to the Poincaré exponents' stability properties, we have

- $|\lambda_i| < 1$ results in stability.
- $|\lambda_i| > 1$ results in instability.
- $|\lambda_i| = 1$ gives no information about the stability.

In [96], it is explained that the monodromy matrix derived from a periodic orbit has at least one eigenvalue with a modulus of one. On the other hand, based on the next theorem, one can imply existance of two eigenvalues with modulus of one.

Theorem 3.2.2. *If λ is an eigenvalue of the monodromy matrix of a time invariant system, then λ^{-1} is also an eigenvalue.*

Since the monodromy matrix of a periodic orbit as a reference solution of the three-body problem is a 6×6 matrix, and according to the Theorem 3.2.2, the eigenvalues are related in the following way [17]

$$\lambda_1 = \frac{1}{\lambda_2},\ \lambda_3 = \frac{1}{\lambda_4},\ \lambda_5 = \lambda_6. \tag{3.34}$$

Therefore, there are exactly two eigenvalues with modulus less than one. Furthermore, there are also exatly two eigenvalues with modulus greater than one, and two eigenvalues with modulus one. Bray and Goudas in [15] presented a fast and simple way to compute the eigenvalues of the monodromy matrix for a periodic orbit in the three-body problem. Parker also summerized this way as following. Suppose

$$\alpha = 2 - \text{trace}(\Phi(T, 0)), \tag{3.35}$$

$$\beta = \frac{\alpha^2 - \text{trace}(\Phi^2(T, 0))}{2} + 1, \tag{3.36}$$

$$p = \frac{\alpha + \sqrt{\alpha^2 - 4\beta + 8}}{2}, \tag{3.37}$$

$$q = \frac{\alpha - \sqrt{\alpha^2 - 4\beta + 8}}{2}, \tag{3.38}$$

then, we have

$$\lambda_1 = \frac{1}{\lambda_2} = \frac{-p + \sqrt{p^2 - 4}}{2}, \tag{3.39}$$

$$\lambda_3 = \frac{1}{\lambda_4} = \frac{-q + \sqrt{q^2 - 4}}{2}, \tag{3.40}$$

$$\lambda_5 = \lambda_6 = 1. \tag{3.41}$$

These eigenvalues can be used to calculate the corresponding eigenvectors. In the next section, the stable and unstable eigenvalues will be used to construct numerically the invariant stable and unstable manifolds.

3.3 Computing Invariant Manifolds

The eigenvectors of the monodromy matrix prepare local approximation of the stable and unstable subspaces. While studying the eigenvectors of a periodic orbit, it is critical to note that the eigenvectors only possess a good approximation of the direction of the corresponding subspaces very close to the periodic orbit. Therefore, to investigate a more global approximation, it is crucial to consider the globalized manifolds for completing the

periodic orbit's picture of the stablity and instabilty. To this end, suppose that the stable and unstable eigenvectors of the monodromy matrix are v^s and v^u, respectively. Then one selects a fixed point x_i on the periodic orbit corresponding to the time t_i. Suppose that the corresponding stable and unstable vectors at the point x_i are v_i^s and v_i^u, respectively, which are indeed

$$v_i^s = \Phi(t_i, t_0)v^s, \tag{3.42}$$

$$v_i^u = \Phi(t_i, t_0)v^u. \tag{3.43}$$

To compute the stable manifold, the considered fixed point on the halo orbit should be perturbed by a small perturbation ϵ in the direction of the stable vector, i.e.

$$x_i^{W_s} = x_i + \epsilon \frac{v_i^s}{\|v_i^s\|}. \tag{3.44}$$

The corresponding state for unstable manifold as (3.44) is

$$x_i^{W_u} = x_i + \epsilon \frac{v_i^u}{\|v_i^u\|}. \tag{3.45}$$

Note that the normalization of the stable and unstable vectors is necessary, since the states resulted in Equation 3.45 grows exponentially. To compute the global manifold, the perturbed states should be integrated along the system. In both Equations 3.44 and 3.45, there is an initial displacement from the periodic orbit denoted by ϵ. The small perturbation cuases a better approximation of the manifold, but it tends to diverge from the orbit much slower than a larger perturbation. On the other hand, this perturbation cannot be chosen arbitrarily large, since the linear approximation must remain whitin a valid range. In the Sun-Earth system, ϵ is usually varies between 100 and 200 kilometers. But in this dissertation, whole manifolds are computed with $\epsilon = 7.0E-8$ which is almost 10 kilometers. If more than one fixed point x_i be considered on the halo orbit, then the manifolds form a tube made of trajectories corresponding to each point along the halo orbit. Figure 3.9 shows the instant points on a halo orbit which are indeed twenty points considered equidistantly along the halo orbit. The trajectories of stable manifolds corresponding to each of these points shape a tube which can be seen in three-dimensional. Furtheremore, two-dimensional views of the stable tube projected on x-y and x-z planes are also shown in this figure. To see the rest of the stable manifold shown in Figure 3.9, Figure 3.10 shows the enterior and exterior part of the stable manifold associated to the same halo orbit around L_2 of the Sun-Earth system in three different views. Due to the concept of assymptotic stability of the stable manifolds, a spacecraft following one of

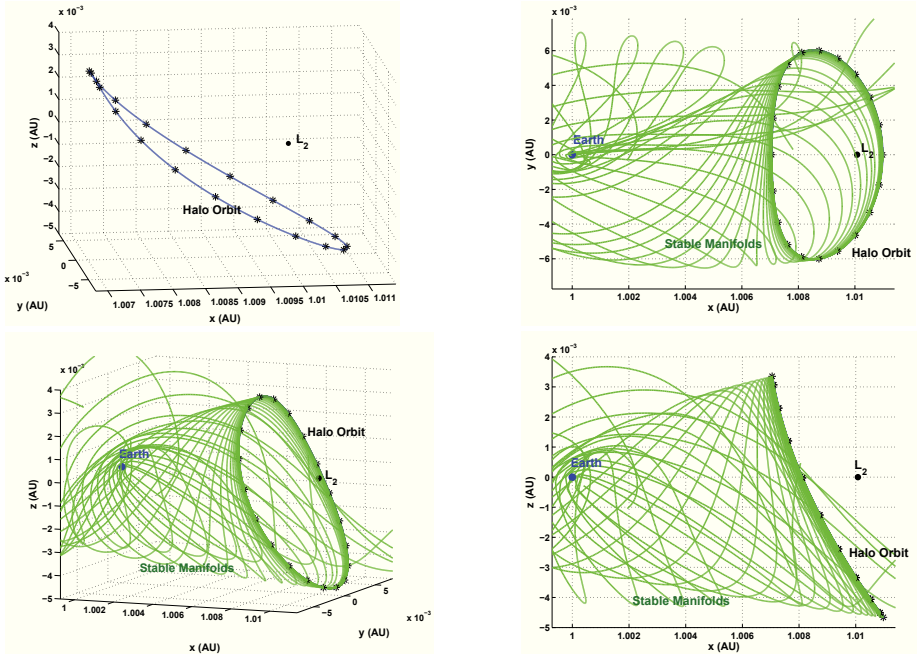

Figure 3.9: Different plots of stable manifolds associated with a halo orbit around L_2 in the Sun-Earth system. This tube of stable manifolds is constructed using 20 fixed points which are shown along the halo orbit (up left).

stable trajectories will asymptotically reach the halo orbit. That means the spacecraft's arrival at the halo orbit will happen in infinity. This fact does not make any problem for mission design, since it can be solved by an extra *Halo-Insert Maneuver* (HIM). To see the behaviour of the stable trajectories approaching the halo orbit, the propagated stable manifolds in different times are sketched in Figure 3.11. The time intervals for propagation of the stable manifolds are 179.23, 217.07, 250.92, 286.76, 322.61, 358.45, 393.77 and 429.57 days. In this figure, one can see that the particle spends a long period of time orbiting quite close to the halo orbit before departing from it. In the second figure, after 217.07 days, the spacecraft is still orbiting the halo orbit. In the last figures embedded in Figure 3.11, the stable manifolds pass the way toward the Earth and cross the vicinity of the Earth. The minimum distance of these close approaches of each trajectory to the Earth are calculated and Figures 3.12 and 3.13 summerize the results. In these figures, six halo orbits of a family around the L_2 libration point in the Sun-Earth system are considered on which fifty instant points as initial conditions to construct the stable trajectories. Each color is relevent to the information of a specific halo orbit. The minimum distance of the first perigee of stable manifolds among these six halo orbits is 2167.26 km from the Earth's surface. This minimum approach takes place in the first perigee (197.38 days) of

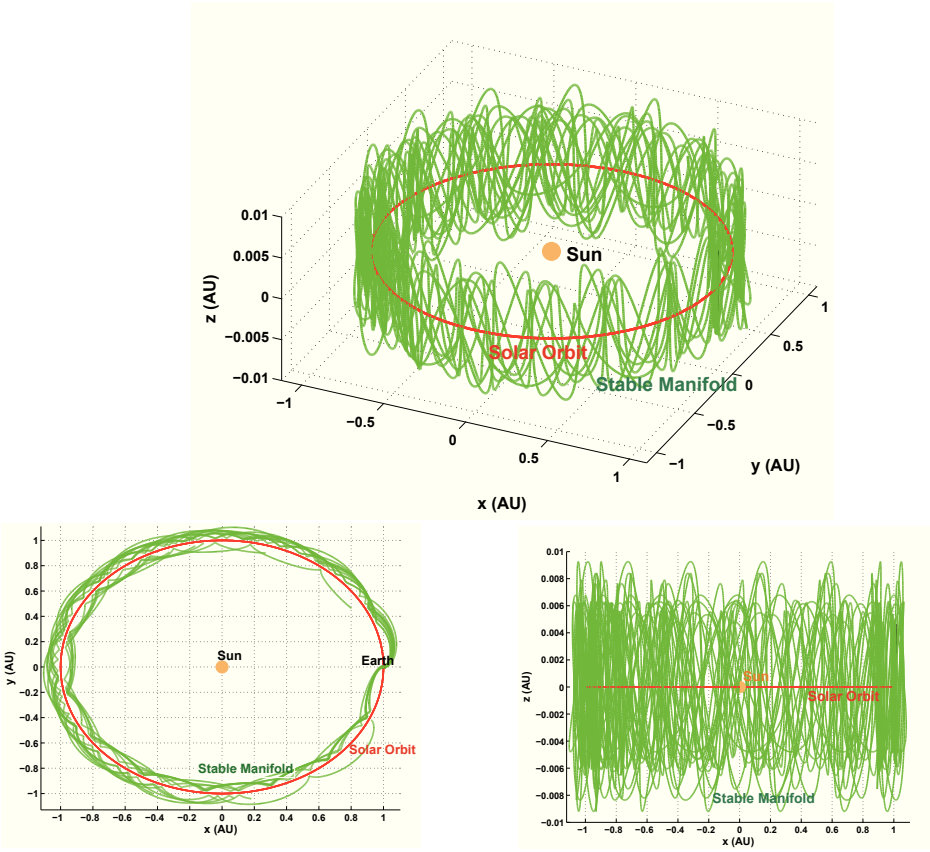

Figure 3.10: Different plots of a set of interior and exterior stable manifolds associated with a halo orbit around L_2 in the Sun-Earth system.

the stable trajectory departing from the fifth instant point on the halo orbit with Jacobi constant 3.0007 and 179 days period.

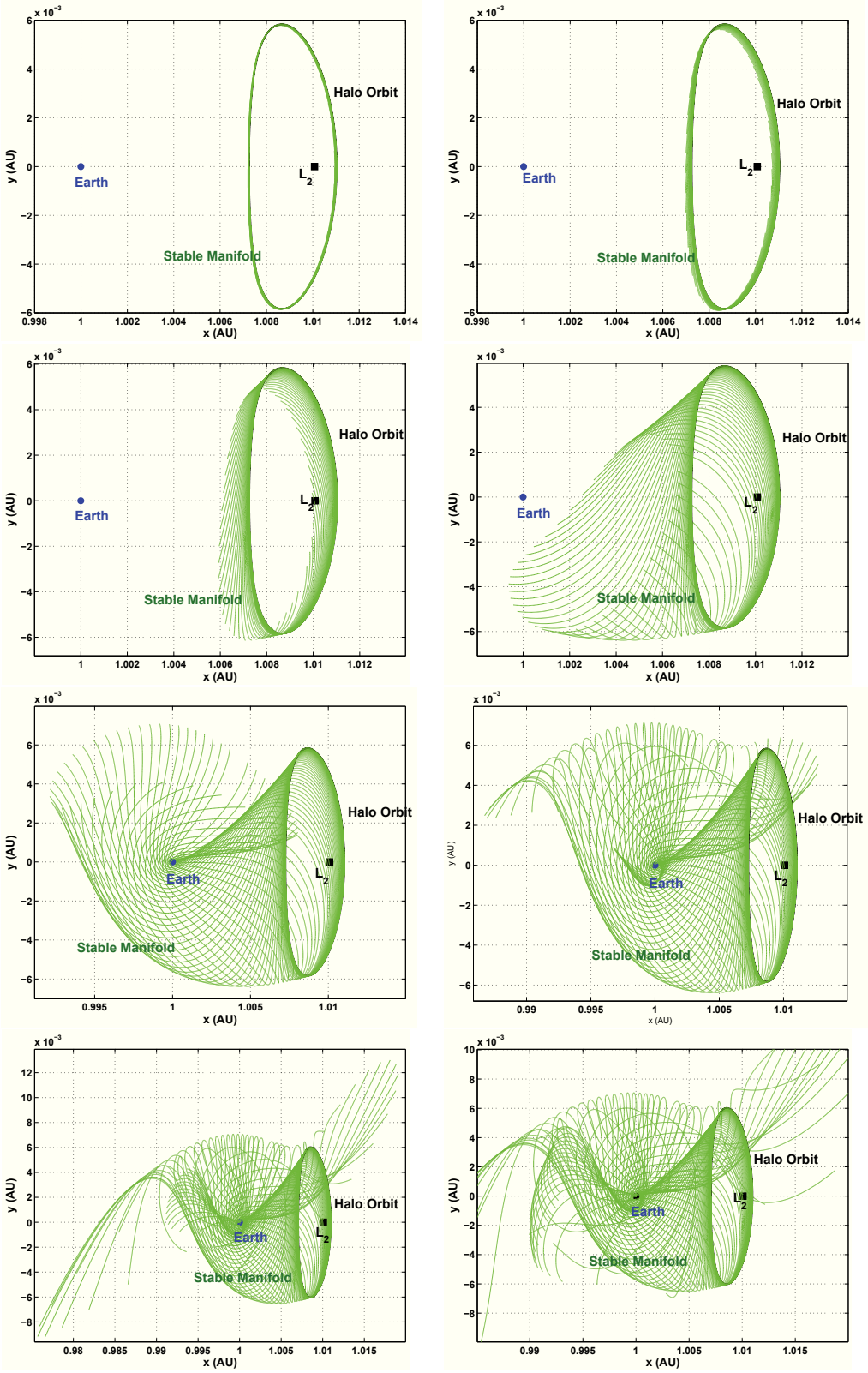

Figure 3.11: The propagation of the stable manifold associated to a halo orbit around L_2 in the Sun-Earth system. The time durations of propagation are $t = 179.23$, 217.07, 250.92, 286.76, 322.61, 358.45, 393.77, and 429.57 days.

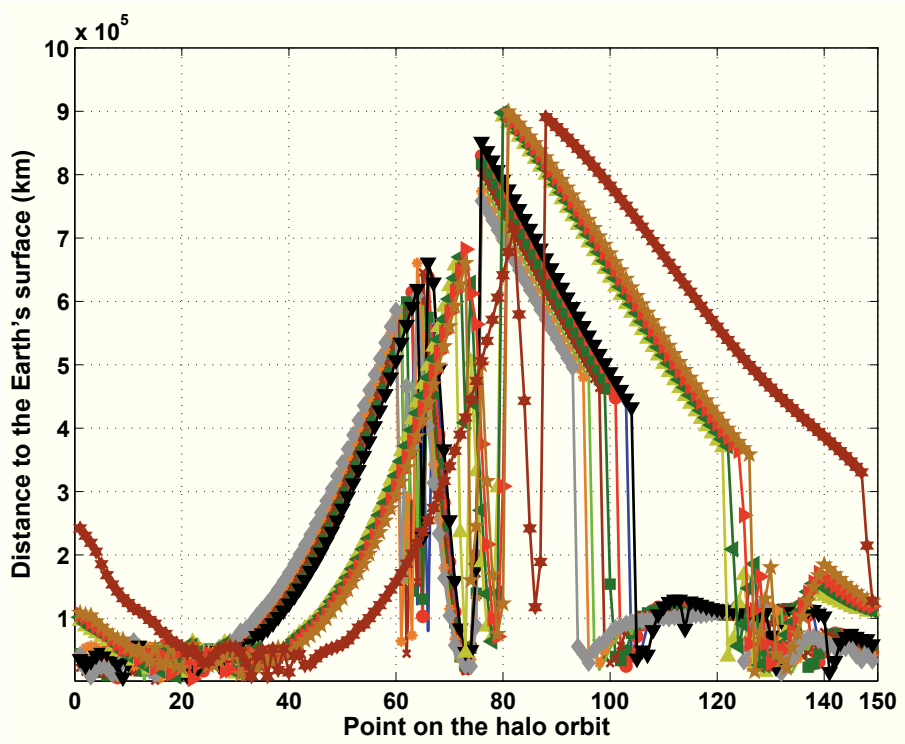

Figure 3.12: Distance analysis of 50 trajectories making stable manifold tubes for thirteen halo orbits around L_2 in the Sun-Earth system. The y-axis is scaled linearly.

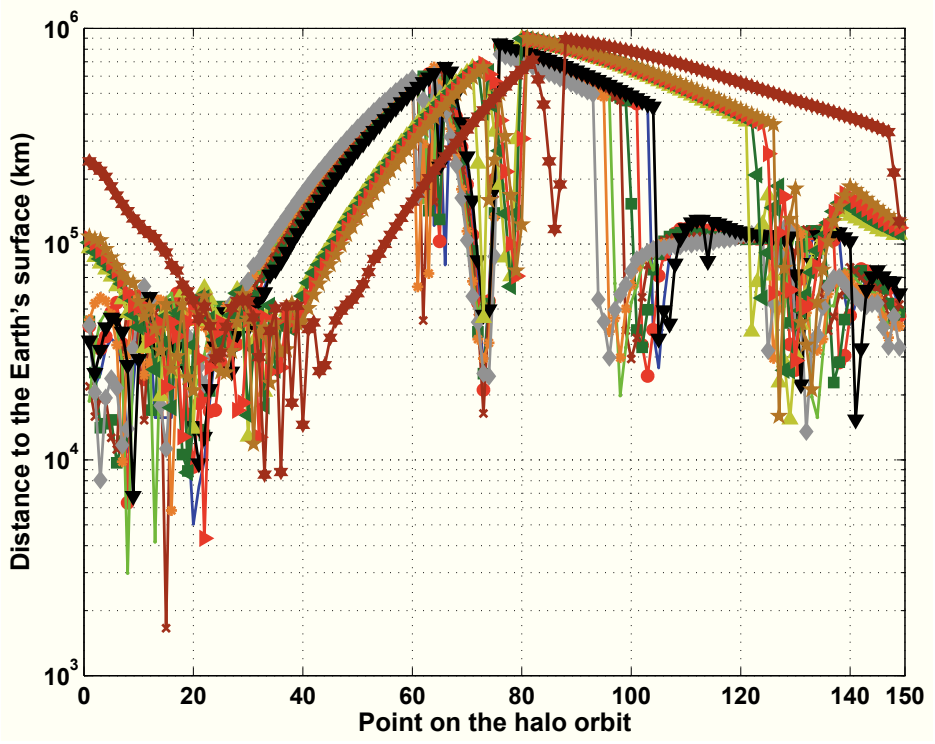

Figure 3.13: Distance analysis of 50 trajectories making stable manifold tube for thirteen halo orbits around L_2 in the Sun-Earth system. The y-axis is scaled logarithmically.

Chapter 4

Optimization

As mentioned before, the approach of this dissertation uses the optimization theory to model and solve the transfer problem. Therefore, the concept of optimization is important in understanding the method used here, and shall be explained in more details. An optimization problem generally deals with a set of independent variables or parameters which can vary to achieve the optimal value of an objective function. These parameters may be restricted by some conditions which are called *constraints*. Optimization problems can be categorized into two different categories; *Static Optimization* and *Optimal Control*. Static optimization problems are an optimization problem which time is not a parameter in it. Lack of continuous parameters in this kind of optimization problems is the reason that it is also called *Discrete Optimization*. On the other hand, the optimal control deals with the optimization problems which usually have time as independent variable and elements vary continuously with respect to the time. Hence, it is sometimes referred as *Continuous Optimization*.

4.1 Static Optimization

The aim is to find a set of parameters, $x \in \mathbb{R}^n$, which optimizes (minimize or maximize) a performance index which is a functional $J(x) : \mathbb{R}^n \to \mathbb{R}$. Without loss of generality, the optimization problems in this dissertation are all considered as minimization problem. It is clear that a maximization problem can be easily converted to a minimization problem with considering the $-J(x)$ as the objective function. The optimization can be subject to a set of equality or inequality constraints. If there is no such constraints on x, the optimization problem is called *Unconstrained Optimization*. This problem is the simplest

optimization problem which is

$$\text{Minimize } J(x), \tag{4.1}$$

for all $x \in \mathbb{R}^n$. In this problem, a local minimum x^* occurs when an arbitrary violation of x makes an increase in the objective function, i.e.

$$\exists N_{x^*} \subseteq \mathbb{R}^n \ \forall x \in N_{x^*},\ J(x^*) \leqslant J(x), \tag{4.2}$$

where N_{x^*} is an open neighbourhood of x^*. If the objective function $J(x) \in C^2$, and a local minimum x^* exists, two following conditions must be satisfied. These conditions are usually referred as *Necessary Conditions for Optimality* for an unconstrained problem.

1. $\|\nabla_x J(x^*)\| = 0$,
2. $\nabla^2_{xx} J(x^*)$ is positive semi-definite.

In practice, the values of optimization variables cannot vary freely and it is often necessary to impose some constraints. The most general form of a constrained optimization problem contains of nonlinear equality and inequality constraints as

$$\begin{aligned} &\text{Minimize } J(x) \\ &\text{s.t.} \begin{cases} c_i(x) = 0, & i = 1, \ldots, n_e, \\ c_j(x) \leqslant 0, & j = n_e + 1, \ldots, n_e + n_i, \end{cases} \end{aligned} \tag{4.3}$$

where $J : \mathbb{R}^n \to \mathbb{R}$ and $c_i, c_j : \mathbb{R}^n \to \mathbb{R}$ for $i = 1, \ldots, n_e$ and $j = n_e + 1, \ldots, n_e + n_i$ are also assumed to be of class C^2 on $\mathbb{R}^n$. Furthermore, n_e and n_i are the numbers of equality and inequality constraints, respectively. The constrained static optimization problem 4.3 is usually called *Nonlinear Programming* or shortly *NLP*. The first thing comes after the concept of constraints is the definition of a set consists of whole points which satisfy these constraints. This is the *set of admissible points*, *feasible set* or *admissible set*, that is

$$S = \{x \in \mathbb{R}^n | c_i(x) = 0,\ i = 1, \ldots, n_e, \text{ and } c_j(x) \leqslant 0,\ j = 1, \ldots, n_i\}. \tag{4.4}$$

Similar to the unconstrained case, a feasible point, i.e. $x^* \in S$ is a local minimum of the NLP 4.3 when

$$\exists N_{x^*} \subseteq \mathbb{R}^n \ \forall x \in N_{x^*} \cap S,\ J(x^*) \leqslant J(x). \tag{4.5}$$

In the optimization theory, a local minimum is also called an *optimal solution*. To characterize the admissible points in the neighbourhood of the possible solution, we shall

distinguish between the constraints which hold exactly and those that do not. At the admissible point $x \in S$, the constraint $c_j(x) \leqslant 0$ for $j = n_e + 1, \ldots, n_e + n_i$ is known as an *active* constraint, if $c_j(x) = 0$. And it is said to be *inactive*, if $c_j(\bar{x}) < 0$. The set of indices of active constraints of problem 4.3 at point x is denoted by $I(x)$ and defined as

$$I^a(x) = \{1, \ldots, n_e\} \cup \{i \in \{n_e + 1, \ldots, n_e + n_i\} | c_i(x) = 0\}. \tag{4.6}$$

Note that in the case $c_j(x) < 0$ for $j = n_e + 1, \ldots, n_e + n_i$, this constraint is *satisfied* at x. Only the active constraints restrict admissible perturbations at x, since an inactive constraint will remain strictly satisfied within a sufficiently small neighbourhood of x. The concepts of active and inactive constraints are basic in derivation of optimality necessary conditions. To do so, suppose that C is the vector of all constraints in the problem 4.3, that is $C = (c_1, \ldots, c_{n_e}, c_{n_e+1}, \ldots, c_{n_e+n_i})^T$, and $C^a(x) = (c_i)_{i \in I^a(x)}$ is the vector of active constraints at x. The Lagrangian function $\mathcal{L} : \mathbb{R}^n \times \mathbb{R}^{n_e+n_i} \to \mathbb{R}$ for this problem is introduced as

$$\mathcal{L}(x, \eta) = J(x) + \eta^T C, \tag{4.7}$$

where the vector $\eta = (\eta_1, \ldots, \eta_{n_e+n_i})^T \in \mathbb{R}^{n_e+n_i}$ is the *Lagrange multiplier* vector.

The first order necessary optimality conditions for a prescribed optimal solution x^* of the problem 4.3 can be achieved by several approaches, see [29] and [30]. In this dissertation, this theorem is described using the Lagrangian function as below.

Theorem 4.1.1. *Let x^* be an optimal solution of an NLP, and assume $\nabla_x C^a(x^*)$ (the Jacobian of the active constraints) is full ranked. Then there is a unique multiplier $\eta \in \mathbb{R}^{n_e+n_i}$ which the followings hold.*

$$\frac{\partial \mathcal{L}}{\partial x}(x^*, \eta) = \frac{\partial J}{\partial x}(x^*) + \eta^T \nabla_x C(x^*) = 0, \tag{4.8}$$

$$\eta_i \geqslant 0, \ \forall i \in I^a(x^*), \tag{4.9}$$

$$\eta_i = 0, \ \forall i \notin I^a(x^*). \tag{4.10}$$

This theorem is famous in studying the nonlinear optimization theory and is so called *Karush-Kuhn-Tucker* or *KKT* which is originally named after William Karush, Harold W. Kuhn, and Albert W. Tucker who first published the conditions in this theorem, see [60], [56] and [57]. Note that the second condition, namely 4.9, provides a useful mechanism to identify the active constraints. Precisely, if any Lagrange multiplier is negative, the corresponding constraint is not active and should be deleted from the active set. As mentioned, the KKT conditions are necessary for a solution of an NLP to be optimal,

provided the mentioned regularity conditions are satisfied. In some cases such as convex problems, the necessary conditions are also sufficient for optimality, but in general the necessary conditions are not sufficient. It was shown that the larger class of functions in which KKT conditions guarantees global optimality are the so called invex functions[1] [69]. So if equality constraints are affine functions, inequality constraints and the objective function are continuously differentiable invex functions, then the KKT conditions are sufficient for global optimality [69]. There are simple examples which KKT conditions are all satisfied, but the point x^* is neither a minimum nor maximum. These kind of points are known as *saddle points*. To figure out that x^* is an optimal solution, additional information so called *Second Order Sufficient Conditions* (SSC) is necessary. These conditions guarantee that the point x^* which satisfies the KKT conditions is actually an optimal solution of the NLP 4.3. In following, these conditions are given as a theorem.

Theorem 4.1.2. *Suppose that J, c_i for $i = 1, \dots, n_e + n_i$ in NLP 4.3 are of C^2-class, η^a are the Lagrange multipliers corresponding to the active constraints, and also assume x^* is admissible point in this problem which satisfies the KKT-conditions. Let*
1) $\nabla_x C^a(x^*)$ is full rank,
2) $\eta^a > 0$,
3) $v^T \nabla^2_{xx} \mathcal{L}(x^*, \eta^*) v > 0$, $\forall v \in \ker(\nabla_x C^a(x^*))$, $v \neq 0$,
then there exists a constant α and $\epsilon > 0$ which

$$J(x) \geqslant J(x^*) + \alpha \|x - x^*\|^2, \ \forall x \in S, \ \|x - x^*\|^2 \leqslant \epsilon, \tag{4.12}$$

that means x^* is a local minimum of the NLP problem 4.3.

Note that the third condition in this theorem expresses that the Hessian of the Lagrangian is positive definite on $ker(\nabla_x C^a(x^*))$. This makes it difficult to check the conditions in the theorem. On the other hand, NLP problem 4.3 is considerably more complicated than to be analytically solvable. Therefore, there must be numerical methods to solve the NLP and check the necessary and sufficient conditions. There are lots of numerical methods to solve an NLP. Among these wide range of methods, the *Sequential Quadratic Programming* or *SQP* is one of the most widely used NLP algorithms. This methods is actually one of the most successful methods used for solving the NLP in general

[1] An invex function is a differentiable function $f : \mathbb{R}^n \to \mathbb{R}$ for which there exists a vector valued function g such that

$$\forall x, y \in \mathbb{R}^n \ f(x) - f(y) \geqslant g(x, y) \nabla f(y). \tag{4.11}$$

Invex functions were introduced by Hanson [39] as a generalization of convex functions. Hanson also showed that if the objective and the constraints of an optimization problem are invex with respect to exactly one function, then the Karush-Kuhn-Tucker conditions are sufficient for a global minimum, see [39].

form. It relies on a profound theoretical foundation and provides powerful algorithmic tools for the solution of medium- and large-scale technical relevant problems.

4.1.1 Sequential Quadratic Programming

Lets consider the NLP problem as 4.3. The SQP is an iterative procedure which models the NLP for a given $x^{(k)}$ $k = 1, 2, \ldots$ by a *quadratic programming* (QP) subproblem. Then SQP solves this QP subproblem and uses the subproblem's solution to construct the new iteration which is $x^{(k+1)}$. The sequence of $(x^{(k)})_{k=1}^{\infty}$ made by this process is supposed to converge to an optimal solution of the NLP. The main aspect in each iteration is the construction of the quadratic subproblem which should reflect the local properties of the NLP with respect to the current iteration. Considering the notations used in explanation of the NLP 4.3, the objective function of the quadratic subproblem is a local approximation of the original objective function $J(x)$ as

$$J(x) \approx J(x^{(k)}) + \nabla_x J(x^{(k)})(x - x^{(k)}) + \frac{1}{2}(x - x^{(k)})^T \nabla^2_{xx} J(x^{(k)})(x - x^{(k)}). \tag{4.13}$$

The equality constraints $c_i(x)$, $i = 1, \ldots, n_e$, and the inequality constraints $c_j(x)$, $j = n_e + 1, \ldots, n_i$ in the problem 4.3 are also approximated by their affine approximations as

$$c_i(x) \approx c_i(x^{(k)}) + \nabla_x c_i(x^{(k)})(x - x^{(k)}), \quad i = 1, \ldots, n_e, \tag{4.14}$$

$$c_j(x) \approx c_j(x^{(k)}) + \nabla_x c_j(x^{(k)})(x - x^{(k)}), \quad j = n_e + 1, \ldots, n_i. \tag{4.15}$$

This approximations lead to the new QP subproblem in the k-th iteration as following

$$\begin{aligned} &\text{Minimize } \nabla_x J(x^{(k)})^T (x - x^{(k)}) + \frac{1}{2}(x - x^{(k)})^T \nabla^2_{xx} J(x^{(k)})(x - x^{(k)}) \\ &\text{s.t. } \begin{cases} c_i(x^{(k)}) + \nabla_x c_i(x^{(k)})(x - x^{(k)}) = 0, & i = 1, \ldots, n_e, \\ c_j(x^{(k)}) + \nabla_x c_j(x^{(k)})(x - x^{(k)}) \leqslant 0, & j = n_e + 1, \ldots, n_i. \end{cases} \end{aligned} \tag{4.16}$$

4.1.2 Sensitivity Analysis of the Parametric NLP

Lets consider *parametric nonlinear programming* problems involving a parameter $p \in P \subseteq \mathbb{R}^{n_p}$. A general parametric NLP problem denoted by NLP(p) with equality and inequality constraints can be considered similar to NLP problem 4.3 as

$$\begin{aligned} &\text{Minimize } J(x, p) \\ &\text{s.t. } \begin{cases} c_i(x, p) = 0, & i = 1, \ldots, n_e, \\ c_j(x, p) \leqslant 0, & j = n_e + 1, \ldots, n_e + n_i, \end{cases} \end{aligned} \tag{4.17}$$

where $J : \mathbb{R}^n \times P \to \mathbb{R}$ and $c_i, c_j : \mathbb{R}^n \times P \to \mathbb{R}$ for $i = 1, \ldots, n_e$ and $j = n_e+11, \ldots, n_e+n_i$ are also assumed to be of class C^2 on $\mathbb{R}^n \times P$. Note that the NLP problem 4.3 is a special case of parametric NLP problem 4.17 with a fixed parameter such as $p_0 \in P$.

Suppose that the nonlinear programming problem (NLP(p_0)) is already solved and we have the optimal solution corresponding to the p_0 in hand. For this fixed reference or *nominal* parameter p_0, the problem NLP(p_0) is called the *unperturbed* or *nominal* problem. Now, we are interested to study the differential properties of the optimal solutions of a perturbed problem NLP(p) with respect to parameters p in a neighbourhood of the nominal parameter p_0. The next theorem mostly presented as the second order sufficient conditions 4.1.2 guarantees differentiability of the optimal solutions with respect to parameters p, and gives a set of explicit formulae for the parameter derivatives, so called *sensitivity differentials*, see [29] and [28].

Theorem 4.1.3. *Let (x_0, η_0) be an admissible point which satisfies the SCC 4.1.2 for the nominal problem NLP(p_0). Then there exists a neighborhood $P_0 \subseteq P$ of p_0 and continuously differentiable functions $x : P_0 \to \mathbb{R}^n$ and $\eta : P_0 \to \mathbb{R}^{n_e+n_i}$ with the following properties:*
1) $x(p_0) = x_0$, $\eta(p_0) = \eta_0$,
2) the active sets are constant in P_0, i.e. $\forall p \in P_0$ $J(x(p), p) \equiv J(x_o, p_0)$,
3) $\nabla_x C^a(x, p)$ is full rank for all $p \in P_0$,
4) for all $p \in P_0$, $(x(p), \eta(p))$ satisfies the SSC 4.1.2 for the perturbed problem NLP(p).
Furthermore, in the P neighborhood of p_0

$$\begin{pmatrix} \nabla^2_{xx}\mathcal{L}(x_0, \eta_0, p_0) & \nabla_z C^a(x_0, p_0)^T \\ \nabla_z C^a(x_0, p_0) & 0 \end{pmatrix} \begin{pmatrix} \frac{dx}{dp}(p_0) \\ \frac{d\eta}{dp}(p_0) \end{pmatrix} = - \begin{pmatrix} \nabla^2_{xp}\mathcal{L}(x_0, \eta_0, p_0) \\ \nabla^2_p C^a(x_0, p_0) \end{pmatrix}, \quad (4.18)$$

where $\nabla^2_{xx}\mathcal{L}$ denotes the Hessian of the Lagrangian.

Since the coefficient matrix of $\left(\frac{dx}{dp}(p_0), \frac{d\eta}{dp}(p_0)\right)^T$ in 4.18 is non-singular on the assumption of Theorem 4.1.3, $\frac{dx}{dp}(p_0)$ and $\frac{d\eta}{dp}(p_0)$ can be calculated explicitly by solving the linear equation system 4.18. For more discussion, see [28], [19] and [20].

4.2 Optimal Control (Continuous Optimization)

Optimal control deals with the problem of seeking a control signal for a given system such that a certain optimality criterion is achieved. This problem includes a cost functional which is a function of state, control variables even their values at initial and/or final conditions. Indeed, the optimal control problem tries to control a set of differential

equations describing the paths of the controls that in such a way that they minimize the cost functional. A general form of an optimal control problem goes as follows. Minimize the continuous-time cost functional

$$J(x,u) = \Phi(x(t_0), u(t_f), t_0, t_f)) + \int_{t_0}^{t_f} f_0(x(t), u(t), t)dt, \tag{4.19}$$

subject to the first-order ordinary differential equation constraints

$$\dot{x}(t) = f(x(t), u(t), t) \;\; \forall t \in [t_0, t_f], \tag{4.20}$$

and probably algebraic path constraints

$$b(x(t), u(t), t) \leqslant 0 \;\; \forall t \in [t_0, t_f], \tag{4.21}$$

with the boundary (initial and final) conditions

$$\phi(x(t_0), x(t_f), t_0, t_f) = 0, \tag{4.22}$$

where $x(t) \in \mathbb{R}^n$ denotes the state of the system, $u(t) \in \mathbb{R}^m$ is the control, t is the independent variable (mostly, time) in the time interval $[t_0, t_f]$, t_0 is the initial time and t_f is the final time. The function Φ appearing in the objective function J is so called the *endpoint cost*. Note that the second constraint is in general inequality and thus may not be active. That means it might be nonzero at the optimal solution. It is also noted that the optimal control problem as stated above may have multiple solutions (i.e., the solution may not be unique). Thus, it is most often the case that any solution to the optimal control problem is locally minimizing. Furthermore, the functions Φ, f_0, f, b and ϕ are assumed to be sufficiently smooth on appropriate open sets. A point $(x(t_i), u(t_i))$ for a $t_i \in [t_0, t_f]$ is called feasible when it satisfies whole constraints. A piecewise continuous control $u(t)$ defined on the interval $[t_0, t_f]$ is said to be admissible. The final time t_f is either fixed or free. An optimal control problem with a free final time t_f can be reduced to an augmented control problem with a fixed final time by the time transformation $t = s.t_f$ introducing the new time variable $s \in [0, 1]$. If the system dynamic equations contains t, the system and their control is called *non-autonomous*, and it can be reformulated as an *autonomous* problem (t does not appear in the system) by considering the time variable t as an additional state.

An optimal control problem can be categorized in different classifications which their treatments are also different. This categorization is founded on different kind of optimal control problem's elements. Difference in form of objective function is not critical, since

objective functions of *Mayer*, *Lagrange* and *Bolza* forms are equivalent, because one can achieve each one of them from another by introducing an additional state variables. The most important categorization is based on the linearity/nonlinearity of the objective and constraint functions. Between these classes of optimal control problems, the specific type which we concern with during this dissertation is quadratic optimal control problem.

To solve an optimal control problem, there are two different approaches. In the classical development, it is well-known that the variational method of optimal control theory, which typically consists of the calculus of variations and Pontryagin's methods [82], can be used to derive a set of necessary conditions that must be satisfied by an optimal control law and its associated state-control equations. These necessary conditions of optimality lead to a (generally nonlinear) two-point boundary-value problem that must be solved to determine the explicit expression for the optimal control. Except in some special cases, the solution of this two-point boundary-value problem is difficult, and in some cases not practical to obtain. This approach is known as the *indirect method*. Various alternative computational techniques for optimal control problems have been developed. The most general approach is the *direct method*. In this method the variables are discretized so that the resulted problem after discretization becomes an NLP problem.

4.2.1 Direct Method for Solving Optimal Control Problem

As mentioned before, direct methods discretize the continuous optimal control problem and constructs an NLP. Generally this discretization can be divided into two classes. In the first class, the methods discretize both state and control variables and take them as the decision variables in the resulted discrete NLP problem. This class which is called *full-discretization* class leads to a high dimensional NLP. In the other class, only control variables are discretized and considered as the NLP decision variables. The state variables of the optimal control problems are calculated as functions of controls using appropriate numerical integration methods. The obtained NLP using the second class of discretization is small, but dense. One can mention to different pseudospectral methods such as Legendre-Gauss-Lobatto method and Tau method as instant methods in full-discretization class. Since, only the partial discretization frame is used in this dissertation, we explain this class in more details in the next section.

Partial discretization of optimal control problem

Optimal control problems are usually of high dimension. Therefore, to have a practical NLP problem after discretization, it is mandatory to keep the dimension of the NLP problem as small as possible. To this aim, let N_d be a positive integer representing the

meshsize (the number of discretization points). Without lose of generality, we choose equidistant mesh points τ_i, $i = 1, \ldots, N_d$, with

$$\tau_i = t_0 + (i-1)h, \ i = 1, \ldots, N_d, \ h = \frac{t_f - t_0}{N_d - 1}. \tag{4.23}$$

In the partial discretization class, We only discretize the control variables as optimization variables and adding the unknown initial state. Then we have

$$z = (x^1, u^1, \ldots, u^{N_d}) \in \mathbb{R}^{N_z}, \tag{4.24}$$

which z is the decision variable of the discretized problem and $N_z = n + mN_d$. The states of the system are computed using an appropriate integration rule such as Euler approximation as below.

$$\begin{aligned} x^1(z,p) &= x^1, \\ x^{i+1}(z,p) &= x^i(z,p) + hf(x^i(z,p), u^i, p), \ i = 1, \ldots, N_d - 1. \end{aligned} \tag{4.25}$$

All calculations described in this section were formed by the code NUDOCCCS of Büskens [19] and [20], which has implemented also various higher order approximations for state and control variables.

4.2.2 Real-Time Control Based on Sensitivity Analysis

We consider parametric optimal control problem subject to sets of state and control constraints. A general parametric optimal control problem denoted by OCP(p) involves a parameter $p \in P \subseteq \mathbb{R}^{n_p}$ can be considered similar to an OCP as

$$\begin{aligned} &\text{Minimize } J(x,u) = \Phi(x(t_0), u(t_f), t_0, t_f), p) + \int_{t_0}^{t_f} f_0(x(t), u(t), t, p)dt, \\ &\text{s.t.} \begin{cases} \dot{x}(t) = f(x(t), u(t), t, p) \ \ \forall t \in [t_0, t_f], \\ b(x(t), u(t), t, p) \leqslant 0 \ \ \forall t \in [t_0, t_f], \\ \phi(x(t_0), x(t_f), t_0, t_f, p) = 0. \end{cases} \end{aligned} \tag{4.26}$$

Note that the optimal control problem introduced in Section 4.2 is a special case of the more general form parametric OCP 4.26 with a fixed parameter such as $p_0 \in P$. Suppose that for this fixed reference or nominal parameter p_0, the parametric optimal control problem OCP(p_0) is partially discretized and solved. The sensitivity analysis of the NLP(p) resulted from discretization provides conditions and formulae such that one can estimate how sensitive the solutions are with respect to the parameters p. As

discussed before, the sensitivity analysis of an NLP(p) gives this sensitivity information for its solutions. Since in the method used in this dissertation, the continuous OCP(p) is transcribed into an NLP(p), therefore one can use the well developed theory and tools of NLP sensitivity analysis to OCP. Suppose that z is the decision variable of the NLP. Then the differentiability property allows us to construct an approximation of the perturbed solution by considering the following first order Taylor expansion

$$\begin{aligned} z(p) &= z(p_0 + \Delta p) \\ &\approx \tilde{z}(p) = z(p_0) + \frac{dz}{dp}(p_0)\Delta p, \end{aligned} \tag{4.27}$$

which uses the explicit sensitivity differentials. This expression gives an an approximation for the perturbed solution, if there is any deviation p from the nominal parameter p_0. Since the sensitivity differentials and $z(p_0)$ are computed *off-line*, thus this approximation can be quickly computed. The computation of the expression 4.27 only requires only matrix multiplications.

In first step, the sensitivity differential $\frac{dz}{dp}(p_0)$ given in 4.18 is evaluated. To deal with the linear approximation 4.27, one has to consider the changes of the active constraints. Although 4.27 results in acceptable real-time approximations for small Δp, it can cause larger deviations from the active constraints for larger Δp and leads to a non-admissible solution with constraint-deviation

$$\varepsilon_1 = C^a(\tilde{z}(p), p) \neq 0. \tag{4.28}$$

Introducing an auxiliary parameter $q \in \mathbb{R}^{N_a}$ for every active constraint in 4.17, one deals with the following problem

$$\begin{aligned} &\text{Minimize } J(z, p) \\ &\text{s.t. } C^a(z, p) - q = 0. \end{aligned} \tag{4.29}$$

Choosing the nominal value of q which is $q_0 = 0$, the problem 4.29 is equivalent to the problem 4.17. Actually, the parameters can be considered as $(p, q) \in \mathbb{R}^{N_p+N_a}$. Since one of the problems 4.17 or 4.29 satisfies the conditions of Theorem 4.1.3 if the other one does, therefore one can compute the sensitivity differentials $\frac{dz}{dq}(q_0)$ and $\frac{d\eta}{dq}(q_0)$ in the same way as 4.18. By using the new sensitivity differentials, we hope that a better approximation of the form of 4.27 can be found to improve the optimality and admissibility of the real-time

approximation. Considering 4.27 and 4.28, this approximation is given by

$$\begin{aligned} z(p) \approx \tilde{z}_2(p) &= \tilde{z}(p) + \frac{dz}{dq}(q_0)\varepsilon_1 \\ &= \tilde{z}(p) + \frac{dz}{dq}(0)C^a(\tilde{z}(p), p), \end{aligned} \tag{4.30}$$

Let $\tilde{z}_1(p)$ denotes the same $\tilde{z}(p)$, then the improving steps 4.28 and 4.30 can be considered as an iterative process to construct sequences $(\varepsilon_k)_{k\in\mathbb{N}}$ and $(\tilde{z}_k)_{k\in\mathbb{N}}$ as the parameter and solution sequences, respectively. Since the nominal solution $z(p_0)$ as well as the sensitivity differentials $\frac{dz}{dp}(p_0)$ and $\frac{dz}{dq}(q_0)$ can be computed off-line, steps like 4.30 do not need any derivative computational cost. Moreover, the terms of form $\frac{dz}{dq}(0)C^a(\tilde{z}_i(p), p)$, can be considered as a correcting *feedback step* for ε_i-error correction.

In the following, the feedback closed loop is briefly presented. The loop continues until a prescribed accuracy ε_∞ is achieved.

1. Initialize $\tilde{z}_1(p) = z(p_0) + \frac{dz}{dp}(p_0)\Delta p$, $k = 1$ and choose the desirable accuracy ε_∞.
2. While $\|C^a(\tilde{z}_k(p), p)\|_2 > \varepsilon_\infty$ do the following
   - $\tilde{z}_{k+1}(p) = \tilde{z}_k(p) - \frac{dz}{dq}(0)G^a(\tilde{z}(p), p)$,
   - $k = k + 1$.

For more details about the feedback rule and the convergence rate of $\tilde{z}_k(p)$, see [21]. Since the decision variables in the discretized OCP(p_0) are the control variables, therefore the sensitivity differentials yields approximations for the sensitivity of the optimal controls at the mesh points as follows.

$$\frac{\partial u}{\partial p}(\tau_i, p_0) \approx \frac{du^i}{dp}(p_0), \;\; i = 1, \ldots, N_d. \tag{4.31}$$

Using updates of the control and corresponding updated state makes us able to design a new strategy for transfer mission correction. The use of this real-time control based on parametric sensitivity analysis will be discussed in Chapter 6.

Chapter 5

Halo Orbit Transfer

Determining an optimal and efficient trajectory transferring a spacecraft from a parking orbit around the Earth to a halo orbit around a libration point still remains a challenge. Attacking to this problem by using the targeting techniques causes a high level of complexity [66]. Using the shooting methods has the design procedure that is usually starts with a set of initial conditions near Earth. Then these initial conditions are propagated forward in time. They are adjusted to achieve an acceptable result. The procedure is complicated by the fact that there are no analytical expressions or approximations to provide a guess to initiate the process. Unfortunately, there is a lack of control over the final complete solution; the high sensitivity of the resulting halo orbit transfer with respect to the slight changes in the initial conditions near the Earth makes it very difficult to achieve a set of precise characteristics that may be specified for the desired halo or Lissajous orbit. Since the real and natural flow is not close enough to the Earth and on the other hand passing this distance from the Earth to the manifold takes much energy, therefore the direct insertion into the stable manifold sounds not reasonable. These aspects and facts to be presented in this chapter present the difficulties associated with the computation of this kind of non-geocentric transfers. With assumption that one even can solve the halo transfer, these hardships can also be spread to the trajectory correction steps. In this chapter, a full model of the Earth-halo transfer with investigated details are going to be presented. This model consists of the dynamics and optimization requirements plus different practical constraints. These requirements and constraints are completely described in different sections.

5.1 Low Earth Orbits

As stated earlier, the first element of the Earth-halo transfer problem is the set of initial conditions. At the initial time t_0, the spacecraft is supposed to be located in a *Low Earth Orbit* or *LEO* which is generally defined as an orbit within the locus extending from the Earth's surface up to an altitude of 2000 kilometers. Despite the commonly accepted definition for LEO which is between 160-2000 kilometers above the Earth's surface, we do not consider the altitude less than 300 kilometers since it is not practical due to the large atmospheric drag. It should be mentioned that the exosphere's influence can be considered as a drag factor, but because of the very slight amount of this factor, it is usually ignored in the Earth-halo missions. LEO is commonly used to locate the satellites. The altitude of a LEO selected for a satellite is regarded to the application. Usually communication satellites require to be located in the geostationary orbits (GEO) to move at the same angular velocity as the Earth. The orbits used as temporary parking for interplanetary missions are LEO with altitude less than GEO range. To describe the initial orbit, LEO, we use a modified set of Gauss coordinates defined as following

$$\begin{cases} e_x = e\cos(\Omega+\omega), \\ e_y = e\sin(\Omega+\omega), \\ h_x = \tan(\frac{i}{2})\cos\Omega, \\ h_y = \tan(\frac{i}{2})\sin\Omega, \\ L = \Omega+\omega+\nu, \end{cases}$$

where P is the semi-latus rectum of the ellipse, e the eccentricity, ν the true anomaly, Ω the ascending node longitude, ω the argument of perigee and i the inclination. We use the following equations to convert those coordinates to the Cartesian position and velocity (in an inertial geocentric reference frame)

$$\mathbf{X}=\begin{pmatrix} x \\ y \\ z \\ \dot{x} \\ \dot{y} \\ \dot{z} \end{pmatrix}=\begin{pmatrix} \frac{P}{\beta W}\xi\cos L+2h_xh_y\sin L \\ \frac{P}{\beta W}\left(\gamma\cos L+2h_xh_y\sin L\right) \\ \frac{P}{\beta W}2Z \\ \frac{1}{\beta}\alpha(2h_xh_y\vartheta-\beta\nu) \\ \frac{1}{\beta}\alpha\left(\gamma\vartheta-2h_xh_y\nu\right) \\ \frac{1}{\beta}\alpha\left(2h_x\vartheta+2h_y\nu\right) \end{pmatrix},$$

where $\alpha=\sqrt{\frac{\mu_0}{P}}$, $\beta=1+h_x^2+h_y^2$, $\gamma=1-h_x^2+h_y^2$, $\xi=1+h_x^2-h_y^2$, $\nu=e_y+\sin L$, $\vartheta=e_x+\cos L$, μ_0 is the Earth gravitational constant and $W=1+e_x\cos L+e_y\sin L$, $Z=h_x\sin L-h_y\cos L$. As an example, one can consider $P(t_0)=11.625Mm$, $e_x(t_0)=$

0.75, $e_y(t_0) = 0$, $h_x(t_0) = 0.0612$, $h_y(t_0) = 0$ and $L(0) = \pi$. This LEO is mainly used in this dissertation as the initial condition at a specific time.

5.2 Spacecraft Properties

The most important aspect of a spacecraft is the thrust. Indeed, thrust is the force which moves the spacecraft through the space. The quantity of the thrust is force, therefore it is a vector quantity having both a magnitude and a direction. The engine works on the fuel and accelerates the exhausted fuel to the rear of the engine. Based on the Newton's third law, the thrust generated in the opposite direction from the accelerated fuel, pushes the spacecraft in the desired direction. The magnitude of the thrust depends on the amount of the fuel that is accelerated and on the difference in velocity of the exhaust through the engine. A general conclusion of the thrust equations for different engines with various propulsion systems shows that the amount of thrust depends on the mass of the fuel. To evaluate the amount of mass change, one can apply a useful factor corresponding to the engine. This factor is denoted by I_{sp} and so called *Specific Impulse*. It is usual to describe and compare the efficiency of various rockets and engines using this factor. Indeed, it shows the amount of impulse generated by a certain amount of propulsion per unit time by representing the derivative of the impulse with respect to the used propellant. This means the higher I_{sp}, the lower fuel mass rate needed to generate the given thrust. The new generations of propulsion systems, ion thrusters, reach even 10000 seconds as specific impulse.

Generally, the specific impulse I_{sp} which is precisely impulse per unit weight in the Earth level of propellant, is described as

$$I_{sp} = \frac{T_{max}}{\dot{m} g_e}, \tag{5.1}$$

where T_{max} is the maximum thrust produced by the engine as force in N (newtons), $\dot{m}$ is the mass rate in kilograms per second $^{kg}/_{s}$, and g_e is the Earth gravitational acceleration at the sea level. There are other ways to define a specific impulse which we will not use those definitions in this dissertation. Note that in this way, I_{sp} is measured in seconds (s), and the mass flow is negative, since propellant is being expelled. Using this definition makes it easy to compare the engine even in different unit systems. On the other hand, it physically means that if the thruster could be adjusted to equal the initial weight of its propellant, the specific impulse shows already the time the propellant would last.

Since between all the electric thrusters, ion thrusters have been the most seriously considered commercially and academically in the quest for interplanetary missions and

orbit raising maneuvers, therefore we consider a ion thruster with $I_{sp} = 3000\ s$. Indeed, since these thrusters require very high change in velocity overall that can be built up over long periods of time, they are seen as the best solution for interplanetary missions. Recent use of these thrusters can show the increasing interest in mission designs using them. *SERT* (Space Electric Rocket Test), *Deep Space 1* in 1990s, *Artemis* in 2001, *Hayabusa* in 2003, *Smart 1* also in 2003, *Dawn* in 2007 and *GOCE* in 2009 are several missions which used ion thrusters in last years. Furthermore, *BepiColombo* in 2014, *GSAT-4*, *LISA Pathfinder*, etc. are the missions planned to use the ion thrusters in the next few years that emphasize the importance of consideration ion thruster in our model.

5.3 Sun Influences

One of the many important perturbations that a motion analysis must take into account is the effect of the solar radiation pressure acting on the spacecraft. This perturbation due to the solar radiation pressure force in the spacecraft's trajectory has been investigated since 1960, see [72], [85] and [22]. In those works, the solar radiation pressure has been considered by averaging the force over the sunlit portion of the spacecraft's orbit [14]. However, in all these investigations the solar radiation pressure has been assumed constant and directed away from Sun, see [72], [85] and [22]. Indeed, for a spacecraft shaped other than a perfectly reflecting sphere, there is a component of solar radiation pressure (SRP) force in the plane normal to the Sun-spacecraft direction. In fact, the SRP force exploited on a spacecraft specifically designed for halo orbit mission highly depends on the shape of the spacecraft. Because of the Sun shield used on the spacecraft to protect the sensitive optic tools from the Sunlight, the effective area can be assumed to be flat and respectively large. This helps us to model SRP force on a flat plate. Here, the solar radiation pressure is modeled as a varying force in the direction away from Sun to Earth varying with the distance. However, optimization of low thrust transfer trajectories would be further complicated by this perturbation effects that should be taken into consideration.

Assume that P_0 is the pressure of the force exerted at the unit area in one AU (149,597,870 kilometers) away from Sun by the Sun's radiation. It is $P_0 = 4.65\text{E}{-}6\ /Nm^2$ for the reference distance 1 AU. The force on the spacecraft area A_{SC} with outward normal vector $\hat{\mathbf{n}}$ is

$$\mathbf{F}_0(t) = P_0\Big(\frac{1_{AU}}{r}\Big)^2 A_{SC} \cdot \langle \hat{\mathbf{r}}(t), \hat{\mathbf{n}} \rangle (-\hat{\mathbf{r}}(t)), \tag{5.2}$$

where $\hat{\mathbf{r}}$ is a unit vector along the Earth-Sun line, see [72], [85] and [22]. Considering the fractions respected specularly and diffusely, the force exploiting on the spacecraft surface,

the resulting force will be

$$\mathbf{F}(t) = \mathbf{F}_0(t) + P_0\Big(\frac{1_{AU}}{r}\Big)^2 A_{SC} \cdot \langle \hat{\mathbf{r}}(t), \hat{\mathbf{n}} \rangle (-\hat{\mathbf{r}}(t)) + F_s + F_d, \tag{5.3}$$

where F_s and F_d are the radiations reflected specularly and diffusely, respectively. Therefore, the acceleration is

$$\mathbf{a}_{SRP}(t) = \frac{1}{m}\Big(P_0\Big(\frac{1_{AU}}{r}\Big)^2 A_{SC} \cdot \langle \hat{\mathbf{r}}(t), \hat{\mathbf{n}} \rangle (-\hat{\mathbf{r}}(t)) + F_s + F_d\Big). \tag{5.4}$$

The acceleration $\mathbf{a}_{SRP} = (a_{SRP_1}(t), a_{SRP_2}(t), a_{SRP_3}(t))^T$ is the extra factor which should be taken into consideration in different three- and four-body frames. Note that we do not consider the Earth shadow, because for the trajectories designed here, there is no intersection with the area behind the Earth.

5.4 Direct Transfer Optimal Control Problem

As mentioned before, although shooting techniques in combination with differential corrections schemes have been successfully employed in the computation of halo transfers, they are time consuming to investigate a range of necessary parameters.

To employ the optimal control theory, the halo orbit transfer problem with the three-body dynamics is formulated as an optimal control problem in the following.

$$\begin{aligned}
&\text{Minimize } J(x(t), u(t), t)\\
&\text{s.t.} \quad \begin{cases}
\dot{x}_1 = x_4,\\
\dot{x}_2 = x_5,\\
\dot{x}_3 = x_6,\\
\dot{x}_4 = 2x_5 + x_1 - (1-\mu)\frac{x_1+\mu}{r_{13}^3} - \mu\frac{x_1-1+\mu}{d_{23}^3} + \frac{u_1 T_{max}}{m} + a_{SRP_1}(t),\\
\dot{x}_5 = -2x_4 + x_2 - (1-\mu)\frac{x_2}{r_{13}^3} - \mu\frac{x_2}{d_{23}^3} + \frac{u_2 T_{max}}{m} + a_{SRP_2}(t),\\
\dot{x}_6 = -(1-\mu)\frac{x_3}{r_{13}^3} - \mu\frac{x_3}{r_{23}^3} + \frac{u_3 T_{max}}{m} + a_{SRP_3}(t),\\
\dot{m}(t) = -\frac{\|u(t)\| T_{max}}{g_e I_{sp}},\\
h(x(t_0), t_0) = 0,\\
g(x(t_f), t_f) = 0,\\
-1 \le u(t) \le 1,\\
m_{min} \le m(t) \le m_{max},\\
C(x(t), u(t), t) \leqslant 0,
\end{cases}
\end{aligned} \tag{5.5}$$

where r_{13} and r_{23} are as defined in 2.12 and 2.13. And $h : \mathbb{R}^{n+1} \to \mathbb{R}^n$, $g : \mathbb{R}^{n+1} \to \mathbb{R}^r$,

$0 \leqslant r \leqslant n$. Actually, the equation $h(x(t_0), t_0) = 0$ determines the initial conditions which is supposed to be the equation of the prescribed LEO introduced in Section 5.1. Note that the further necessary conditions at the initial time will be applied by the extra constraints. The equation $g(x(t_f), t_f) = 0$ is indeed the final condition that determines the periodic orbit which is the destination at the final time t_f. The final time t_f is free. This optimal control problem with free final time can be reduced to an augmented optimal control problem with a fixed final time by a transformation $t = s \cdot t_f$ with the new time variable $s \in [0, 1]$. Due to the mass which is not normalized and bounded between m_{min} and m_{max}, the thrust must be bounded into the box $-1 \leq u(t) \leq 1$. A percentage of the mass is considered as m_{min} which can be interpreted the mass of the spacecraft itself, as opposed to expendable fuel. This percentage is about 6% for the James Webb Telescope and 22% for the Genesis. In this dissertation, the ratio of the spacecraft mass to the total mass is considered to be 50%. This is a conservative estimate for a spacecraft, but makes the problem more challenging. Indeed, for a mission which lasts a few days, this is not an issue, but for the missions modeled here, it becomes an important constraint in the simulation.

The objective function is traditionally considered as the differences in the velocity during the mission. This factor, Δv, is selected to be the sum of the magnitude of the velocity increments as

$$\Delta v = \sum_k |\Delta v_k|. \tag{5.6}$$

This kind of objective function have been indeed used for impulsive transfers, especially transfer of the spacecrafts equipped by chemical engines. On the other hand, the most important consequence of this kind of objective function is the lack of continuity which would have considerably complicated solving optimal control problem. To adapt the objective function in order to be suitable for the smooth and continuous thrust of electrical engines and ion thrusters, one can substitute 5.6 by the following objective function

$$J = \|u(t)\|_2^2, \tag{5.7}$$

which is often used as the familiar quadratic objective function. With this function as cost function, the optimization problem is seeking to minimize the magnitude of the thrust in each direction.

Note that the ordinary differential dynamics of the optimal control problem 5.5 is the circular restricted three-body problem which is augmented by the solar radiation pressure. The halo orbit transfer problem in four-body dynamics will be discussed later in 5.6.

5.4.1 More Constraints

The transfer trajectory is assumed to be originated from a parking LEO. To ensure that the transfer trajectory originates on a desired parking orbit, it is necessary to add constraints to the initial points that are defined on the parking LEO orbit and very first part of the transfer trajectory. Besides the altitude of the LEO, an apse must be ensured, too. On the other hand, the spacecraft cannot pass its way through the Earth, therefore there must be a constraint to restrict this kind of passage. One can formulate this restriction as the below constraint.

$$(x(t) - (1-\mu))^2 + y^2(t) + z^2(t) \geqslant R_E, \tag{5.8}$$

which R_E can be considered as the altitude of the prescribed LEO plus the radius of the Earth, since $(1-\mu, 0, 0)$ is the position of the center of the Earth. Furthermore, the usage of the thrust cannot be arbitrary. The thrust magnitude is restricted as mentioned in Section 5.2. Moreover, some times there should be a constraint even on the direction of the thrust. As discussed before, some missions need to keep away the spacecraft and its equipments from the sunlight, or maybe keep the instant tester instruments facing the Sun. To ensure that, one has to augment a proper constraint to the problem which can be formulated as

$$\tan(\theta) \leqslant \frac{\|u_2(t) + u_3(t)\|_2}{\|u_1(t)\|_2}, \tag{5.9}$$

which θ is the angle between the thrust and the Sun-Earth axis.

5.5 Optimal Results of Three-Body Transfers

The transfer optimal control problem and its elements have been described so far. The initial and final conditions, the underlying system dynamics, a reasonable objective function, and different necessary constraints are all explained. The actual mission design can now proceed. Now, we report the results from testing the methods and algorithms described in Chapter 4. One can see that the mission design problem is in fact solvable without any simplification, especially breaking the problem into several steps and making assumptions about the orbit, or not considering practical factors. Another purpose is to show the flexibility of the optimal control model to be adapted and employed in different missions. For example, solving the transfer problem to a halo orbit around L_1 and L_2 or even transfer to a quasi-periodic orbit around these points do not need extra system identification and modelling efforts. Although this approach can be applied to any

Lagrange point transfer, we first design and control missions around the Sun-Earth L_2 points. The ideal trajectory to be achieved is supposed to be useful for the James Webb Space Telescope [76] with special angle constraints described in 5.4.1.

5.5.1 Halo transfer around L_2

The first guess for the LEO departure control signal is inspired from the difference between velocities of the LEO parking orbit and the closest stable manifold of the halo orbit that was generated previously. This manifold can be obtain using the distance analysis shown in Figures 3.12 and 3.13. Of course, this difference might be bigger than the ability of a low-thrust engine to compensate for it, but the results confirm that the optimal control model can handle this difficulty by considering the maximum thrust constraint. On the other hand, an initial guess for the final time has been taken from the practical missions as $t_f = \frac{2\pi}{3} \simeq 121$ days. The maximum thrust is considered differently to show the flexibility of the optimal control model. For the first mission, a very big halo orbit around L_2 is considered. Namely, a halo orbit with almost 673190 km, 204950 km and 1645600 km x-, y- and z-altitudes, respectively. This halo orbit with this properties can not be used for a mission design, but is is selected here to show the reusability and of course the robustness of the optimal control solver. On the other hand, the maximum thrust has been given as $T_{max} = 20\ N$ and as mentioned in 5.2, the specific impulse is $I_{sp} = 3000\ s$. The transfer optimal control problem is transcribed to an NLP using 81 discretization points. NUDOCCCS can reach the desirable accuracy after 529 major iterations. The

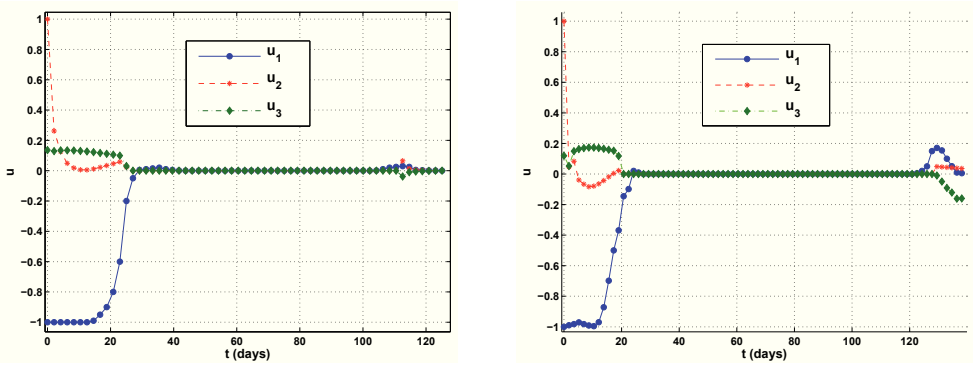

Figure 5.1: Optimal controls for the missions transferring to the halo orbits around L_2. The control signals in three x-, y- and z- directions corresponding to the first and the second missions are shown in left and right, respectively.

optimal control signals are presented in Figure 5.1-Left. As it is appear in this figure, the controls try to use the maximum thrust to change the spacecraft's velocity from the LEO

velocity to the new conditions. In most part of the trajectory the engines are off until the spacecraft is close to the halo orbit. To handle the new conditions, controls use a little thrust in all three dimensions to overcome the velocity difference. The amount of force which is used in this mission is $J = 8.9815\ N$. The four trajectories shown in Figure 5.2 show this transfer in two-dimensional views of this trajectory projected on $x-y$, $x-z$ and $y-z$ planes and a three-dimensional view. This transfer takes almost 125 days.

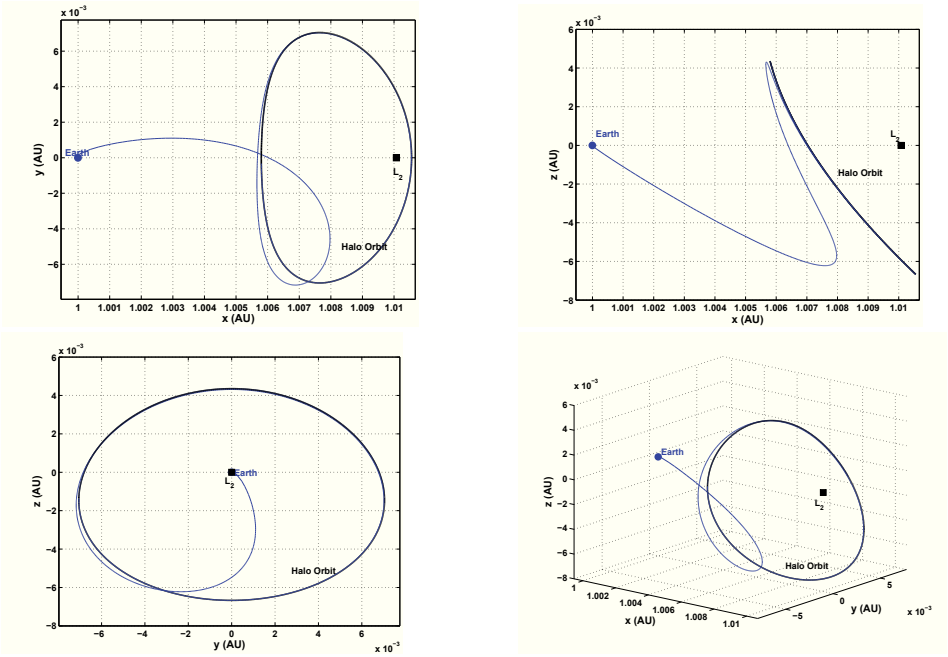

Figure 5.2: The first transfer trajectory from LEO to a southern halo orbit around L_2 with big x-, y- and z-altitudes is shown in two- and three-dimensional views.

As the second example, we consider another southern halo orbit with x-, y- and z-altitude as 718070 km, 204950 km and 149600 km. The final time guess is the same as before, but the maximum thrust is given as $T_{max} = 18\ N$. Although, the shape of the halo orbit is quite similar the previous one, this orbit is closer to the libration point L_2 which means it is further from the Earth. Since the thruster uses less force, therefore we expect a mission which takes longer than the first mission. After testing different numbers of discretization, the optimal solution is achieved with 71 discretization points after solving 457 quadratic programming subproblems. The optimal trajectory is shown in different two and three dimensional views in Figure 5.3. The main structure of the trajectory looks quite similar to the first example, but it takes almost 138 days as we expected. The optimal controls (Figure 5.1-Right) have been changed slightly. The main change is in the last days of the mission. In last days (halo entrance), controls use a

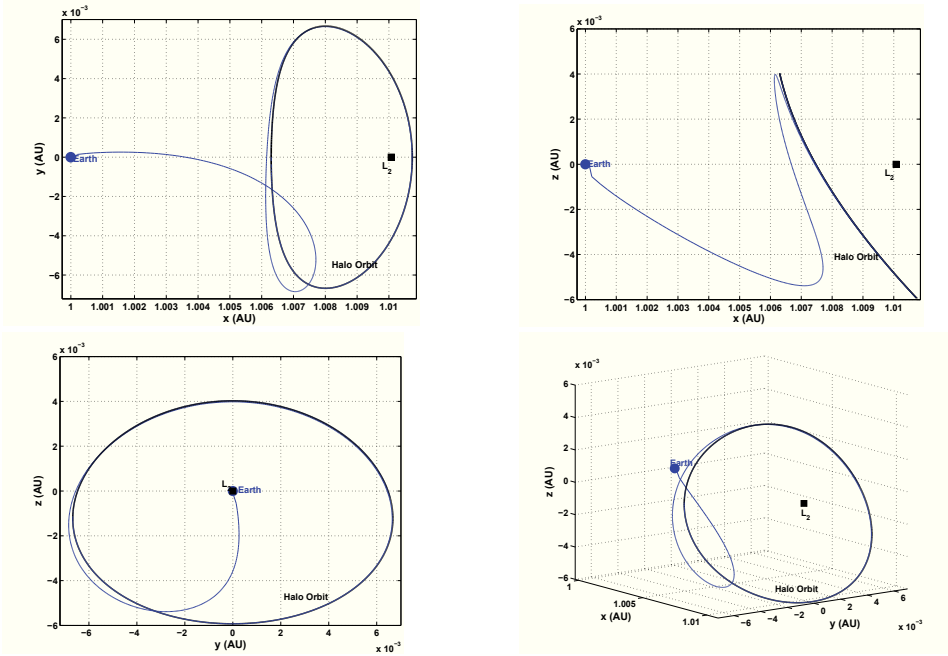

Figure 5.3: The second transfer trajectory from LEO to a southern halo orbit around L_2 with big x-, y- and z-altitudes (smaller than Figure 5.2) is shown in two- and three-dimensional views.

certain amount of thrust to put the spacecraft with a proper velocity on the halo orbit. The total force exploited by the thruster to control the mission is $J = 9.2957\ N$.

As the third example, we considered a halo orbit with 493670 km in x-direction, 173530 km in y-direction and 107710 km in z-direction. Although the considered orbit's altitudes in all three directions are indeed smaller than previous two halo orbits, it is still big for practice. Nevertheless, to show that the optimal control approach is true, applicable and robust, it is considered as the third example for the final place to locate the spacecraft. Lets consider the maximum thrust less than two previous missions as $T_{max} = 15\ N$. Since the final orbit is further away from the Earth and weaker thruster is being used, therefore one can expect a longer mission or more thrust usage. NUDOCCCS converges to the optimal solution with 121 discretization points after solving 1273 major subproblems. Figure 5.4-Left shows the optimal control signals for this mission. This figure also shows that this mission takes almost 170 days, and the optimal control variables during these days are similar to the optimal control variables in the previous two examples. As one can see the corresponding trajectory shown in Figure 5.5 is also similar to the previous trajectories. The necessary force to end this mission is $J = 7.2911\ N$.

The fourth example concerns with a halo orbit with a smaller altitudes. This orbit is

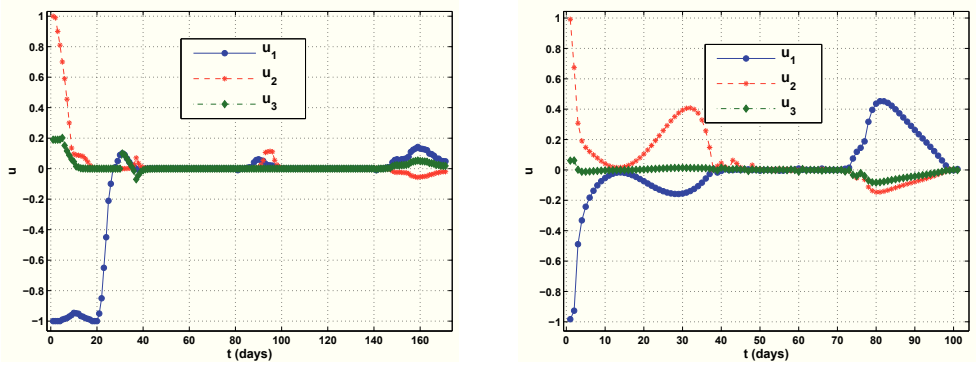

Figure 5.4: Optimal controls for the missions transferring to the halo orbits around L_2. The control signals in three x-, y- and z- directions corresponding to the third and the fourth missions are shown in left and right, respectively.

also southern and its altitudes in x-, y- and z-directions are almost 598390 km, 173530 km and 107710 km, respectively. Therefore, this halo orbit is smaller than the previous orbits in every direction. This kind of halo orbits with these altitudes are usually used to design a mission. The properties of the spacecraft are the same but the maximum thrust has been considered a little more as $T_{max} = 30\ N$. Although, the halo orbit is further away from the Earth, the higher thrust compensates for this difficulty. The Optimal control solver solves 2498 quadratic nonlinear programming subproblems to converge to the optimal solution with 121 discretization points. This mission takes almost 103 days. As one can see, T_{max} was enough to compensate for the far distance. The optimal control signals are shown in Figure 5.4-Right. It is clear that the control variables governing this mission are quite different from two previous missions. They vanish in very first days and become nonzero again very fast. These reactions in first 40 days of the mission lead to a totally different trajectory which can be seen in Figure 5.6. This retrograde trajectory spends almost 40 days in the other side of the Earth and quite away from the final halo orbit, but after 70 days it starts to locate and adjust the velocity to the halo position and velocity. This second phase can be seen as a big pick in the control variables at 70 to 100 days. The total force used for this mission is $J = 12.4928\ N$.

For the fifth attempt, a northern halo orbit is considered. Actually, this orbit is the corresponding symmetric orbit of the first halo orbit. Therefore the altitudes of this orbit are the same as the first orbit, i.e. 673190 km, 204950 km and 1645600 km in x-, y- and z-directions, respectively. The first guess for the LEO departure control signal is inspired from the difference between velocities of the LEO parking orbit and the closest stable manifold of the halo orbit (like the southern orbit examples). For this example the maximum thrust is given as $T_{max} = 50\ N$ and as always the specific impulse is

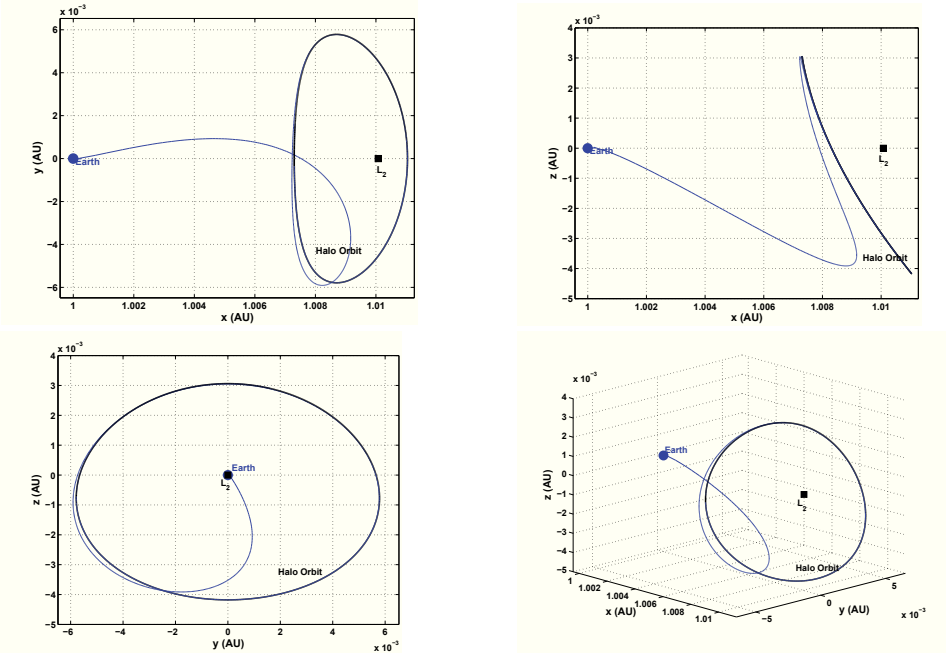

Figure 5.5: The third transfer trajectory from LEO to a southern halo orbit around L_2 with big x-, y- and z-altitudes (smaller than two previous orbits) is shown in two- and three-dimensional views.

$I_{sp} = 3000\ s$. This amount of thrust is the highest so far. Since the main structure of the halo orbit is the same as the first halo orbit, a relatively short mission is expected. Therefore, the initial guess for the final time is $t_f = \frac{2\pi}{5} \simeq 75$ days. The transfer optimal control problem is transcribed to an NLP using 81 discretization points. The solver can reach the desirable accuracy after 851 major iterations. The optimal control signals are presented in Figure 5.7-Left. This mission uses $J = 16.5347\ N$ and takes almost 82 days to reach the desired halo orbit. The four trajectories shown in Figure 5.8 show this transfer in two-dimensional views of this trajectory projected on $x-y$, $x-z$ and $y-z$ planes and a three-dimensional view.

As the sixth example, the corresponding symmetrical northern halo orbit of the second orbit is given. This orbit has the same altitudes as 718070 km, 204950 km and 149600 km in x-, y- and z-directions. To test the ability of the optimal control solver, the maximum thrust is given as $T_{max} = 4\ N$ which is very low thrust. The specific impulse is the same $I_{sp} = 3000\ s$. One can anticipate a very long mission because of the low thrust engine. Therefore, $t_f = \pi$ would be a good guess for the final time. After testing different numbers of discretization, the optimal solution is achieved with 61 discretization points after solving 2566 quadratic subproblems. The optimal trajectory is shown in different

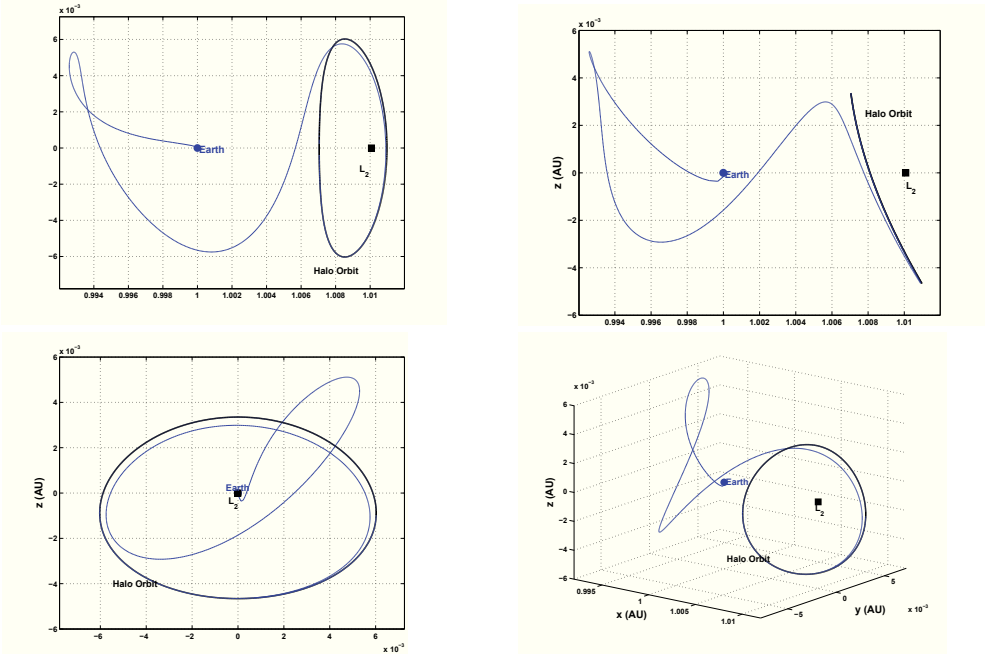

Figure 5.6: The fourth transfer trajectory from LEO to a southern halo orbits around L_2 with reasonable x-, y- and z-altitude (smallest orbit) is shown in two- and three-dimensional views.

two and three dimensional views in Figure 5.9. The main structure of the trajectory looks quite similar to the fifth example and symmetrical to the second example, but it takes almost 207 days as we expected. The optimal controls (Figure 5.7-Right) shows the usage of the low thrust and the relatively complication of the mission. The total force exploited by the thruster to control the mission is $J = 4.1888\ N$.

The symmetrical halo orbit corresponding to the third example is given as the seventh transfer problem. The halo orbit with 493670 km in x-direction, 173530 km in y-direction and 107710 km in z-direction which mostly is in northern part is considered as the final destination. The maximum thrust is $T_{max} = 35\ N$ which is 20 N more than the third example. Since the initial and final conditions are the same, one can anticipate that the current mission lasts less than the third example. The optimal control solver converges to the optimal solution with 111 discretization points after solving 1330 major subproblems. Figure 5.10-Left shows the optimal control signals for this mission. As we expected, this mission takes exactly 88 days which is almost half of the third mission time. The difference in the optimal controls can be recognize easily by two big picks of u_1 in Figure 5.10. The optimal trajectory is shown in Figure 5.11. The total force to end this mission is $J = 18.3260\ N$ which is almost twice the third example total force. It means that this

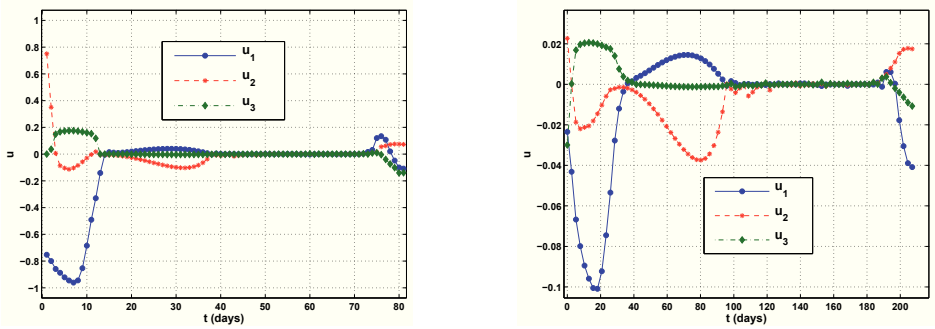

Figure 5.7: Optimal controls for the missions transferring to the northern halo orbits around L_2. The control signals in three x-, y- and z- directions corresponding to the fifth and the sixth missions are shown in left and right, respectively.

extra force exploited by a stronger engine compensates the shorter mission duration.

The last L_2 transfer example concerns with a northern halo orbit which is actually symmetrical to the halo in fourth example. Its altitudes in x-, y- and z-directions are almost 598390 km, 173530 km and 107710 km, respectively. The properties of the spacecraft are the same but the maximum thrust has been considered 10 N less as $T_{max} = 20\ N$. NUDOCCCS solves 1224 quadratic nonlinear programming subproblems to converge to the optimal solution with 61 discretization points. This mission takes almost 121 days. The optimal control variables are shown in Figure 5.10-Right. Also, the optimal trajectory is presented in Figure 5.12. The total force used for this mission is $J = 9.2648\ N$.

Periodic orbits information and results regarding transfers are summarized in Table 5.1. The first column points to the example which corresponding halo orbit's distance to the Earth is mentioned as d_{EO} in the second column. The maximum thrust used for each transfer T_{max}, the number of discretization points d_N, length of the mission in days and the total thrust used during the mission are consecutively shown in this table.

5.5.2 Halo transfer around L_1

As mentioned before, the bounded orbits around first libration point in the Sun-Earth/Moon three-body system are usually used for missions that study the Sun and its influences such as solar winds. To locate the spacecraft in a periodic orbit around L_1, the transfer optimal control problem is modelled as before, Section 5.5.1. The objective function, underlying system dynamics, main constraints on trajectory and controls and other necessary elements are given as before. The initial conditions are also considered as same as Section 5.5.1 which is the LEO parking explained in Section 5.1. The main difference between halo transfers in two sections 5.5.1 and 5.5.2 is the final conditions which explain the peri-

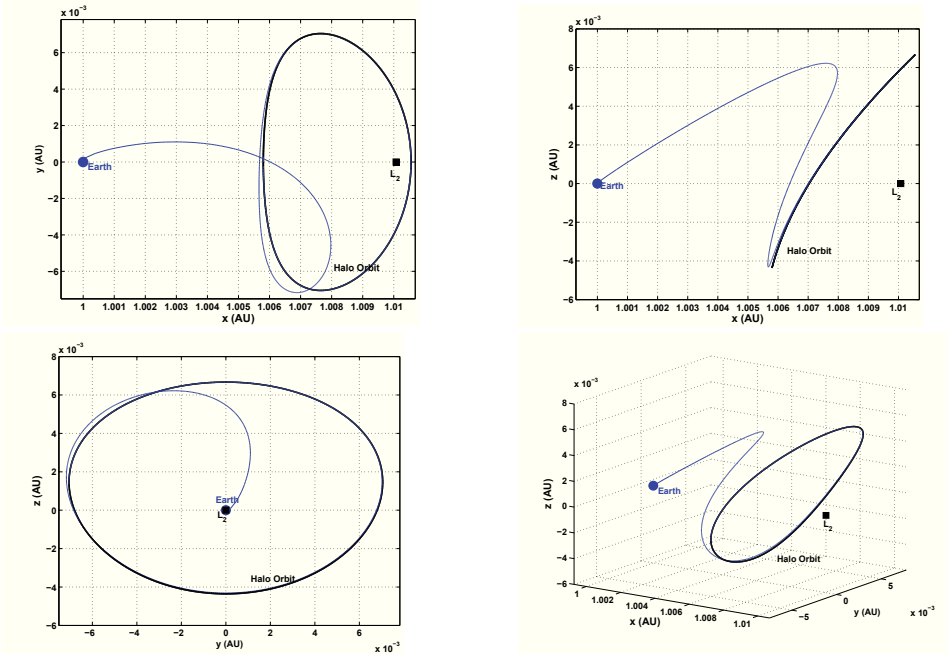

Figure 5.8: The fifth transfer trajectory from LEO to a northern halo orbit around L_2 with big x-, y- and z-altitudes (the same altitudes as the first mission) is shown in two- and three-dimensional views.

odic orbit around two different libration points. This shows that the modelling of transfer problem as an optimal control problem can even be used to design a totally different mission in the same manner. This reusability is one of the most important advantages of this approach. Like the way used before, the first guess for the LEO departure control signal is taken from the difference between velocities of the LEO and the closest stable manifold of the halo orbit that was generated previously. Despite showing the optimal trajectories to L_2 in four different two- and three-dimension views, for the transfers to L_1, we only show the three-dimensional view of the optimal trajectory.

For L_1 halo transfer, four halo orbits with a big range of altitudes are considered. Their symmetrical orbits are also taken into account as the next four examples. For these eight missions, the spacecrafts are also differently equipped with thrusters. The first example deals with a transfer to a halo orbit with 456273 km, 1421170 km and 583431 km in x-, y- and z-directions, respectively. On the other hand, the maximum thrust is given as $T_{max} = 50\ N$, and the specific impulse is $I_{sp} = 3000\ s$. The transfer optimal control problem is transcribed to an NLP using 121 discretization points. The solver can reach the desirable accuracy after 2437 major iterations. This transfer takes almost 66 days which with such a big thrust for a ion thruster, it was expected. The amount of

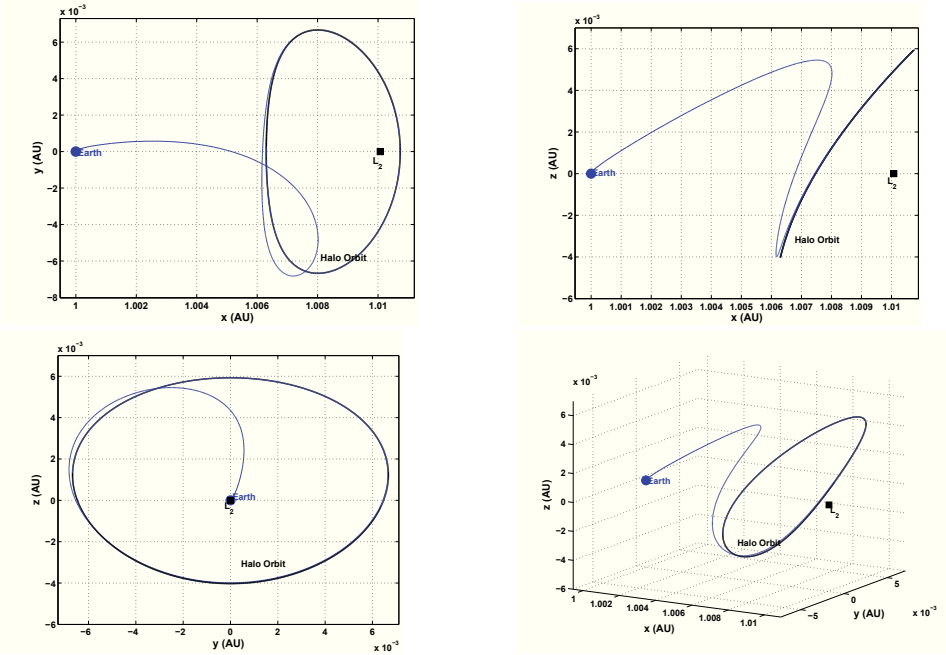

Figure 5.9: The sixth transfer trajectory from LEO to a northern halo orbit around L_2 with big x-, y- and z-altitudes (smaller than fifth orbit) is shown in two- and three-dimensional views.

force which is used in this mission is $J = 18.5891\ N$. The trajectory shown in Figure 5.13-Left shows this transfer in a three-dimensional view.

A halo with x-, y- and z-altitudes as 422047 km, 1065877 km and 437573 km respectively, around L_1 is the second destination for a spacecraft equipped by engine with $T_{max} = 25\ N$. The only thing which is guessed differently from the first mission is the final time which is estimated to be more than 66 days. We put the initial guess as $t_f = \frac{2\pi}{3} \simeq 121$ again. The continuous optimal control problem is discretize with 141 points. The nonlinear programming problem is solved after 1128 major iterations. The result shows that this transfer lasts for almost 111 days and uses $J = 15.5269\ N$. The corresponding optimal trajectory is shown in Figure 5.13-Right.

As the third example of the transfers to periodic orbits around L_2, we consider a halo orbit with 418874 km in x-direction, 688150 km in y-direction and 299195 km in z-direction. Lets consider the maximum thrust less than two previous missions as $T_{max} = 15\ N$. Since the final orbit is further away from the Earth and weaker thruster is being used, therefore one can expect a longer mission or more thrust usage. The optimal control solver converges to the optimal solution with 151 discretization points after solving 1736 major subproblems. This mission takes almost 122 days and the optimal trajectory

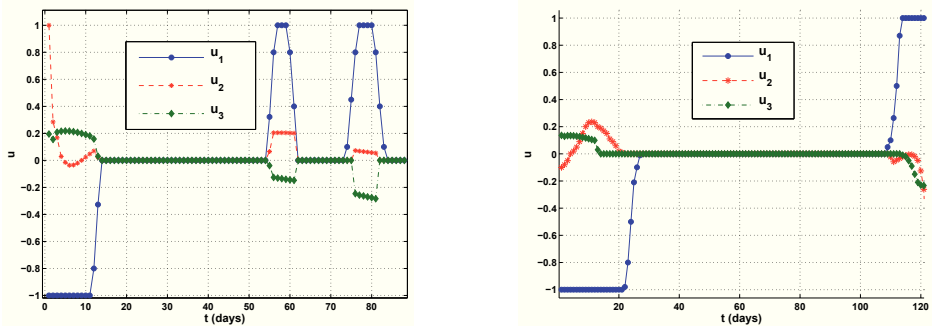

Figure 5.10: Optimal controls for the missions transferring to the northern halo orbits around L_2. The control signals in three x-, y- and z- directions corresponding to the seventh and the eighth missions are shown in left and right, respectively.

Mission	d_{EO} (km)	T_{max} (N)	N_d	t_f (days)	J (N)
1st	1083423.263	20	81	125	8.9815
2nd	1116385.068	18	71	138	9.2957
3rd	1180686.420	15	121	170	7.2911
4th	1164175.199	30	121	102	12.4928
5th	1083423.263	50	81	82	16.5347
6th	1116385.068	4	61	207	4.1888
7th	1180686.420	30	111	88	18.3260
8th	1164175.199	20	61	121	9.2648

Table 5.1: Transfers from LEO to eight halos around L_2 by spacecrafts which are differently equipped with vaious thrusters.

during these days is shown in Figure 5.14-Left. The necessary force to end this mission is $J = 12.9112$ N.

The fourth example concerns with a halo orbit with smaller altitudes. This orbit is also northern and its altitudes in x-, y- and z-directions are almost 397784 km, 344075 km and 134638 km, respectively. All properties of the spacecraft are the same but the maximum thrust has been considered a little less as $T_{max} = 10$ N. NUDOCCCS solves 1498 quadratic nonlinear programming subproblems to converge to the optimal solution with 91 discretization points. This mission takes almost 162 days. The trajectory can be seen in Figure 5.14-Right. The total force used for this mission is $J = 8.1924$ N.

The next four examples take the southern symmetrical halo orbit corresponding to each one of the previous orbits. As the fifth example of the periodic orbit around L_1, the halo orbit with 456273 km, 1421170 km and 583431 km in x-, y- and z-directions is given. Most of this orbit is above the $z = 0$ plane. The spacecraft is equipped with a low

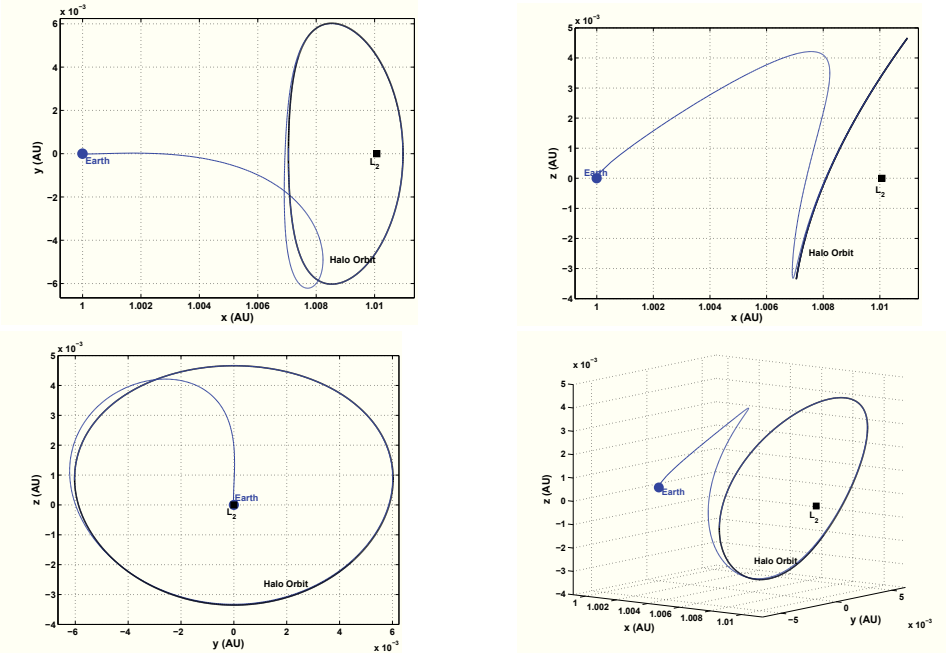

Figure 5.11: The seventh transfer trajectory from LEO to a northern halo orbit around L_2 with big x-, y- and z-altitudes (the same altitudes as the first mission) is shown in two- and three-dimensional views.

thrust engine which its maximum thrust is $T_{max} = 5\ N$. The optimal control problem is discretized by $N_d = 171$ points. The upcoming discrete nonlinear programming problem is solved in 3228 iterations. The optimal solution shows that this mission takes almost 208 days and uses $J = 8.0435\ N$. The trajectory is shown in Figure 5.15-Left.

The next example considers the corresponding symmetrical southern halo orbit of the second orbit. This orbit has the same altitudes 422047 km, 1065877 km and 437573 km in x-, y- and z-directions. The maximum thrust is given as $T_{max} = 25\ N$, and the specific impulse is the same $I_{sp} = 3000\ s$. After testing different numbers of discretization points, the optimal solution is achieved with 61 discretization points after solving 398 quadratic subproblems. The optimal trajectory is shown in a three dimensional view in Figure 5.15-Right. The total force exploited by the thruster to control the mission is $J = 12.8198\ N$.

The symmetrical halo orbit corresponding to the third example is given as the seventh L_1 transfer problem. The altitudes in x-, y- and z-directions are 418874 km, 688150 km and 299195 km. The maximum thrust is $T_{max} = 35\ N$. NUDOCCCS converges to the optimal solution with 91 discretization points after solving 1425 major subproblems. The optimal trajectory during almost 68 days is shown in Figure 5.16-Left. The total force to

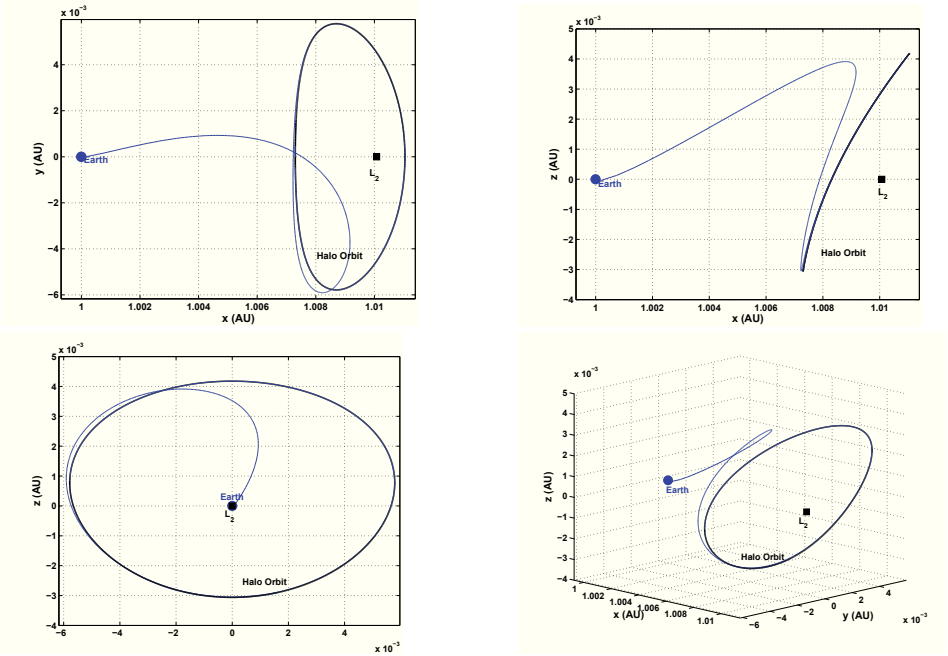

Figure 5.12: The eighth transfer trajectory from LEO to a northern halo orbit around L_2 with small x-, y- and z-altitudes is shown in two- and three-dimensional views.

end this mission is $J = 17.0653\ N$.

In the last example of the L_1 transfer, a halo orbit with a smaller altitudes is given. This orbit is also southern and its altitudes in x-, y- and z-directions are almost 397784 km, 344075 km and 134638 km, respectively. All properties of the spacecraft are the same but the maximum thrust is given as $T_{max} = 10\ N$. This is the maximum thrust of the fourth example. The Optimal control solver solves 956 quadratic nonlinear programming subproblems to converge to the optimal solution with 91 discretization points. This mission takes almost 162 days which is equal to the fourth mission's duration. The optimal trajectory shown in Figure 5.16 is symmetrical with respect to the trajectory in fourth example. This similarity can be explained because of the symmetric properties of the halo orbits, the underlying system dynamics. On the other hand, there is no extra asymmetric constraint such as the angle constraints forced for the L_2 transfers. As we expect the total force used for this mission is almost the same amount of the fourth example, i.e. $J = 8.1925\ N$. All results and information about these eight transfer from LEO to different periodic orbits around L_1 are summarized in the Table 5.2.

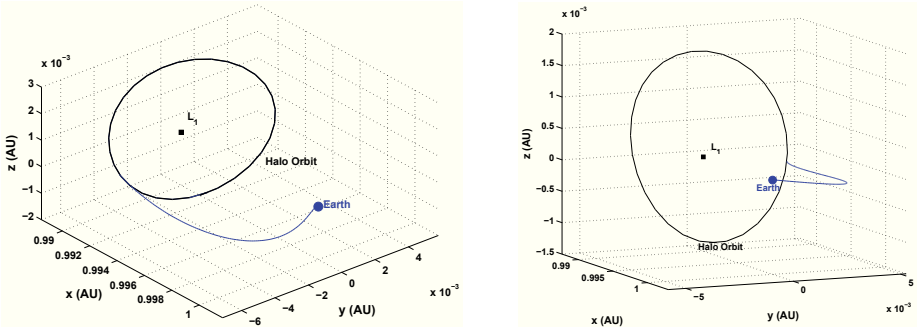

Figure 5.13: The first and second transfer trajectories from LEO to two different northern halo orbits around L_1 are shown in three-dimensional views at left and right, respectively.

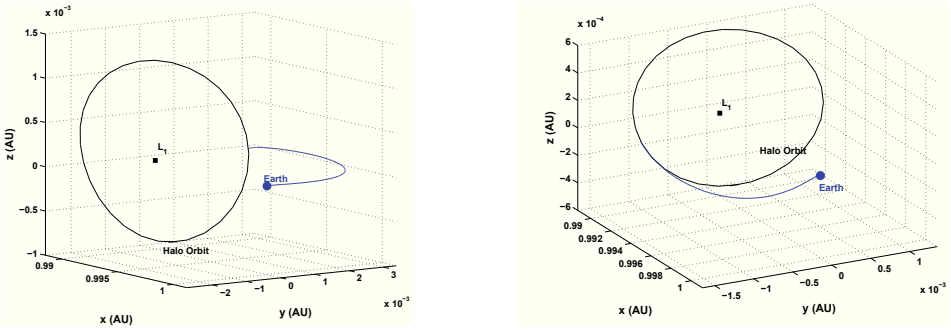

Figure 5.14: The third and fourth transfer trajectories from LEO to two different northern halo orbits around L_1 are shown in three-dimensional views at left and right, respectively.

5.5.3 Lissajous orbit transfer

The focus of this section is the determination of a transfer to quasi-periodic orbit around libration points. This shows the flexibility and usability of our approach solving different transfer problems. As before, the transfer problem is considered as an optimal control problem, and the only element which differs from the previous models is the final condition. In new problem, the final condition is given as a quasi periodic orbit, see Section 3.1.1. To show the robustness and usability of the optimal control approach, four Lissajous orbits are considered which two of them are in the vicinity of L_1 and the rest are around L_2.

The first transfer which is shown in the left figure of the Figure 5.17-Left is going to be terminated on a Lissajous orbit that does not revolve so fast in-plane and out-of-plane. But the second transfer shown in Figure 5.17-Right, is constructed with in-plane and out-of-plane equal to 20 which makes it to revolve many times in the $z = 0$ plane and out of it. This makes the transfer problem much more difficult, but the optimal control

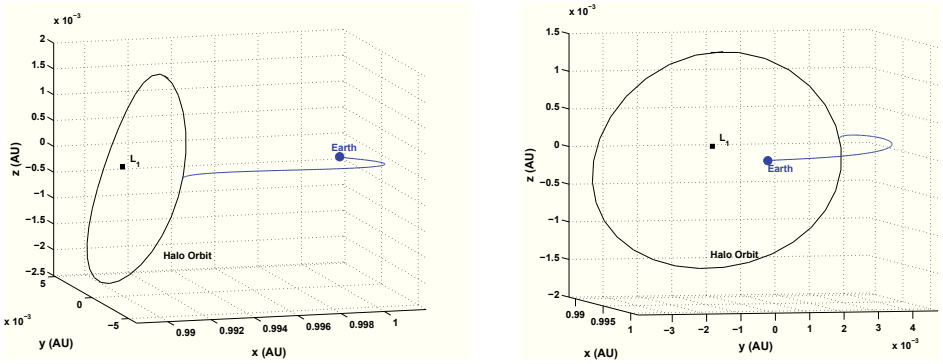

Figure 5.15: The first and second transfer trajectories from LEO to two different southern halo orbits around L_1 are shown in three-dimensional views at left and right, respectively.

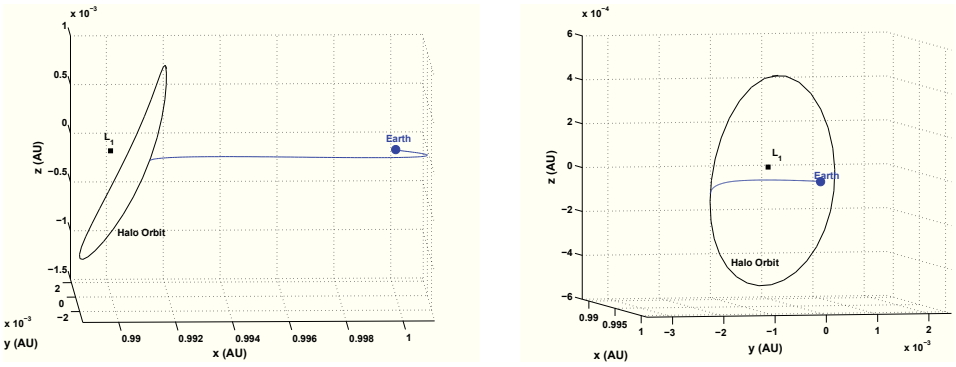

Figure 5.16: The third and fourth transfer trajectories from LEO to two different southern halo orbits around L_1 are shown in three-dimensional views at left and right, respectively.

solver after solving 3442 subproblems converges to the optimal solution.

The transfers to the Lissajous orbits around L_2 are also arranged in the same way. The first one terminates at arriving to a Lissajous orbit with in-plane and out-of-plane frequencies equal to 7. But the second orbit is constructed with both frequencies equal to 21. These two transfers are also shown in Figure 5.18. Table 5.3 summarizes the results about these four transfers with information of the corresponding final quasi-periodic orbit. Note that in this table, first the quasi-periodic orbit is identified by in-plane and out-of-plane amplitudes, frequencies and phases explained in Section 3.1.1 and denoted by A_x, A_z, λ, ν, ϕ and ψ, respectively.

Mission	d_{EO} (km)	T_{max} (N)	N_d	t_f (days)	J (N)
1st	1226286.508	50	121	66	18.5891
2nd	1269045.882	25	141	111	15.5269
3rd	1335081.998	15	151	122	12.9112
4th	1428991.711	10	91	162	8.1924
5th	1226286.508	5	171	208	8.0435
6th	1269045.882	25	61	119	12.8198
7th	1335081.998	35	91	68	17.0653
8th	1428991.711	10	97	162	8.1925

Table 5.2: Transfers from LEO to eight halos around L_1 by spacecrafts which are differently equipped with various thrusters.

Lissajous Orbit around L_1
$A_x = 1367324$ km, $A_z = 700000$ km, $\lambda = 8$, $\nu = 8$, $\phi = \frac{\pi}{2}$, $\psi = 0$

d_{EO} (km)	T_{max} (N)	N_d	t_f (days)	J (N)
1128261.285	50	171	67	21.09189

Lissajous Orbit around L_1
$A_x = 1000000$ km, $A_z = 500000$ km, $\lambda = 20$, $\nu = 20$, $\phi = 0$, $\psi = \frac{\pi}{2}$

d_{EO} (km)	T_{max} (N)	N_d	t_f (days)	J (N)
11965405.112	5	211	188	19.2966

Lissajous Orbit around L_2
$A_x = 1326597$ km, $A_z = 700000$ km, $\lambda = 7$, $\nu = 7$, $\phi = 0$, $\psi = \frac{\pi}{2}$

d_{EO} (km)	T_{max} (N)	N_d	t_f (days)	J (N)
1335081.998	50	157	59	22.1292

Lissajous Orbit around L_2
$A_x = 1000000$ km, $A_z = 500000$ km, $\lambda = 21$, $\nu = 21$, $\phi = \frac{\pi}{2}$, $\psi = \frac{\pi}{2}$

d_{EO} (km)	T_{max} (N)	N_d	t_f (days)	J (N)
1409981.017	5	151	198	18.9144

Table 5.3: Transfers from LEO to four Lissajous orbits with different orbital elements around L_1 and L_2 by spacecrafts which are differently equipped with various thrusters.

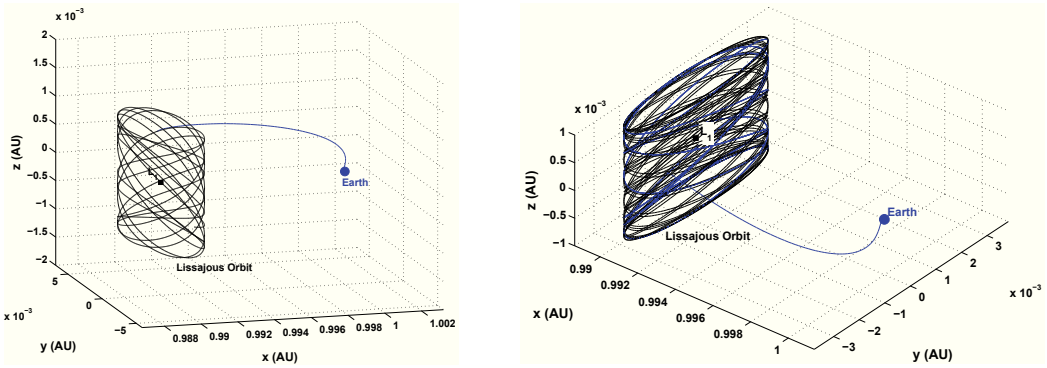

Figure 5.17: Transfer trajectories from LEO to two different Lissajous orbits around L_1 are shown in three-dimensional views.

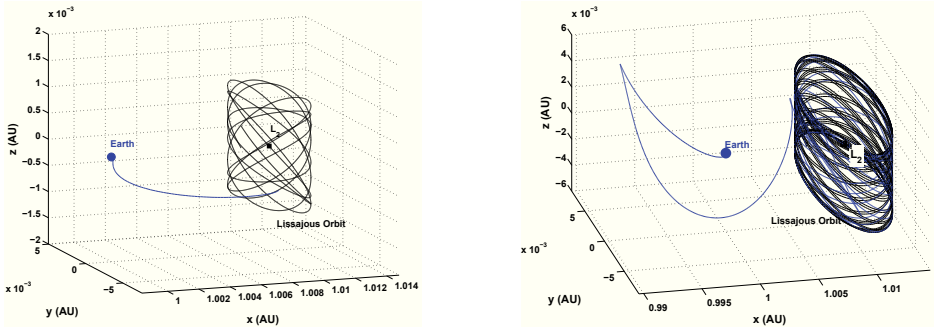

Figure 5.18: Transfer trajectories from LEO to two different Lissajous orbits around L_2 are shown in three-dimensional views.

5.6 Optimal Results of Four-Body Transfers

In this section, we consider the transfer problem with underlying system dynamics as the four-body problem. The four-body model that we use to simulate the transfer is the bicircular model which is already explained in Section 2.1.3.2. The bicircular model is derived from the Sun-Earth three-body problem with extra term regarding the Moon's gravitational influence. The mission conditions are given as same as the missions in three-body frame in Sections 5.5.2 and 5.5.3. As before for transfers to orbits around L_1, no asymmetric constraint will be augmented to the problem, but for the L_2 missions, the angle constraint will be added so the problem will not be symmetric any more. To study the extra influence of the Moon on the optimal solution, all conditions and constraints are considered the same as before. This allows us to compare the results concerning one concrete mission in two different frames. As before, the optimal control approach is employed to model the transfer problem. One can see in bicircular four-body equations 2.27

Mission	d_{EO} (km)	T_{max} (N)	N_d	t_f (days)	J (N)
1st	1083423.263	20	151	143	17.5161
2nd	1116385.068	18	133	160	17.9972
3rd	1180686.420	15	211	179	19.9211
4th	1164175.199	30	213	122	22.8297
5th	1083423.263	50	121	101	24.3575
6th	1116385.068	4	221	230	17.7412
7th	1180686.420	30	219	109	29.0069
8th	1164175.199	20	175	143	17.8194

Table 5.4: Transfers from LEO to eight halos around L_2 in four-body frame by spacecrafts which are differently equipped with various thrusters.

and 2.28 that this system is non-autonomous, since t appears in the ordinary differential equations. It is explained in Section 4.2 that an autonomous optimal control problem can be reformulated as an autonomous problem by considering the time variable t as an additional state.

5.6.1 Four-body transfers to halo orbits around L_2

The halo orbits are given as exactly same as the eight halo orbits in Section 5.5.1. On the other hand, the optimal control solver could not converge to the optimal solution using the same initial guesses for final final time t_f and controls u_i, for $i = 1, 2, 3$. That is because of the structure of the four-body problem and its properties. As mentioned before, not only the asymmetry, but also the lack of well-known solutions and knowledge about their manifolds can be the reason of this difficulty about four-body transfer problem. To handle this situation, the initial guesses have to be adjusted to the new problem. Since the knowledge about the bounded solutions and their manifolds is not solid, and there is not a well developed method to construct them, therefore the estimation of a guess for the three components control vector is not easy. Besides, having a periodic or a quasi-periodic orbit does not guarantee achieving good properties like halo orbits in three-body problem.

To overcome this hardship, a large range of sets of initial guesses must be tested to become closer to a reasonable solution. The results regarding the eight four-body transfers are presented in Table 5.4 . One can see with the same initial and final conditions, there are meaningful differences between three-body and four-body mission costs, see Table 5.1. Due to results in Table 5.4, it is clear that missions designed in four-body frame are more energy and time consuming than the missions in three-body frame. The

Mission	d_{EO} (km)	T_{max} (N)	N_d	t_f (days)	J (N)
1st	1226286.508	50	211	74	29.1951
2nd	1269045.882	25	201	119	26.6357
3rd	1335081.998	15	151	133	23.5878
4th	1428991.711	10	131	188	17.9271
5th	1226286.508	5	153	209	18.0015
6nd	1269045.882	25	151	127	21.9910
7rd	1335081.998	35	121	91	29.6844
8th	1428991.711	10	175	181	19.4618

Table 5.5: Transfers from LEO to eight halos around L_1 in four-body frame by spacecrafts which are differently equipped with various thrusters.

fifth column of Table 5.4 shows the duration of these missions which are almost 20 days more in average. On the other hand, the last column confirms that the total force used for each mission is almost 8 N more. Since the four-body model is more realistic and complete, one can expect extra force to conquer these complications. Even the number of discretization points jumps up significantly. This means NUDOCCCS spends much more time to converge to the optimal solution.

5.6.2 Four-body transfers to halo orbits around L_1

As before, to compare the results with the three-body transfers, the halo orbits are given as exactly same as the eight halo orbits in Section 5.5.2. Just like the four-body transfers to L_2, the optimal control solver cannot converge to the optimal solution using the same initial guesses for the final time t_f and controls u_i, for $i = 1, 2, 3$ which have been used in Section 5.5.2. Therefore, the initial guesses have to be adjusted again to the new situation. As before, a large range of sets of initial guesses must be tested to become closer to a reasonable solution. Eight transfers to the halo orbits are presented in Table 5.5. Although the initial and final conditions are all the same as conditions in examples given in Section 5.5.2, there are again big differences between three-body and four-body mission results. These results also confirm that the four-body transfers to periodic orbits around L_1 need more energy and time than three-body transfers. The four-body transfers shown in Table 5.5 last averagely 10 days more. On the other hand, the total force used for each mission is even more than 10 N.

5.6.3 Four-body transfers to Lissajous orbits

In this section, we continue our approach to solve the transfer problem to quasi-periodic orbits around libration points in the Sun-Earth-Moon-spacecraft four-body system. The most difficult part of this task is estimating the initial values for the free final time and control variables. The solver NUDOCCCS cannot converge to the optimal solution with the guesses made in 5.5.3. Therefore, the optimal solutions of the three-body transfers to Lissajous orbits in Section 5.5.3 are used. Fortunately, the solver responses very well to these estimations and converges to the optimal solutions. To compare the results achieved in three- and four-body frames, the initial and final conditions are considered as the same conditions as in Section 5.5.3. Table 5.6 shows the results about four transfers with information of the corresponding final quasi-periodic orbit. Similar to Table 5.3, first the quasi-periodic orbit is identified by in-plane and out-of-plane amplitudes, frequencies and phases which are denoted as in Section 3.1.1 by A_x, A_z, λ, ν, ϕ and ψ, respectively.

In Table 5.6, it is clear like L_1 and L_2 transfers in four-body frame, the Lissajous transfers are also more energy and time consuming than the same missions in three-body frame. Note that the numbers of discretization points, N_d in this table are meaningfully decreased, because the initial guesses for the t_f and controls were close to the local optimizers. Therefore, as a general conclusion of this section, one would imply that for solving a complicated transfer problem in four-body frame, such as Lissajous transfer, one should first solve the same problem in three-body frame and use the optimal solution as an initial guess for the four-body frame.

Lissajous Orbit around L_1
$A_x = 1367324$ km, $A_z = 700000$ km, $\lambda = 8$, $\nu = 8$, $\phi = \frac{\pi}{2}$, $\psi = 0$

d_{EO} (km)	T_{max} (N)	N_d	t_f (days)	J (N)
1128261.285	50	111	75	23.3541

Lissajous Orbit around L_1
$A_x = 1000000$ km, $A_z = 500000$ km, $\lambda = 20$, $\nu = 20$, $\phi = 0$, $\psi = \frac{\pi}{2}$

d_{EO} (km)	T_{max} (N)	N_d	t_f (days)	J (N)
11965405.112	5	113	189	19.9841

Lissajous Orbit around L_2
$A_x = 1326597$ km, $A_z = 700000$ km, $\lambda = 7$, $\nu = 7$, $\phi = 0$, $\psi = \frac{\pi}{2}$

d_{EO} (km)	T_{max} (N)	N_d	t_f (days)	J (N)
1335081.998	50	91	65	23.0164

Lissajous Orbit around L_2
$A_x = 1000000$ km, $A_z = 500000$ km, $\lambda = 21$, $\nu = 21$, $\phi = \frac{\pi}{2}$, $\psi = \frac{\pi}{2}$

d_{EO} (km)	T_{max} (N)	N_d	t_f (days)	J (N)
1409981.017	5	101	202	20.0973

Table 5.6: Transfers from LEO to eight halos around L_1 by spacecrafts which are differently equipped with various thrusters.

Chapter 6

Real-Time Mission Correction

Correction steps play an important role in space mission design processes. The nominal trajectories, no matter generated by which method, cannot be trusted. There are some extra factors that make the nominal trajectory and strategies impractical by themselves. These factors which disturb the spacecraft following the pre-designed mission are *disturbances* such as solar radiation pressure and/or solar winds, *displacements* caused by inaccurate thrusts, *errors* especially LEO departure error and so on. The only factor taken into account is the solar radiation pressure, Section 5.3. To deal with the rest of extra factors which are not taken into account in any element of transfer model, we continue using the optimization approach. As studied in last chapters, the transfer problem is modelled as an optimal control problem. This modelling allows us to solve the optimal control problem with a wide range of methods. The direct methods has been chosen to solve the continuous problem. Between all methods which are classified as direct method, we selected the partial discretization method. Selecting this method gives us the opportunity to numerically compute the necessary reasonable-sized matrices and sensitivity differentials. These elements have been used to design a real-time control to correct the errors exploiting in time interval $[t_0, t_f]$. The aim of this chapter is to study this real-time control for libration point missions. The only perturbation that we consider in this dissertation is the LEO departure error which happens because of the inaccuracy in the departure thrust. It means the perturbation is embedded as the parameters in the initial conditions (initial velocity). Treating the other perturbations is similar provided they are recognized and measured. The numerical results will show the feasibility and applicability of this new correction strategy for different missions in three- and four-body frames.

6.1 Mission Correction of Three-Body Transfers

In this section, we shall recall the three-body transfer studied in Section 5.5. As explained in that section, different transfers can be designed to each of L_1 and L_2 points. Not only the periodic orbits around these points have been taken into account, but also quasi-periodic orbits were considered as the destination of the mission. Now, we aim to use the iterative real-time process explained in Section 4.2.2 to control the spacecraft transferring to these different locations.

Suppose that the optimal control problem defined by Equation 5.5 is given. This problem can be seen as a parametric optimal control problem with the nominal parameters $p_0 = (0,0,0)^T$ in the initial velocity, and $q_0 = (0,0,0,0,0,0)^T$ in the final conditions (final position and velocity). The appearance of the parameters in the initial conditions is already explained. The discussion concerning the parameter vector q_0 will be explained later. Based on the earlier discussion, p denotes the parameters caused by launch velocity error from the LEO, and it consists of three components showing the errors in three different directions. Clearly, the transfer with absence of any error in the launch velocity ($p_0 = (0,0,0)^T$) is equivalent to the nominal optimal transfer.

Lets consider the mission presented as the second example in Section 5.5.2. The nominal transfer using a thruster with $T_{max} = 25\ N$ force and $I_{sp} = 3000\ s$ specific impulse, takes almost 111 days and uses $J = 15.5269\ N$. The unperturbed problem is solved by $N_d = 141$ discretization points. On the other hand, for the nominal optimal solution, all conditions in Theorem 4.1.3 are satisfied, particularly positive definiteness of the Hessian matrix on the kernel of the Jacobian of C^a with the smallest eigenvalue $\nu_{min} = 2.6744\text{E}{-}04 > 0$. Therefore one can use the explicit formulae 4.18 to calculate the sensitivity differentials $\frac{dz}{dp}(p_0)$ and $\frac{dz}{dq}(q_0)$ which are originally $\frac{du}{dp}(t_i, p_0, q_0) \approx \frac{du_i}{dp}(0,0)$ and $\frac{du}{dq}(t_i, p_0, q_0) \approx \frac{du_i}{dq}(0,0)$ as sensitivity of optimal control signals with respect to the parameters.

Based on the fact that the optimization variables after discretization of OCP(p) with partial discretization method are the discretized control variables (state variables are calculated by integration of the differential constraints with the given controls), the approximation of the form 4.27 is only used to improve the control variables. Therefore, the first step of the real-time iteration process is

$$\tilde{u}^{[1]}(p,q) = u(p_0,q_0) + \frac{du}{dp}(p_0,q_0)\Delta p. \tag{6.1}$$

Considering the value of $\tilde{u}^{[1]}(p,q)$ from this equation, we integrate the differential constraints of optimal control problem 5.5 to get the state $\tilde{x}^{[1]}(p,q)$, and check its admissibility. Since the state are achieved by integration from the actual initial boundary point, the only constraint of the transfer optimal control problem that can be violated is the final condition which is the equation of the destination orbit. By using the notations in 5.5, we have

$$\varepsilon_1 = \Delta q = g(\tilde{x}^{[1]}(\tilde{t}_f^{[1]}, p, q), \tilde{t}_f^{[1]}(p,q), q) \neq 0. \tag{6.2}$$

Now, we use the parameter q which is showing the violation in the final conditions and it is indeed the set of six parameters embedded in final position and velocity. We use q and $\frac{du}{dq}(p_0, q_0)$ to construct the next step of the real-time iterative process as following

$$\tilde{u}^{[2]}(p,q) = \tilde{u}^{[1]}(p,q) + \frac{du}{dq}(p_0,q_0)\Delta q. \tag{6.3}$$

Similar to the previous iteration, we compute the ε_k and $\tilde{u}^{[k]}(p,q)$ for $k = 2, 3, \ldots$ until the specified precision ε_∞ is achieved.

The process explained in the Equations 6.1, 6.2 and 6.3 shows the general real-time mission correction. To see the feasibility and applicability of this process, we shall consider some actual LEO departure errors and present the numerical results. The first given perturbation in the initial velocity is equal to $p_1 = (1,1,1)^T m/s$ where $1 m/s = 3.3573\text{E}{-}5\, AU/TU$ which TU is the astronautical time unit in the Sun-Earth/Moon three-body problem and the Sun-Earth-Moon-spacecraft bicircular four-body problem based on the Sun-Earth/Moon three body, i.e. $TU = 5019110.28\ s$. This amount of error usually happens in practice. The second error vector is $p_2 = (7,7,7)^T\, m/s$ where $7 m/s = 2.3501\text{E}{-}4\, AU/TU$. This error is the upper bound of the practical errors. This amount of velocity error is big and usually considered to check the applicability of correction methods. Furthermore, to point out the robustness of the real-time correction process, a huge perturbation of $p_3 = (70,70,70)^T\, m/s$ where $7 m/s = 2.3501\text{E}{-}3\, AU/TU$ is also given. This error is not only impractical and impossible to happen during a mission, but also is able to destroy the whole plans and strategies designed before the launch.

Table 6.1 shows the numerical results achieved by the real-time iterative process for the second transfer in Section 5.5.2. In this table, ε_k shows the error defined as 6.2, i.e. the violation in satisfaction of final conditions. Also, ϵ_k^F, defined as following, shows the

changes of the objective function in the k-th iteration.

$$\begin{aligned}\epsilon_1^F &= F(\tilde{u}^{[1]}, \tilde{x}^{[1]}, p, q_0) - F(u(p_0), x(p_0), p_0, q_0),\\ \epsilon_k^F &= F(\tilde{u}^{[k]}, \tilde{x}^{[k]}, p, q) - F(u(p_0, q_0), x(p_0, q_0), p_0, q_0),\ \ k = 2, 3, \ldots.\end{aligned} \tag{6.4}$$

To be more precise, the errors at the final position and velocity are separately written in the table, so one can clearly see the improvements achieved in each iteration. For each perturbation $p = p_1, p_2, p_3$, the first row in Table 6.1 corresponds to $k = 0$ which means no correction has been employed. Therefore, the errors in the $k = 0$ row are achieved only by integration of the system dynamics from the perturbed initial boundary to be corrected iteratively in next iterations $k = 1, 2, \ldots$. On the other hand, since one meter is equal to 6.68459E-12 AU, we consider $\varepsilon_\infty = 1$ cm $=$ 6.68459E-14 AU as desired precision to be achieved. Since the objective function is total force used during the mission, the positiveness of ϵ_k^F in the whole iterations describes the extra usage of thrust to correct the errors. Note that for $k = 0$, the computed trajectory is perturbed and left without correction, thus ϵ_0^F does not mean any thing and left blank. One can see the convergence of the method in successive ϵ_k^Fs. For $p = (1, 1, 1)^{m/s}$ and $p = (7, 7, 7)^{m/s}$, the sequence of ϵ_k^F converges in two and three iterations, respectively. Even for the unreal perturbation $p = (70, 70, 70)^{m/s}$, it converges with three significant digits precision in four iterations. In Figure 6.1, the biggest parameter ($p_3 = (70, 70, 70)^T$ $^{m/s}$ in initial velocity) is selected to see more clearly what happens when the iterative real-time correction method is applied. One can see the nominal optimal trajectory, violated trajectory and the corrected trajectories. In this figure, the perturbed trajectory is recognizable even in such a big scale. Based on the data from Table 6.1, this trajectory ends 97866.926 km far from the desired final destination. It is clear that the first corrected trajectory does not satisfy the final constraint. It actually ends 1251.536 km away from the halo orbit. This successive process goes on until the displacement from final constraint be less than one centimeter which happens in seventh iteration.

The second mission is the first Lissajous transfer to L_2 in Section 5.5.3. The underlying system dynamics is three-body problem. We shall review the quasi-periodic orbit and mission's properties again. The in-plane and out-of-plane amplitudes are $A_x = 1326597$ km, $A_z = 700000$ km, respectively. Furthermore, the in-plane and out-of-plane frequencies and phases are also respectively $\lambda = 7$, $\nu = 7$, $\phi = 0$, $\psi = \frac{\pi}{2}$. The transfer to such an orbit using a $T_{max} = 50$ N thruster as shown in Table 5.3 takes almost 59 days and $J = 22.1292$ N of force. We shall perturb the initial velocity when the spacecraft may leave the LEO by errors p_1, p_2 and p_3 as before. The results shown in Table 6.2 confirms the ability of the proposed real-time mission correction method. Even for the unreal

	$p = p_1$					
			Position Displacement		Velocity Violation	
k	ϵ_k^F (kg)	$\|\varepsilon_k\|_2$	AU	km	AU/TU	m/s
0		8.654E-5	1.007E-5	1506.450	8.595E-5	2.560
1	+1.551E-3	1.370E-8	2.992E-10	4.491E-1	1.337E-8	3.981E-4
2	+1.539E-3	2.029E-12	9.691E-13	1.450E-4	1.7826e-12	5.310E-8
3	+1.539E-3	8.256E-14	3.181E-14	4.759E-6	7.618E-14	2.269E-9
4	+1.539E-3	0.0E0	0.0E0	0.0E0	0.0E0	0.0E0

	$p = p_2$					
			Position Displacement		Velocity Violation	
k	ϵ_k^F (kg)	$\|\varepsilon_k\|_2$	AU	km	AU/TU	m/s
0		6.901E-4	7.015E-5	10494.290	6.865E-4	20.4489
1	+1.059E-2	6.814E-7	9.125E-8	13.651	6.753E-7	2.011E-2
2	+1.004E-2	7.827E-10	8.920E-11	1.334E-2	7.776E-10	2.316E-5
3	+1.003E-2	2.405E-12	7.093E-13	1.061E-4	2.298E-12	6.844E-8
4	+1.003E-2	9.437E-14	7.540E-15	1.128E-6	9.407E-14	2.802E-9
4	+1.0023-2	0.0E0	0.0E0	0.0E0	0.0E0	0.0E0

	$p = p_3$					
			Position Displacement		Velocity Violation	
k	ϵ_k^F (kg)	$\|\varepsilon_k\|_2$	AU	km	AU/TU	m/s
0		5.573E-3	6.542E-4	97866.926	5.534E-2	164.850
1	+0.165	7.027E-5	8.366E-6	1251.536	6.977E-5	2.078
2	+0.109	8.636E-7	5.991E-8	8.9624	8.615E-7	2.566E-2
3	+0.109	2.607E-8	3.995E-9	5.976E-1	2.576E-8	7.673E-4
4	+0.108	7.185E-10	3.357E-11	5.022E-3	7.177E-10	2.138E-5
5	+0.108	2.009E-11	1.338E-12	2.002E-4	2.004E-11	5.971-7
6	+0.108	6.368E-13	3.656E-14	5.469E-6	6.357E-13	1.894-8
7	+0.108	0.0E0	0.0E0	0.0E0	0.0E0	0.0E0

Table 6.1: Violation of objective function, constraints, final position and velocity computed by the real-time correction process for different initial errors. This correction strategy is designed for a mission transferring to L_1 halo orbit in three-body frame explained in the second example of Section 5.5.2.

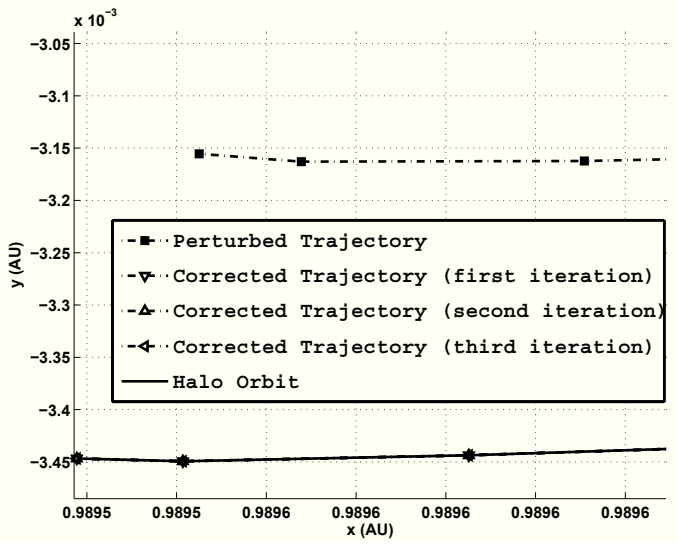

Figure 6.1: The last part of the nominal, perturbed and corrected trajectories for $p_3 = (70, 70, 70)^{m}/_{s}$. The nominal trajectory shown in this figure is obtained as the second example of L_1 transfers in three-body frame. See the details of the nominal optimal solution in Section 5.5.2.

perturbation p_3, the correction process convergence after ten iterations.

6.2 Mission Correction of Four-Body Transfers

In this section, we shall recall the four-body transfer studied in Section 5.6. As explained in that section, different transfers can be designed to each of L_1 and L_2 points. Not only the periodic orbits around these points have been taken into account, but also quasi-periodic orbits were considered as the destination of the mission. Now, we aim to use the iterative real-time process explained in Section 4.2.2 to control the spacecraft transferring to these different locations.

Lets consider the first L_2 transfer in four-body frame explained in Section 5.6.1. This mission transfers the spacecraft to a halo orbit 1226286.508 kilometers away from the parking LEO using a $T_{max} = 50\ N$ thruster. This mission takes almost 74 days to reach the destination with proper position and velocity. As one can see in Table 5.4, the total force use of this mission is $J = 29.1951\ N$. Again, the initial velocity at the LEO departure is perturbed by three different errors p_1, p_2 and p_3. Table 6.3 also shows the results obtained by the real-time correction process. Lets consider the biggest perturbation p_3. This process can correct the position displacement and velocity violation in ten iterations. Note that the perturbed trajectory ends 154965.190 kilometers away

	$p = p_1$					
			Position Displacement		Velocity Violation	
k	ϵ_k^F (kg)	$\|\varepsilon_k\|_2$	AU	km	$^{AU}/_{TU}$	$^{m}/_{s}$
0		1.678e-04	1.205E-5	1802.654	1.674E-4	4.986
1	+1.897E-2	3.948E-8	3.002E-9	4.491E-1	3.937E-8	1.172E-3
2	+1.897E-2	3.907E-11	2.913E-12	4.357E-4	3.896E-11	1.160-06
3	+1.897E-2	4.808E-13	3.487E-14	5.216E-6	4.795E-13	1.428E-8
4	+1.897E-2	0.0E0	0.0E0	0.0E0	0.0E0	0.0E0

	$p = p_2$					
			Position Displacement		Velocity Violation	
k	ϵ_k^F (kg)	$\|\varepsilon_k\|_2$	AU	km	$^{AU}/_{TU}$	$^{m}/_{s}$
0		1.091E-3	9.551E-5	14288.092	1.087E-3	32.3774
1	+1.239E-1	1.394E-6	1.019E-7	15.244	1.390E-6	4.140E-2
2	+1.233E-1	1.002E-8	8.894E-10	1.330E-1	9.983E-9	2.973E-4
3	+1.229E-1	5.515E-11	4.392E-12	6.570E-4	5.498E-11	1.638E-6
4	+1.229E-1	0.0E0	0.0E0	0.0E0	0.0E0	0.0E0

	$p = p_3$					
			Position Displacement		Velocity Violation	
k	ϵ_k^F (kg)	$\|\varepsilon_k\|_2$	AU	km	$^{AU}/_{TU}$	$^{m}/_{s}$
0		1.163E-2	9.894E-4	148012.132	1.159E-2	345.220
1	+1.457	1.673E-4	9.779E-5	14629.176	1.358E-4	4.045
2	+1.501	1.007E-5	8.903E-7	133.187	1.003E-5	2.988E-1
3	+1.488	5.994E-7	4.563E-8	6.826	5.977E-7	1.782E-2
4	+1.485	4.204E-8	3.299E-9	4.935E-1	4.191E-8	1.248E-3
5	+1.486	2.491E-9	1.810E-11	2.708E-3	2.491E-9	7.420E-5
6	+1.486	1.501E-10	1.100E-11	1.645E-3	1.497E-10	4.459E-6
7	+1.486	9.822e-12	9.018E-13	1.349E-4	9.781E-12	2.913E-7
8	+1.486	9.488e-13	7.399E-14	1.107E-5	9.459E-13	2.817E-8
9	+1.486	7.253E-13	5.015E-14	7.502E-6	7.236E-13	2.155E-8
10	+1.486	0.0E0	0.0E0	0.0E0	0.0E0	0.0E0

Table 6.2: Violation of objective function, constraints, final position and velocity computed by the real-time correction process for different initial errors. This correction strategy is designed for a mission transferring to Lissajous orbit around L_2 in three-body frame explained in the second example of Section 5.5.3.

from the closest point of halo orbit. On the other hand, the errors in all iterations are relatively bigger than both previous examples, because of the complication of the system dynamics in four-body problem [86].

6.3 Discussion

This chapter presented a new method for libration point mission correction in different underlying systems. A mission transferring to a periodic orbit around L_1 in three-body system, a mission to a quasi-period orbit around L_2 in three-body system, and eventually a mission to a halo orbit around L_2 in four-body system are perturbed and treated in real-time manner. At this point, some questions come up. Due to the structure of a formation mission, is it possible to use such a strategy for mission correction in formation flights? How can it be applied? All spacecraft should be controlled in real-time fashion independently, or only one leading controlled spacecraft is enough? Which spacecraft is the best choice to design the real-time control? And lots of other questions regarding real-time control of formation flights. Therefore, this problem is still open and full of unclear aspects and unsolved problems that can be the subject of a research.

	$p = p_1$					
			Position Displacement		Velocity Violation	
k	ϵ_k^F (kg)	$\|\varepsilon_k\|_2$	AU	km	$^{AU}/_{TU}$	$^{m}/_{s}$
0		1.830E-4	1.407E-5	2104.249	1.825E-4	5.435
1	+2.687E-2	4.049E-8	3.157E-9	4.723E-1	4.037E-8	1.202E-3
2	+2.689E-2	4.174E-11	3.255E-12	4.869E-4	4.161E-11	1.239E-6
3	+2.689E-2	4.942E-13	3.650E-14	5.461E-6	4.929E-13	1.468E-8
4	+2.689E-2	0.0E0	0.0E0	0.0E0	0.0E0	0.0E0

	$p = p_2$					
			Position Displacement		Velocity Violation	
k	ϵ_k^F (kg)	$\|\varepsilon_k\|_2$	AU	km	$^{AU}/_{TU}$	$^{m}/_{s}$
0		1.286E-3	9.887E-5	14790.967	1.283E-3	38.2087
1	+1.879E-1	1.668E-6	1.282E-7	19.177	1.662E-6	4.951E-2
2	+1.888E-1	1.162E-8	9.062E-10	1.356E-1	1.158E-8	3.450E-4
3	+1.888E-1	5.790E-11	4.523E-12	6.767E-4	5.772E-11	1.719E-6
4	+1.888E-1	1.577E-13	1.049E-14	1.569E-6	1.573E-13	4.687E-9
5	+1.888E-1	0.0E0	0.0E0	0.0E0	0.0E0	0.0E0

	$p = p_3$					
			Position Displacement		Velocity Violation	
k	ϵ_k^F (kg)	$\|\varepsilon_k\|_2$	AU	km	$^{AU}/_{TU}$	$^{m}/_{s}$
0		1.349E-2	1.036E-3	154965.190	1.345E-2	400.708
1	+1.873	1.656E-4	1.272E-5	1902.579	1.652E-4	4.920
2	+1.873	1.177E-5	9.205E-7	137.710	1.173E-5	3.495
3	+1.878	6.174E-7	4.815E-8	7.202	6.156E-7	1.833E-2
4	+1.878	4.473E-8	3.498E-9	5.232	4.460E-8	1.328E-3
5	+1.878	2.774E-9	2.167E-10	3.242E-2	2.765E-9	8.237E-5
6	+1.878	1.878E-10	1.471E-11	2.201E-3	1.876E-10	5.589E-6
7	+1.878	1.181E-11	9.224E-13	1.380E-4	1.177E-11	3.507E-7
8	+1.878	1.018E-12	7.769E-14	1.162E-5	1.016E-12	3.025E-8
9	+1.878	7.778E-13	5.777E-14	8.643E-6	7.757E-13	2.310E-8
10	+1.87859	0.0E0	0.0E0	0.0E0	0.0E0	0.0E0

Table 6.3: Violation of objective function, constraints, final position and velocity computed by the real-time correction process for different initial errors. This correction strategy is designed for a mission transferring to L_2 halo orbit in four-body frame explained in the second example of Section 5.6.1.

Chapter 7

Conclusions and Prospects

This dissertation is a contribution to the investigation of a new approach to design the space missions. The mission designs have been done traditionally using some sophisticated methods which are very sensitive with respect to slight changes. Therefore, the aim of this dissertation was to study the new approach, its theory and tools. The new approach is based on the theory of optimal control. To explain the optimization approach, one has to have the mathematical model which was fortunately prepared upon different efforts since 18th century. On the other hand, to start using the optimization theory, one also has to have information about the behaviour of the system in some specified areas, such as the vicinity of the Earth etc. To this end, different underlying system dynamics have been explained such as three-body problem and its simplified versions, different four-body models etc. Consideration of the three-body problem has lots of advantages which made us to study this problem in a special chapter. different types of solutions, such as equilibrium points, two- and three-dimensional orbits. These orbits were classified differently in periodic orbits, quasi-periodic orbits etc.

Using the information about the underlying system dynamics, an optimal control problem is formulated. In this problem, a reasonable objective function with differential and algebraic equation constraints with possibility to extend to different initial and final conditions is modelled. This optimal control problem is solved by a partial discretization direct method. This method discretizes the optimal control problem in a special fashion and transcribes it into a nonlinear programming problem. This transcription allows us to use well developed theory of static optimization and take advantage of the theory of parametric sensitivity analysis. Due to the properties of transfer problem, one can use the sensitivity differentials to estimate the sensitivity of optimal solutions with respect to different practical perturbations.

The perturbation considered in this dissertation is the errors in low Earth orbit departure. Treatment of other types of perturbations is also similar to this. The errors

in LEO leaving part of he mission modelled as parameters embedded in initial velocity. Based on the parametric sensitivity analysis and its explicit formulae, the sensitivity of the optimal solutions with respect to errors is estimated. Using a linear approximation taken from the Taylor expansion of new control rule, a process to design new controls is derived. This process updates the control rules such that all constraints (final conditions in transfer problems) are satisfied. Since computation of Hessian and Jacobian matrices can be done off-line, this process can be deployed in real-time fashion.

The field of mission design to different orbits around libration points is still growing and there are many more problems to solve. This dissertation presents an extensive study for different transfer problems and shows that many of them are solvable with the optimization approach. Furthermore, the new real-time method for updating the control rules in transfer problems opens a new window to a different way of mission correction design. In this dissertation, different types of missions, to both L_1 and L_2 in the Sun-Earth/Moon three-body problem and also the Sun-Earth-Moon-spacecraft are corrected by the real-time correction method. It can be interesting for researchers in this field to check the possible use of this methods for formation flight in general form and/or system to system missions. Since these two types of missions are very complicated even to achieve the transfer solution, the design of correction maneuvers can be challenging.

Appendix

This appendix is devoted to prepare the relations and equations regarding conversion from one reference frame to another. The main body of this discussion is taken from Jeff Parker [77]. The reference frames which are discussed in this dissertation are the Sun-Earth or the Sun-Earth/Moon inertial frame and the Sun-Earth/Moon synodic frame. These reference frames are briefly explained in the following:

The Sun-Earth/Moon inertial reference frame which is centered at the barycenter of two masses, the Sun and the Earth/Moon. This frame does not rotate with motion of any of these bodies.

The Sun-Earth/Moon synodic reference frame which is centered at the barycenter of two bodies. This frame rotates with a constant angular speed equal to the mean rotation rate of the Earth and the Sun about their barycenter. The x-axis of the system goes from the barycenter which is very close to the Sun's surface through the Earth. And the z-axis coincides with the angular momentum vector of the system. Of course, the y-axis completes the right handed triad rule. This reference frame is main subject of this dissertation.

In Section 2.1.2.1, it is necessary to have some formulae regarding transformation of the Sun-Earth/Moon three-body from inertial to synodic frame. To this end, several conversions are necessary. We discuss this transformation in both two sides, i.e. from the inertial frame to the synodic frame and vice versa.

Inertial Frame to Synodic Frame

Lets state the coordinates in the standard inertial frame of the circular restricted three-body problem as

$$X_I = (x_I, y_I, z_I, \dot{x}_I, \dot{y}_I, \dot{z}_I)^T, \tag{1}$$

and the coordinates in the synodic reference frame of the circular restricted three-body problem as

$$X_S = (x_S, y_S, z_S, \dot{x}_S, \dot{y}_S, \dot{z}_S)^T. \tag{2}$$

Note that the subscripts I and S specify the coordinates in inertial and synodic frames, respectively. To make the conversion clear, one should note that the conversion assumes that the Sun and the Earth revolve around the barycenter in circular orbits in the inertial frame. Now, We shall obtain the equations converting the coordinates in inertial frame X_I to the inertial reference frame with X_S coordinates. Suppose that at the time of the conversion, the synodic frame is rotated by an angle θ with respect to the inertial frame, i.e. the Earth in the CRTBP at the time of conversion has revolved about the barycenter by the angle θ in a counter-clockwise manner from the x-axis of the inertial reference frame. Now, lets define the transformation $T_{-\theta}$ as

$$T_{-\theta} = \begin{pmatrix} \cos(-\theta) & -\sin(-\theta) & 0 \\ \sin(-\theta) & \cos(-\theta) & 0 \\ 0 & 0 & 1 \end{pmatrix} = \begin{pmatrix} \cos(\theta) & -\sin(\theta) & 0 \\ -\sin(\theta) & \cos(\theta) & 0 \\ 0 & 0 & 1 \end{pmatrix}. \tag{3}$$

Lets denote the AU (astronautical distance unit) in kilometers as D_N which is actually 149597870 kilometers. Furthermore, suppose that T_N also denotes TU (astronautical time unit) in seconds which is 5022410 seconds. Then the following equations may be used to convert the the inertial reference frame to the synodic reference frame.

$$\begin{pmatrix} x_S \\ y_S \\ z_S \end{pmatrix} = T_{-\theta} \begin{pmatrix} x_I \\ y_I \\ z_I \end{pmatrix} \left(\frac{1}{D_N}\right) \tag{4}$$

and

$$\begin{pmatrix} \dot{x}_S \\ \dot{y}_S \\ \dot{z}_S \end{pmatrix} = T_{-\theta} \begin{pmatrix} \dot{x}_I \\ \dot{y}_I \\ \dot{z}_I \end{pmatrix} \left(\frac{1}{D_N} \times \frac{T_N}{1}\right) + \begin{pmatrix} y_S \\ -x_S \\ 0 \end{pmatrix}. \tag{5}$$

Synodic Frame to Inertial Frame

This conversion assumes again that the Sun and the Earth revolve around their barycenter in circular orbits in the inertial frame. At the time of the conversion, it is also assumed

that the synodic frame is rotated by an angle θ with respect to the inertial frame. Assume

$$T_\theta = \begin{pmatrix} \cos(\theta) & -\sin(\theta) & 0 \\ \sin(\theta) & \cos(\theta) & 0 \\ 0 & 0 & 1 \end{pmatrix}. \tag{6}$$

Then the following equations may be used to convert the synodic reference frame to the inertial reference frame.

$$\begin{pmatrix} x_I \\ y_I \\ z_I \end{pmatrix} = T_\theta \begin{pmatrix} x_S \\ y_S \\ z_S \end{pmatrix} (\tfrac{D_N}{1}) \tag{7}$$

$$\begin{pmatrix} \dot{x}_I \\ \dot{y}_I \\ \dot{z}_I \end{pmatrix} = T_\theta \begin{pmatrix} \dot{x}_S - y_S \\ \dot{y}_S + x_S \\ \dot{z}_S \end{pmatrix} (\tfrac{D_N}{1} \times \tfrac{1}{T_N}) \tag{8}$$

Bibliography

[1] http://heasarc.gsfc.nasa.gov/Images/misc_missions/isee3_traj.gif. 7

[2] http://sohowww.nascom.nasa.gov/about/about.html. 8

[3] http://www.ptmcdonald.net/radeffects/SOHO.html. 8

[4] http://map.gsfc.nasa.gov/. 8, 9

[5] http://www.srl.caltech.edu/ACE/. 9

[6] http://genesismission.jpl.nasa.gov/index.html. 10

[7] *The Columbia Encyclopedia, Sixth Edition.* 2001-05. 3

[8] A. Babloyantz, AP. Krishchenko, and A. Nosov. Analysis and stabilization of nonlinear chaotic systems. *Computers & Mathematics with Applications*, **34**:355–368, 1997. 6

[9] B.T. Barden. *Using Stable Manifolds to Generate Transfers in the Circular Restricted Problem of Three Bodies.* Master's thesis, School of Aeronautics and Astronautics, Purdue University, West Lafayette, Indiana, December 1994. 6

[10] J. Barrow-Green. *Poincaré and the Three Body Problem*, **11**. American mathematical Society, Providence Rhode Island, 1997. 4

[11] M. Beckman. Orbit determination issues for libration point orbits. In *Libration Point Orbits and Applications: Proceedings of the conference*, Aiguablava, Girona, Spain, June 2002. 7, 9

[12] C. Beichman, G.M.M. Gómez, M.W. Lo, J. Masdemont, and L. Romans. Searching for life with the Terrestial Planet Finder: Lagrange point options for a formation flying interferometer. *Advances in Space Research*, **34**[3]:637–644, 2004. 11

[13] D.J. Bell. Optimal space trajectories–a review of published work. *Aeronautical Journal*, **72**:141–146, 1968. 3, 4

[14] W.J. Boulton. The effect of solar radiation pressure on the orbit of a cylindrical satellite. *Planet Space Sci.*, **32**[3]:287–296, 1984. 70

[15] T.A. Bray and C.L. Goudas. Doubly-symmetric orbits about the collinear lagrange points. *Astronomical Journal*, **22**[2], 1967. 49

[16] R.A. Broucke. Periodic orbits in the restricted three-body problem with Earth-Moon masses. Technical report, Jet Propulsion Laboratory, Cal. Tech., 1968. 5

[17] R.A. Broucke. Stability of periodic orbitzs in the elliptic, restricted three-body problem with earth-moon masses. *AIAA Journal*, **7**[6]:1003–1009, 1969. 49

[18] Arthur Earl Bryson and Yu-Chi Ho. *Applied Optimal Control: optimization, estimation, and control*. Hemisphere, Washington, 1975. 2

[19] C. Büskens. *Direkte Optimierungsmethoden zur numerischen Berechnung optimaler Steuerungen*. Master's thesis, Institut für Numerische Mathematik, Universität Münster, Münster, Germany, 1993. 60, 63

[20] C. Büskens. *Optimierungsmethoden und Sensitivitätsanalyse für optimale Steuerprozesse mit Steuer-und Zustands-Beschränkungen*. PhD thesis, Institut für Numerische Mathematik, Universität Münster, Münster, Germany, 1998. 60, 63

[21] C. Büskens. *Echtzeitoptimierung und Echtzeitoptimalsteuerung parametergestörter Probleme*. Fachbereich Mathematik und Physik, Universität Bayreuth, Bayreuth, Germany, 2002. 65

[22] G.E. Cook. Luni-solar perturbations of the orbit of an earth satellite. *Geophysical Journal of the Royal Astronomical Society*, **6**:271–291, 1962. 70

[23] G.H. Darwin. Periodic orbits. *Acta Mathematica*, **21**:99–242, 1897. 5

[24] T.N. Edelbaum. How many impulses? *Astronautics and Aeronautics*, **5**[11]:64–69, 1967. 4

[25] R.W. farquhar. *The Control and Use of Libration-Point Satellites*. PhD thesis, Stanford University, Department of Aeronautics and Astronautics, Stanford, CA, 1968. 1, 5

[26] R.W. Farquhar. The flight of ISEE-3/ICE: Origins, mission history, and a legacy. In *AIAA 98-4464, AIAA/AAS Astrodynamics Specialist Conference*, Boston, Massachusetts, USA, August 1998. 7

[27] R.W. Farquhar and A.A. Kamel. Quasi-periodic orbits about the translunar libration point. *Celestial Mechanics*, **7**[4]:458–473, 1973. 5

[28] A.V. Fiacco. *Introduction to Sensitivity and Stability Analysis in Nonlinear Programming Mathematics in Science and Engineering*. Academic Press, New York, 1983. 60

[29] R. Fletcher. *Practical Methods of Optimization*. Wiley & Sons, Chichester/New York, 2nd edition, 1997. 57, 60

[30] P.E. Gill, W. Murray, and M.H. Wright. *Practical Optimization*. Academic Press, 1981. 57

[31] F.W. Gobetz and J.R. Doll. A survey of impulsive trajectories. *AIAA Journal*, **7**[5]:801–834, 1969. 4

[32] G. Gómez, A. Jobra, J. Masdemont, and C. Simò. Final report: Study refinement of semi-analytic halo orbit theory. Technical Report 8625/89/D/MD(SC), ESOC Contract Report, Barcelona, Spain, April 1991. 6

[33] G. Gómez, A. Jobra, J. Masdemont, and C. Simò. Study of the transfer from the Earth to a halo orbit around equilibrium point L_1. *Celestial Mechanics and Dynamical Astronomy*, **56**[4]:541–562, 1993. 6

[34] G. Gómez, C. Simó, J. Llibre, and R. Martinez. *Dynamics and Mission Design near Libration Points, Volume II: Fundamentals: The Case of Triangular Libration Points*. World Scientific Monograph Series in Mathematics, 2001. 30

[35] G.M.M. Gómez and J. Masdemont. Trajectory correction manoeuvres in the transfer to libration point orbits. *Acta Astonautica*, **56**:652–669, 2005. 6

[36] C. Grebog and YC. Lai. Controlling chaotic dynamical systems. *Systems & Control Letters*, **31**:307–312, 1997. 6

[37] J. Guckenheimer and P. Holmes. *Nonlinear oscillations, dynamical systems, and bifurcations of vector fields*. Applied mathematical sciences. Springer-Verlag, 1990. 47

[38] P. Guillaume. New periodic solutions of the three dimensional restricted problem. *Celestial Mechanics*, **10**[4]:475–495, 1974. 5

[39] M.A. Hanson. On sufficiency of the Kuhn-Tucker conditions. *Journal of Mathematical Analysis and Applications*, **80**:545–550, 1981. 58

[40] M. Hènon. Exploration numèrique du problème des trois corps, (i), masses egales, orbites pèriodiques. *Annales d'Astrophysique*, **28**[3]:499–511, 1965. 5

[41] M. Hènon. Exploration numèrique du problème des trois corps, (ii), masses egales, orbites pèriodiques. *Annales d'Astrophysique*, **28**[6]:992–1007, 1965. 5

[42] M. Hènon. Exploration numèrique du problème des trois corps, (iii), masses egales, orbites non pèriodiques. *Bulletin d'Astronomie*, **1**[1]:57–80, 1966. 5

[43] M. Hènon. Exploration numèrique du problème des trois corps, (iv), masses egales, orbites non pèriodiques. *Bulletin d'Astronomie*, **1**[2]:49–66, 1966. 5

[44] M. Hènon. Numerical exploration of the restricted problem. V., Hill's case: Periodic orbits and their stability. *Astronomy & Astrophysics*, **1**:223–238, 1969. 5

[45] Lisa A. Hiday. *Optimal Transfers Between Libration Points in the Elliptic Restricted Three-Body Problem*. PhD thesis, School of Aeronautics and Astronautics, Purdue University, West Lafayette, Indiana, August 1992. 6

[46] G.W. Hill. Review of Darwin's periodic orbits. *Astronomical Journal*, **18**[423]:120, 1898. 5

[47] R.F. Hoelker and R. Silber. The bi-elliptic transfer between co-planar circular orbits. *Proceeding of the Fourth AFBMD/STL symposium–Advances in Ballistic Missile and Space Technology*, **3**:164–175, 1961. 4

[48] Walter Hohmann. *Die Erreichbarkeit Der Himmelskörper: Untersuchungen über Das Raumfahrtproblem*. Munique, 1925. 5

[49] K.C. Howell. Three-dimensional, periodic, '*Halo*' orbits. *Celestial Mechanics*, **32**[1]. 5, 36, 40, 44

[50] K.C. Howell and B.T. Barden. Brief summary of alternative targeting strategies for TCM1, TCM2 and TCM3. Private communication, Purdue University, 1999. 6

[51] K.C. Howell, D.L. Mains, and B.T. Barden. Transfer trajectories from Earth parking orbit to Sun-Earth halo orbits. In *AAS Paper, AIAA/AAS Spaceflight Mechanics Meeting*, pages 94–160, Cocoa Beach, Florida, USA, April 1994. 6

[52] K.C. Howell and H.J. Pernicka. Stationkeeping method for libration point trajectories. *Journal of Guidance, Control and Dynamics*, **16**[3]:151–159, 1993. 2

[53] Samantha I. Infeld. *Optimization of Mission Design for Constrained Libration Point Space Mission*. PhD thesis, Department of Aeronautics and Astronautics, Stanford University, December 2005. 6

[54] D.J. Jezewski and L. Rozendaal. An efficient method for calculating optimal free-space n-impulsive trajectories. *AIAA Journal*, **6**[11]:2160–2165, 1968. 6

[55] E. Julliard-Tosel. Bruns' theorem: the proof and some generalizations. *Celestial Mechanics and Dynamical Astronomy*, **76**:241–281, 2000. 4

[56] W. Karush. *Minima of Functions of Several Variables with Inequalities as Side Constraints*. Master's thesis, Dept. of Mathematics, University of Chicago, Chicago, Illinois, 1939. 57

[57] Tinne Hoff Kjeldsen. A contextualized historical analysis of the kuhn-tucker theorem in nonlinear programming: the impact of world war ii. *Historia Math*, **27**[4]:331–361, 2000. 57

[58] W.S. Koon, M.W. Lo, J.E. Marsden, and S.D. Ross. *Dynamical Systems, the Three-Body Problem and Space Mission Design*. Marsden Books, 2008. ISBN 978-0-615-24095-4. 30

[59] M.J. Kuchner. General astrophysics and comparative planetology with the Terrestrial Planet Finder missions. *JPL Publication*, **05-01**, 2005. 1

[60] H.W. Kuhn and A.W. Tucker. Nonlinear programming. In *Proc. Second Berkeley Symp. on Math. Statist. and Prob.*, pages 481–492, Berkeley, University of California Press, 1951. 57

[61] D.F. Lawden. *Optimal Trajectories for Space Navigation*. Butterworths, London, 1963. 6

[62] D.F. Lawden. Rocket trajectories optimization: 1950-1963. *Journal of Guidance, Control, and Dynamics*, **14**[4]:705–711, 1991. 4

[63] M.L. Lidov and V.Y. Rabinovich. Investigation of families of three-dimensional periodic orbits of the three-body problem. *Cosmic Research*, **17**[3], 1979. 5

[64] P.M. Lion and M. Handelsman. Primer vector on fixed-time impulsive trajectories. *AIAA Journal*, **6**[1]:127–132, 1968. 6

[65] M.W. Lo, B.G. Williams, W.E. Bollman, D. Hahn, J.L Bell, E.A. Hirst, R.A. Corwin, P.H. Hong, K.C. Howell, B.T. Barden, and R.S. Wilson. Genesis mission design. In *AIAA 98-4468, AIAA Space Flight Mechanics*, Boston, Massachusetts, USA, August 1998. 6

[66] E.E.N. Macau. Low-thrust chaotic based transfer from the earth to a halo orbit. *Journal of Theoretical and Applied Mathematics*, **46**:551–564, 2008. 67

[67] A.P. Markeev. Two-dimentional periodic motion of a satellite relative to the center of mass near a collinear libration point. *Cosmic Research*, **17**[3], 1979. 5

[68] S.M. Marsh. *Sun-Synchronous Trajectory Design Using Consecutive Lunar Gravity Assist*. Master's thesis, Purdue University, West Lafayette, Indiana, May 1988. 12

[69] D.H. Martin. The essence of invexity. *Journal of Optimization, Theory and Applications*, **47**:65–76, 1985. 58

[70] R. Mettin. Control of chaotic maps by optimized periodic inputs. *International Journal of Bifurcation and Chaos*, **8**:1707–1711, 1998. 6

[71] F.R. Moulton. *An Introduction to Celestial Mechanics*. The McMillan Company, New York, 1914. 5

[72] P. Musen. The influence of the solar radiation pressure on the motion of an artificial satellite. *Journal of Geophysical Research*, **65**[5]:1391–1396, 1960. 70

[73] Isaac Newton. *Philosophiae Naturalis Principia Mathematics*. Londoni, 1687. 3

[74] J. Nocedal and S.J. Wright. *Numerical Optimization*. Springer series in operations research. Springer, 2006.

[75] NSSDC. National Space Science Data Center. `http://nssdc.gsfc.nasa.gov/`, 2011. 7

[76] J.D. Offenberg and J.G. Bryson. The James Webb Space Telescope. 2005. `http://www.jwst.nasa.gov/`. 1, 11, 74

[77] J.S. Parker. *Low-Energy Ballistic Lunar Transfers*. PhD thesis, University of Colorado, Department of Aerospace Engineering Sciences, 2007. 5, 7, 107

[78] L. Perko. *Differential equations and dynamical systems*. Texts in applied mathematics. Springer, 2001. 46

[79] G.L. Pillbratt, T. Prusti, A.M. Heras, S. Leeks, A.P. Marston, and R. Vavrek. Herschel Space Observatory. *American Astronautical Meeting 204*, pages 01–81, 2004. 11

[80] H.C. Plummer. On oscillating satellites. *Monthly Notices of Royal Astronautical Society*, **63**:436–443, 1903. 5

[81] H.C. Plummer. On oscillating satellites. *Monthly Notices of Royal Astronautical Society*, **64**:98–105, 1903. 5

[82] L.S. Pontryagin, V. Boltyanskii, R. Gamkrelidze and E. Mischenko. *The Mathematical Theory of Optimal Processes Interscience*. Springer, New York, 1962. 62

[83] D.L. richardson. Analytical construction of periodic orbits about the collinear points. *Celestial Mechanics*, **22**:241–253, 1980. 5, 36, 37, 39

[84] A. Roy. *The Foundations of Astrodynamics*. The McMillan Company, London, 1965. 5

[85] H.M. Jones R.W. Parkinson. Effects of solar radiation pressure on earth satellite orbits. *Science*, **131**:920–921, 1960. 70

[86] Majid Salmani, and Christof Büskens. Real-time control of optimal low-thrust transfer to the SunEarth L_1 halo orbit in the bicircular four-body problem. *Acta Astronautica*, **69**:882–891, 2011. 102

[87] R. Serban, W.S. Koon, M.W. Lo, J.E. Marsden, L.R. Petzold, S.D. Ross, and R.S. Wilson. Halo orbit mission correction maneuvers using optimal control. *Automatica*, **38**:571–583, 2002. 6

[88] C. Simó, G. Gómez, J. Llibre, R. Martínez, and J. Rodríguez. On the optimal station keeping control of halo orbits. *Acta Astronautica*, **15**[6-7]:391–397, 1987. 2

[89] E.C. Stone, A.M. Frandsen, R.A. Mewaldt, E.R. Christian, D. Margolies, J.F. Ormes, and F. Snow. The advanced composition explorer. http://www.srl.caltech.edu/ACE/ace-mission-ssr-paper.pdf, 1998. 9, 10

[90] K. Sundman. Mèmoire sur le problème des trois corps. *Acta Mathematica*, **36**:105–179, 1912. 5

[91] V.G. Szebehely. *Theory of Orbits: the Restricted Problem of Three Bodies*. Academic Press, New York, 1967. 3, 16, 19, 20

[92] V.G. Szebehely. *Advances in Celestial Mechanics, a first Course in Theory of Orbits*. University of Texas Press, Austin, 1989. 4, 25

[93] R. taton and C. Wilson. *Planetary astronomy from the Renaissance to the rise of astrophysics*, **2A**. Cambridge University Press, 1989. 4

[94] D.A Vallado and W.D. McClain. *Fundamentals of Astrodynamics and Applications*. Space technology library. Microcosm Press, 2001. 17, 21

[95] W.E. Wiesel. *Modern Astrodynamics*. Aphelion Press, Beavercreek, Ohio. 4, 48

[96] S. Wiggins. *Introduction to applied nonlinear dynamical systems and chaos*. Texts in applied mathematics. Springer, 2003. 48

[97] Hagihara Yusuke. *Celestial Mechanics*. Japan Soc. for the Promotion of Science, Kojimachi u.a., 1975. 3

[98] C.G. Zagouras and M. Kalogeropoulou. Numerical determination of families of three-dimensional orbits bifurcating from planar periodic orbits around both primaries. *Astron. Astrophys. Suppl.*, **32**:307–321, 1978. 5

Optimal Control of Mission Design in Multi-Body Models

Majid Salmani
Zentrum für Technomathematik

Dissertation
zur Erlangung des Grades eines Doktors
der Naturwissenschaften
- *Dr. rer. nat.* -
14.12.2012

Gutachter: Prof. Dr. Christof Büskens
Gutachter: Prof. Dr. Alfred Schmidt